The Challenges and Opportunities of a Hydrogen Internal Combustion Engine

E.C. Peeters

Delft University of Technology

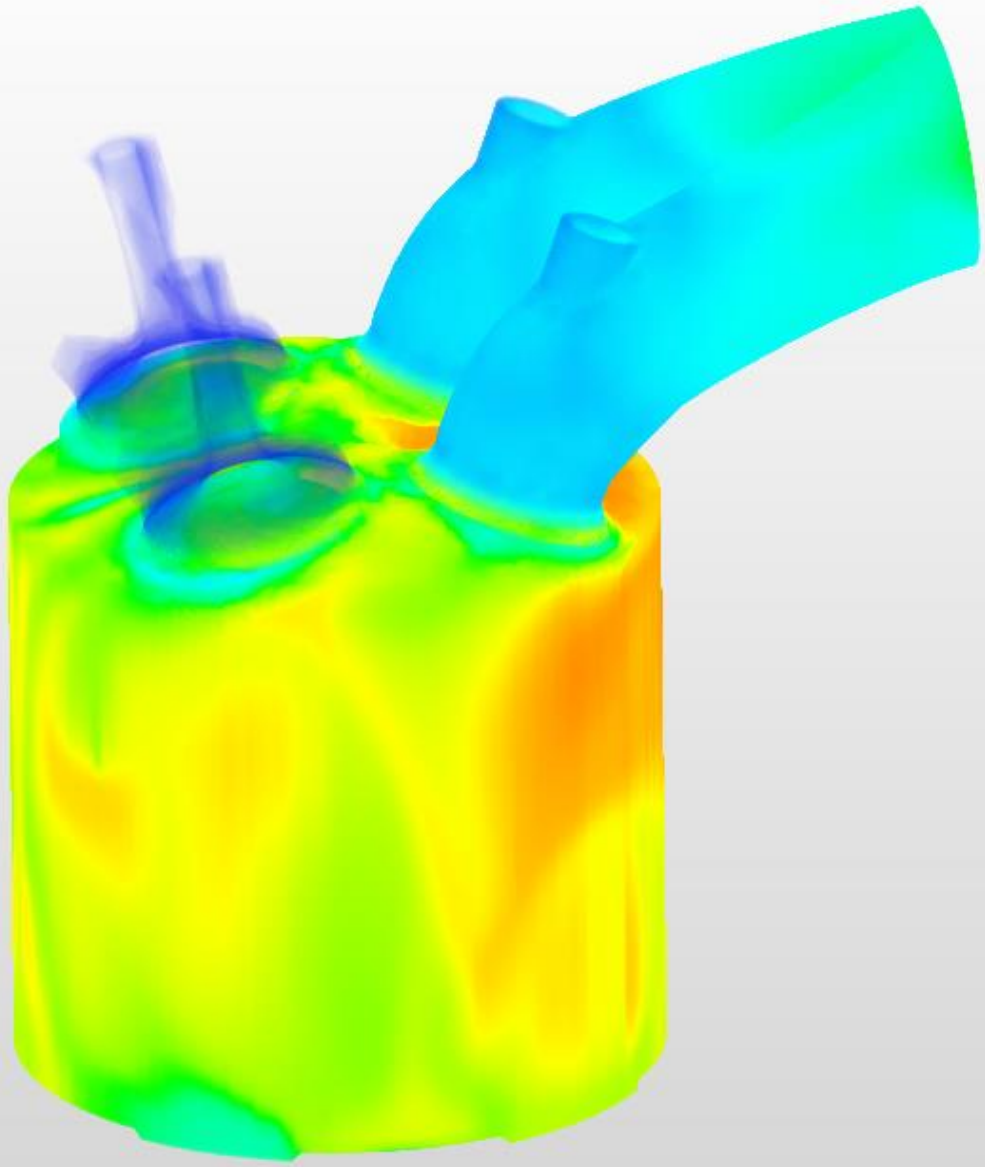

TU Delft Delft University of Technology

Challenge the future

This page is intentionally left blank

The Challenges and Opportunities of a Hydrogen Internal Combustion Engine

by

E.C. Peeters

4547322

to obtain the degree of Master of Science

at the Delft University of Technology

Supervisor: Ir. J.A. Melkert
Advisor: Prof. Dr. Ir. L.L.M. Veldhuis

TU Delft

Preface

This Master's thesis gains insights into the challenges and opportunities of a hydrogen internal combustion engine. It is a continuation of the effort of the collaboration between the Delft University of Technology, Deltion College and the Dutch Electric Aviation Centre (DEAC) to built a flying testbed for sustainable aviation.

I would like to thank my supervisor Joris Melkert and advisor Leo Veldhuis for their supervision, support and feedback. I would also like to thank Kees, Maritte and Stijn for their input, feedback and support.

Erik Peeters
Delft, January 2022

Contents

List of Symbols and Abbreviations

Greek symbol	Meaning
α_T	Turbulent thermal diffusivity
Γ	Reynolds stress
$\overline{\epsilon}$	Dissipation rate of the turbulent kinetic energy
η	Efficiency
$\tilde{\kappa}$	Favre mean flame front curvature
λ	Thermal conductivity
$\overline{\lambda}$	Turbulent thermal conductivity
ρ	Density
$\overline{\dot{\rho}}_k^c$	Source term due to chemical reaction
$\overline{\dot{\rho}}_k^s$	Source term due to spray evaporation
$\overline{\sigma}$	Viscous shear stress
ϕ	Equivalence ratio

Roman symbol	Meaning
A_p	Piston area
c_p	Heat capacity
D	Mixture-averaged molecular diffusion coefficient
D_T	Turbulent diffusivity
F	Force
$\overline{\mathbf{F}}^{\mathbf{s}}$	Rate of momentum gain per unit volume
g	specific body force
h_k	specific enthalpy of species k
I	Identity tensor
J	Heat flux vector
k	Species index
$\overline{k}$	Turbulent kinetic energy
K	Total number of species
l	specific internal energy
p	Pressure
Pr_T	Turbulent Prandtl number
$\dot{Q}_c$	Source term due to chemical heat release
$\dot{Q}_s$	Source term due to spray interactions
$\dot{Q_{spk}}$	Electrical energy discharge rate
r_k	Kernel radius
S_T	Turbulent flame speed
Sc_T	Turbulent Schmidt number
u	Flow velocity vector
v	Laminar kinematic viscosity
v_T	Turbulent kinematic viscosity
V	Volume
W	Work
y_k	Mass fraction of species k

Abbreviation	Meaning
BDC	Bottom Dead Centre
BTDC	Before Top Dead Centre
CFD	Computational Fluid Dynamics
CNG	Compressed Natural Gas
COVID	Coronavirus Disease
DEAC	Dutch Electric Aviation Centre
DOC	Diesel Oxidation Catalyst
DPF	Diesel Particulate Filter
EGR	Exhaust Gas Recirculation
HCCI	Homogeneous Charge Compression Ignition
ICE	Internal Combustion Engine
LPG	Liquefied Petroleum Gas
MON	Motor Octane Number
NO_x	Nitrogen oxides
NTP	Non-Thermal Plasma
PLIF	Planar Laser-Induced Fluorescence
RANS	Reynolds Averaged Navier-Stokes
RON	Research Octane Number
RPM	Revolutions per minute
SCR	Selective Catalyst Reduction
SOI	Start Of Injection
TDC	Top Dead Centre
TWC	Three Way Catalyst

Executive Summary

With the intention to set the first step on the path to sustainable aviation, the TU Delft, the Dutch Electric Aviation Centre (DEAC) and Deltion College have partnered up with the aim to convert a Cessna 337F Skymaster into a flying testbed. One of the goals of this project is to investigate the possibility of converting one of its engines to be run on hydrogen instead of aviation gasoline. Before that can happen though, experiments to asses the safety and viability will be performed on the ground, in a purposely designed test cell. This thesis work is performed in preparation to those engine tests.

Prior to this thesis, a literature study was performed into the challenges of hydrogen internal combustion engines. In this work, the knowledge gained from that study is combined with a CFD study to make recommendations for the conversion of a Lycoming aircraft engine and to gain insights on the challenges and opportunities of hydrogen internal combustion engines.

During this CFD investigation, which is performed using ANSYS Forte, it is found that due to hydrogen's high flame speed, combustion can be very fast and quite severe, resulting in high pressure peaks and low thermal efficiencies. It has, however, been found that by optimising the hydrogen injection, combustion can be slowed down, resulting in lower pressure peaks, lower NO_x emissions and higher power outputs. Additionally, the effects of equivalence ratio, spark timing and indirect vs. direct hydrogen injection on the performance of the engine are investigated. It is found that lower equivalence ratios will result in higher thermal efficiencies, but lower power outputs. Higher equivalence ratios will result in higher NO_x emissions, but this can be mitigated using optimised hydrogen injection. Higher equivalence ratios can also lead to abnormal combustion phenomena such as pre-ignition and knock, so great care must be taken if such equivalence ratios are used. The spark timing can be optimised for different performance parameters, and this should be done for each individual equivalence ratio and engine condition. It is also found that in order to meet the power requirements of an aircraft engine, direct injection should be employed, as indirect injection incurs too high volumetric losses.

The combustion processes of gasoline and hydrogen are compared, where it can be seen that combustion in gasoline happens much slower and much less severe than for hydrogen. It is also observed that using direct and optimised injection, the performance of a gasoline internal combustion engine can be matched using hydrogen. The CFD model is verified and validated, where it is found that the hydrogen flow inside the combustion chamber is highly dependent on the mesh refinement and geometry. As the results of the optimised injection engine cycles depend highly on the hydrogen flow, it is concluded that the CFD results in this work can only be used to inform future engine testing and not as predictive data or as a guide on how to obtain optimised injection. Since the next step in the project is to perform engine testing on a Lycoming IO-360-1AB6 engine, the ANSYS Forte engine model and the Lycoming engine are compared and the application of the knowledge gained in the CFD simulations on the Lycoming engine is discussed. From this, it is concluded that operating the Lycoming engine on hydrogen can be done safely, provided that certain modifications are applied and that great care is taken during every step of the process.

1 Introduction

The trend in aviation has always been one that goes up. Year after year, forecasts have been saying that for the foreseeable future, the aviation industry would grow with 5% per year [1]. The only thing these forecasts could not foresee was a global pandemic, such as the one that hit the world at the start of 2020. As a result, the world shut down and air traffic came almost to a complete halt. It is unknown how fast the aviation industry will be back at the level of 2019 and if the steady pre-COVID growth will return. But even if the annual pre-COVID growth is not met, the aviation industry is still a polluter and something has to be done to make aviation more sustainable.

With the intention to set the first step on the path to sustainable aviation, the Delft University of Technology, the Dutch Electric Aviation Centre (DEAC) and Deltion College have partnered up with the aim to convert a Cessna 337F Skymaster into a flying testbed. One option for this flying testbed, would be to replace one the engines of this aircraft with a hydrogen fuel cell and have that power the propeller through an electric motor. However, currently this is still a developing technology and the costs for both the fuel cell itself and the high purity hydrogen that is required for such a fuel cell are still very high. An alternative solution would be to keep the same engine, but convert it to run on hydrogen. This would be a less invasive and cheaper procedure, plus the hydrogen used in a hydrogen internal combustion engine does not have to be as pure as in a fuel cell and is thus considerably cheaper [2]. Converting existing internal combustion engines could thus be an intermediate step towards using fuel cells or it might even replace fuel cells as the end goal. With future improvements of hydrogen internal combustion engines, the difference in efficiency between fuel cells and hydrogen internal combustion engines might not be as big as is often thought. Delorme et al. [3] predict that in 2045, a hydrogen fuel cell vehicle will only be 9% more efficient than a hydrogen internal combustion engine vehicle.

This conversion from aviation gasoline to hydrogen brings a lot of challenges with it, but also opportunities. The aim of this thesis work is to provide insights into these challenges and opportunities, and to be a preparation for the engine tests that are planned to be performed on a Lycoming IO-360-1AB6 engine. In order to do so, a literature study [4] and computational fluid dynamics (CFD) analyses have been performed. The results of these efforts have been bundled into this report.

This thesis work starts with the research objective and with the research questions that will be answered in chapter 2. To give the reader a basic understanding of internal combustion engines, chapter 3 provides some technical background on internal combustion engines, after which some innovations are discussed that can make these engines more sustainable for the future. chapter 4 discusses abnormal combustion phenomena that might arise from the conversion to hydrogen and provides potential changes to the engine to account for these abnormal combustion phenomena and any other problems that can occur because of the conversion to hydrogen. An overview of the CFD set-up is provided in chapter 5, including the engine geometry, CFD models and meshing, boundary and initial conditions that were used. The results of the performed CFD simulations are discussed in chapter 6, after which verification and validation of the CFD models and simulations are performed in chapter 7. Because the next step in the project is engine testing on the Lycoming IO-360-1AB6 engine, chapter 8 provides a comparison between the Lycoming and the CFD engine and talks about modifications that have to be made to the Lycoming engine. Finally, conclusions about the work performed during this thesis are drawn in chapter 9 and recommendations for future research in general, and for the engine testing in particular are given in chapter 10.

2
Research Objective and Questions

2.1. Research Background and Objectives

The work presented in this thesis is part of a collaborative project by the Delft University of Technology, Deltion College and the Dutch Electric Aviation Centre (DEAC). The final objective of this project is to convert a Cessna 337F Skymaster into a flying testbed for sustainable aviation. This will entail converting one of its aviation gasoline fueled internal combustion engines to run on hydrogen. However, before any work on the Cessna can begin, ground tests will be performed on a Lycoming IO-360-1AB6 four-cylinder engine, to see if such a conversion will yield the hoped results and if operation of such an engine can be done safely. But before any real modifying can be done, the challenges surrounding such a conversion must be known. At the basis of this thesis work lies exactly that task; find out what the challenges are of converting an internal combustion engine to run on hydrogen, what potential solutions there are to these challenges and document whatever other information on hydrogen internal combustion engines might be useful for the eventual conversion process. A literature study has already been performed that looks into the challenges of a hydrogen internal combustion engine [4]. The objective for the thesis work presented here, is to find insights that might help with the conversion and with running the actual engine tests. In order to do this, CFD simulations will be performed and further research will be done.

2.2. Research Question

Can the insights on injection and spark timing gained from a CFD model of a four stroke hydrogen internal combustion engine be used to convert an aviation gasoline internal combustion engine to run on hydrogen and by doing so, can predictions be made on converting aviation gasoline internal combustion engines to hydrogen internal combustion engines on a larger scale?

2.3. Research Sub-questions

- What changes will have to be made to convert an aviation gasoline internal combustion engine to a hydrogen internal combustion engine?
- Can a CFD model be created that accurately models a hydrogen internal combustion engine?
- What are the performance differences between direct and indirect hydrogen injection for hydrogen internal combustion engines?
- How does the combustion cycle of a hydrogen internal combustion engine differ from a gasoline internal combustion engine?
- Can predictions on the safety of converting an internal combustion engine to run on hydrogen be made, based on CFD simulations?
- How do injection timing, spark timing and equivalence ratio affect the performance of a hydrogen internal combustion engine?
- Can optimised hydrogen injection be used to increase the performance of a hydrogen internal combustion engine?

3
Hydrogen Internal Combustion Engines - Background

This chapter aims to give the reader a basic understanding of internal combustion engines and provide an overview of some internal combustion engine innovations. The information in this chapter was largely taken from the literature study that preceded this thesis work, where more extensive explanations on the subjects covered in this chapter can be found [4].

3.1. Technical Background on Internal Combustion Engines

Since the invention of the internal combustion engine (ICE) in the 19th century, ICEs have come in many shapes and sizes. Because ICEs have such a wide range of applications, each with their own requirements, there is no one true internal combustion engine. Many pages could be spend explaining the fascinating differences between all of these engines, but as this section is merely meant to provide some technical background needed for the reader to better understand the work presented in this thesis, only a small part of the spectrum of ICEs is discussed here.
The type of engine discussed here is a reciprocating engine. A reciprocating engine is an engine in which the piston reciprocates back and forth within the cylinder. The piston is mechanically linked to a rotating crankshaft that can be used to drive wheels, propellers or even a generator. The engine can consist of one cylinder or more cylinders, which can be arranged differently, depending on the application. Figure 3.1 shows some possible cylinder lay-outs.

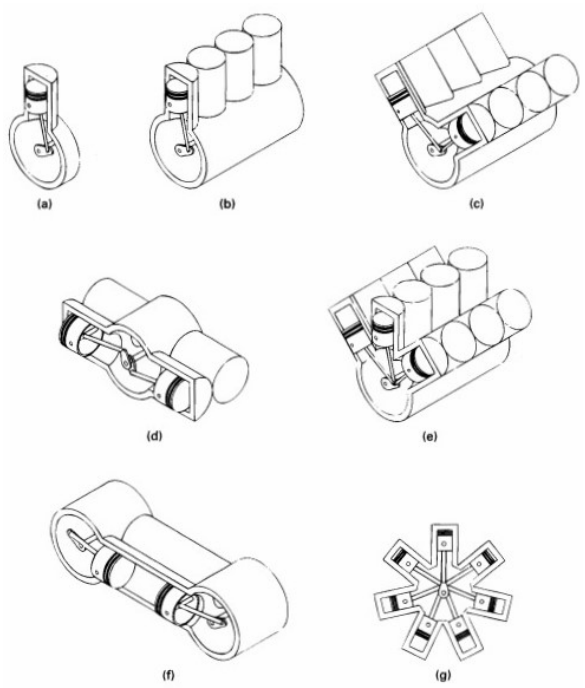

Figure 3.1: Different cylinder arrangements: **a)** single cylinder **b)** in-line or straight **c)** V lay-out **d)** flat engine or opposed cylinder **e)** W lay-out **f)** opposed pistons **g)** radial engine [5]

In this thesis, the internal combustion engine will be discussed on the cylinder level, so not much attention will be given to the actual lay-out of the engine. It is, however, good to note that the engines that will be featured in the project that this thesis work is a part of, will be either single cylinder or opposed cylinder engines.

One of the distinctions that can be made when looking at internal combustion engines, is the number of strokes that the piston makes per engine cycle; either two strokes or four strokes. Two stroke engines are often less complex and lighter than four stroke engines and are mostly used for smaller vehicles, such as mopeds, scooters, or as an outboard motor for a boat. Bigger and heavier vehicles almost always use a four stroke engine, though there have been some examples of two stroke engine cars in the past. All of the engines considered in this thesis work will be four stroke engines. So how does a four stroke engine work? Figure 3.2 shows an example of one engine cycle of a spark ignition, four stroke engine with external fuel mixture. Later on, different configurations will be discussed and explained.

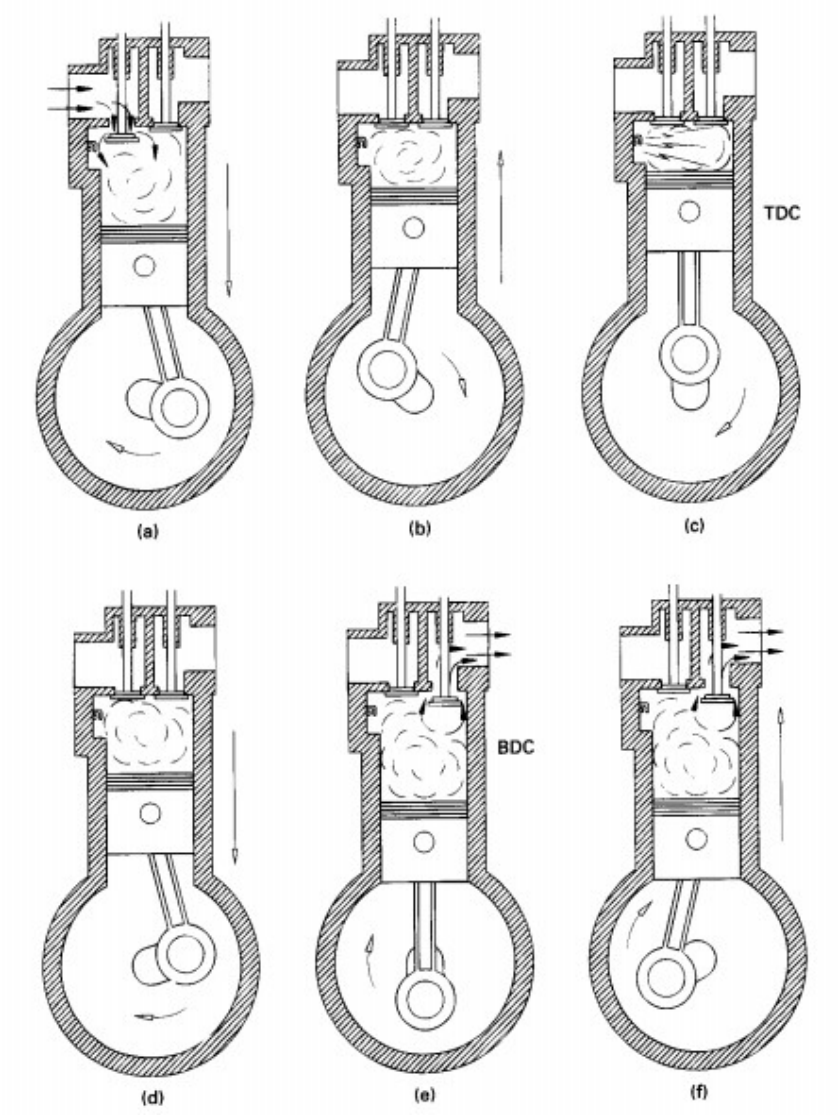

Figure 3.2: Graphical representation of an engine cycle: **a)** Intake stroke **b)** Compression stroke **c)** Combustion **d)** Expansion or power stroke **e)** and **f)** Exhaust stroke [5]

Because it is a cycle, the starting point is of course arbitrary, but let's start at the intake stroke. As can be seen in the drawing, the intake valve is open, which means that when the piston moves down, air is sucked into the cylinder. In this example engine, the fuel and the air are mixed outside the cylinder, so what is coming in during the intake stroke is actually a mixture of fuel and air. The different mixture and injection techniques will be discussed later. Once the piston starts to move up again, the intake valve will be closed and the mixture in the cylinder is compressed. The position where the piston is at its highest point is called

'top dead centre' (TDC). Close to TDC, a spark will be fired that ignites the mixture in the cylinder. The combustion that follows pushes the piston down in what is called the expansion or power stroke. This is actually when the chemical energy of the fuel mixture is delivered to the crankshaft as power. Once the piston reaches the bottom point, which is called 'bottom dead centre' (BDC), the exhaust valve is opened and as the piston moves up, the combusted mixture is pushed out. Once the piston reaches to top, the intake valve is opened and the cycle starts again.

In this report, the position of the piston is often discussed in terms of a certain number of degrees before or after a certain point. For instance, in many of the simulations, the spark plug is fired at '5 degrees BTDC'. To fully understand this report, it is important to understand what this means. The degrees that are mentioned here, relate to the rotation of the crank shaft. One full rotation of the crank shaft is 360 degrees and since the location of the piston is directly related to the rotation of the crank shaft, the location of the piston is expressed in terms of the crank angle. This way of expressing the position of the piston has its benefits over other potential methods (such as for instance expressing it as a percentage of the total volume or as the actual position of the piston in coordinates or in its height). The benefits stem from the fact that the piston is at the same height twice per full crank shaft location. If you were therefore to express its position solely in terms of the height of the piston, you would have two heights per crank shaft rotation that are the same, without placing them at their respective moments in time. By expressing the position of the piston in terms of the crank angle, you know exactly about which point in time you are talking. The '5 degrees BTDC' therefore, mean that the crank angle is 5 degrees removed from the position where the piston is at its highest point and is therefore at 5 degrees before top dead centre (BTDC).

As stated before, this is just an example of the engine cycle of one particular engine. Within the realm of four stroke engines, there are many variations on this, but what stays the same is that that there are four strokes; intake, compression, power/expansion and exhaust. The following is a breakdown of the different features and aspects of different four strokes engines.

3.1.1. Fuel Injection/Mixing

The first aspect where not all four stroke engines are the same, is the way the fuel is injected/mixed. The goal of the fuel system is to have the fuel mixed with the air in the combustion chamber at the moment when ignition happens. The mixing of the air and fuel can either be done inside the cylinder, or outside the cylinder. Let's start with the latter.

Carburettor

One of the options of mixing the fuel with the air is the use of a carburettor. A carburettor is a device that regulates the airflow going to the cylinders, but also mixes in the fuel with the airflow. The carburettor contains a venturi tube, which accelerates the flow and reduces the static pressure of the flow. At the point where the static pressure is lowest, the fuel is exposed to the flow and because of the pressure differential, the fuel will be sucked in and mixed with the flow. Usually, more than one cylinder will be attached to a carburettor, meaning that the carburettor provides the air-fuel mixture for more than one cylinder. Carburettors used to be very common as a fuel delivery system, but have been replaced more and more by injection. This is because of several reasons, some of which are the stated below.

As the mixture is travelling from the carburettor to the combustion chamber, it is still mixing. As a result, the equivalence ratio per cylinder, in a system where multiple cylinders are attached to the same carburettor, will vary. Some cylinders will therefore operate less efficiently.

Because the hydrogen and air have already been mixed before reaching the combustion chamber, the mixture that enters the combustion chamber is highly flammable. Hot spots in the engine can ignite this mixture upon entry and because the intake valve is open at this point in time, the engine could backfire (for more on backfire see subsection 4.1.2).

External Injection

Injection outside the combustion chamber takes place in the inlet manifold and is often referred to as port fuel injection or inlet manifold injection, depending on the timing. The inlet manifold is located directly before the intake valve. A fuel injector is situated here that either continuously injects fuel into the manifold, or injects it at a specified point in the engine cycle. In some engines, the fuel is sprayed directly onto the back of the intake valves. The hot surface then helps mix the fuel with the air. The timing of the fuel injection can vary, from anytime before the intake valve opens, right up until the intake valve closes again. If injection takes place when the intake valve is closed, this is referred to as inlet manifold fuel injection. If the valve is open, it is called port fuel injection. Figure 3.3 shows a schematic of both external and internal injection.

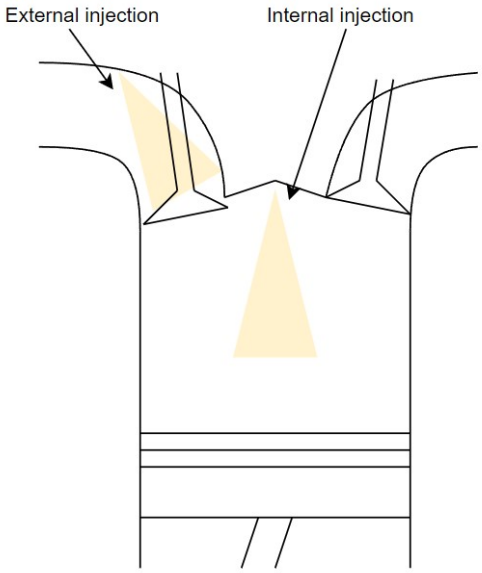

Figure 3.3: Schematic of external and internal injection

The major drawback of using inlet manifold injection is similar to that of using a carburettor; the risk of backfire. As the hydrogen is injected when the intake valve is closed, a combustible mixture is formed in the inlet manifold. When this mixture enters the combustion chamber, it could auto-ignite on any of the hot spots in the combustion chamber. At this point, there will still be some combustible mixture in the inlet manifold which could combust, resulting in backfire. The risk of backfire is much lower with port injection, as the fuel is injected at the same time as the air flows into the cylinder, so almost no combustible mixture is formed in the inlet manifold.

Internal Injection

The fuel can also be added in the combustion chamber itself, again with the use of a fuel injector. The fuel is now added sometime during the combustion stroke. This means that the pressure in the cylinder is rising, so the injection pressure has to be quite high. This means that the so-called direct injection system is often more complex than a port injection system.

A problem that might arise with internal injection is the inhomogeneous mixture that results. The fuel is injected at a later stage in the engine cycle and the air is already in the combustion chamber, so there is both less time to mix and the mixture will be less turbulent, reducing the mixing rate. Instinctively, this is a drawback, as a less homogeneous mixture can lead to a less efficient combustion. On top of that, if the fuel is located near the wall liner and far away from the spark plug, the fuel mixture may not ignite properly and a misfire might occur. However, if done strategically, creating a far from homogeneous mixture in the combustion chamber can have some positive effects on the engine performance, as will be discussed later on.

Because the injector is located inside the combustion chamber, it has to be able to deal with the high temperatures that result from the combustion. This might mean that injectors will have to be manufactured out of different materials than traditional injectors.

Direct injection also has a couple of benefits. Because the intake valve is closed when the fuel is injected, there is no chance for the engine to backfire. Additionally, because injection happens when all of the air is already in the cylinder, there are no volumetric losses. Volumetric losses occur when a carburettor or port injector is used. When the fuel is added to the air, it replaces part of the volume that air took up before. Therefore, there is less oxygen in the combustion chamber. This is especially a problem for hydrogen, because hydrogen is less dense than aviation gasoline. In a stoichiometric hydrogen-air mixture, hydrogen takes up 30% of the total volume, whereas aviation gasoline only takes up 2% [6]. With direct injection, all the air is already in the combustion chamber when the hydrogen is injected, so this problem is negated.

Injection Mechanism

Depending on the timing and the location of injection, the injection process can become quite complicated. However, the basic principle is simple; the injector should deliver the fuel in a controlled manner, at the specified time and at the specified pressure or fuel flow. To do so, many different techniques have been used over the years. Figure 3.4 shows an example of a more recent fuel injector, a modified natural gas, piezoelectric injector.

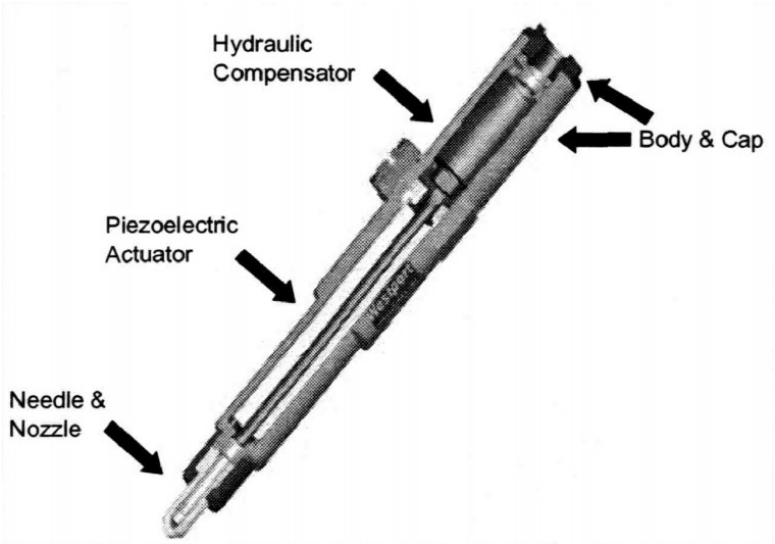

Figure 3.4: Example of a piezoelectric injector [7]

The basic principle of most fuel injectors is the same; the nozzle of the injector is closed off and is opened by activating the injector. The nozzle can be closed off in many different ways, such as a ball, a needle, a reed or a flat disc. For this explanation, we will assume that a needle is used, but later on, other types of injectors are discussed as well.

The needle that is closing off the nozzle, is usually pushed down by a spring, so that when the injector is not activated, the needle closes off the nozzle and no fuel is passed through. Once the needle is lifted, fuel can pass on by. The lifting of the needle can be done using a solenoid coil, which when charged produces a magnetic field and lifts the needle, or the needle can be lifted using a piezoelectric actuator. A piezoelectric actuator makes use of the piezoelectric effect, where a material changes dimensions when a voltage is applied. The benefit of using a piezoelectric actuator like in Figure 3.4 is that the movement of the needle can be controlled very precisely, which means that the fuel flow can also be controlled very precisely.

In a multiple cylinder, direct injection engine, a common rail is used to deliver the fuel to the injectors. A common rail is basically a pressure vessel that is attached to all of the injectors. In this way, the injectors are always supplied with a constant pressure, which is especially important for direct injection, because the injection pressure needs to be very high.

3.1.2. Ignition

Two types of ignition can be distinguished in internal combustion engines; compression ignition and spark ignition. An example of a compression ignition engine is a diesel engine, where the fuel mixture is ignited by the elevated temperature caused by mechanical compression. For a compression ignition engine, the choice for the correct fuel is crucial. Because there is no spark to ignite the fuel at the exact moment you want, you need a fuel that will auto-ignite at the correct timing in the engine cycle. In a compression ignition engine, only air is compressed during the compression stroke. Right at the end of the compression stroke, the fuel is injected, which, due to the high pressure and temperature in the combustion chamber, will ignite spontaneously. The moment at which the fuel combusts is determined by the ignition delay, which is a fuel specific property.

In a spark ignition engine, the fuel mixture is ignited by a spark. The spark timing of the engine is an important parameter that needs to be optimised per engine and per fuel type. The spark plug is fired before TDC. This is because of the ignition delay of the fuel mixture. Time it later, and the piston will have moved down already, decreasing the potential work that can be done, while also decreasing the pressure in the chamber. If the spark comes too early, combustion will happen when the piston is still moving up. In this situation, the movement of the piston and the force of the combustion are opposite, which of course should not happen. The exact timing of the spark is dependent on the geometry of the cylinder, the state of the fuel mixture and the type of fuel.

3.2. Internal Combustion Engine Innovations

Now that the basic workings of internal combustion engines are clear, it is time to look at innovations that can make internal combustion engines cleaner and more sustainable for the future. In this section, a couple of potential innovations are highlighted. It must be noted that this list is far from complete and that the innovations listed here are limited to those that can be applied to internal combustion engines. It would also be possible to replace the internal combustion engine all together and that might very well be where the future is headed, but that falls outside the scope of this project. It must also be noted that the innovations proposed here are not exclusive; an internal combustion engine could both be run on a different fuel and be fitted with an exhaust after-treatment device at the same time.

Homogeneous charge compression ignition (HCCI)

Homogeneous charge compression ignition (HCCI) combines the techniques used in both spark ignition and diesel engines to create an engine that has the fuel efficiency of a diesel engine, but with very low NO_x emissions and no soot production [8, 9]. The principle behind this type of engine is as follows. First, a nearly homogeneous fuel mixture is introduced in the combustion chamber. After the intake valve is closed, the mixture is compressed. This results in pressure and temperature rises and at some point, the fuel mixture will auto-ignite. Due to the lower peak temperatures, the NO_x emissions are almost negligible and because of the high compression ratios, the fuel efficiency can be as much as 30% higher than in a gasoline spark ignition engine [9]. The idea of a HCCI engine has been around for a long time, but it has not yet been widely implemented. One of the reasons for this is that a HCCI engine "does not offer precise control over the start of combustion across wide range of engine speeds and loads." [10]. In spark ignition engines, the start of combustion is (in normal combustion) determined by the spark timing, while in a compression ignition engine, the start of combustion is determined by the injection timing. Different options have been proposed to control the ignition timing in a HCCI engine, some of which are:

- **Exhaust Gas Recirculation** (EGR) is used to dilute the air-fuel mixture in the combustion chamber. This results in a retarded combustion timing, which in turn results in higher obtainable pressures and thus higher engine loads [11].
- **Multiple fuel stratification** can be used to vary the combustion timing in a HCCI engine. By mixing fuels with different octane numbers, the combustion timing can be controlled.
- Varying the **inlet temperature** has a strong effect on the combustion timing in a HCCI engine [12]. Increasing the inlet temperature significantly advances the combustion timing and of course, a lower

inlet temperature means retarded combustion timing.
- Another strong influence on the combustion timing in a HCCI engine is the **compression ratio**. Christensen et al. [13] found that, irrespective of the fuel used, not only does the compression timing have a strong influence on the combustion timing, an increased compression ratio also decreases the necessary intake temperature needed for HCCI to work.

Other downsides of HCCI are the full load restrictions due to pressure limits in the cylinder and potential issues with cold-starting the engine.

After-treatment technologies

With after-treatment, the engine exhaust gas is treated in such a way that the emissions are reduced. The two main forms of emission that are removed using after-treatment are NO_x emissions and particulate matter (PM) emissions. PM emissions consist of soot, unburned or partially burned hydrocarbon, or partially burnt lubricating oil [14]. For NO_x emissions, these are some of the after-treatment technologies:

- The **non-thermal plasma** (NTP) technique uses electricity to ionise the exhaust gas. The resulting plasma radicalises the oxygen, which converts NO to NO_2, which is then converted to N_2 using a catalyst [15]. This type of after-treatment works well in diminishing the emissions, but the energy consumption is quite high.
- In a **selective catalyst reduction** (SCR) system, NO_x is reacted to N_2 and H_2O using a catalyst and a reductant. The downsides of this technique are poor efficiency at lower temperatures and that the reductant needs refilling.
- In an NO_x **trap**, the emitted NO_x is literally trapped and is therefore not emitted to the environment. Although this method is cost effective, the major downside is the fact that at some point, no more NO_x can be adsorbed.

For the PM emissions, there are two main after-treatment methods; diesel oxidation catalyst (DOC) and diesel particulate filter (DPF). As the names suggest, these devices are mostly used on diesel engines, as the PM emissions of such engines are a lot higher than for gasoline internal combustion engines. A DOC converts CO and hydrocarbons to CO_2 and H_2O, whereas a DPF just filters the particles from the exhaust gasses.

Alternative fuels

The last innovation discussed in this report is the use of alternative fuels. Because this project focuses mainly on aviation applications, alternative fuels will in this case mean any other fuel than aviation gasoline.

Both Hosking [16] and Frijters [17] have performed trade-offs for alternative fuels that could be used in an aviation internal combustion engine. Their conclusions were very similar. For future implementations, both conclude that hydrogen is the alternative fuel with the most potential. Hosking does note that currently, liquefied petroleum gas (LPG) is still the best alternative fuel. However, once hydrogen production is scaled up, the availability will go up and the price will go down, and hydrogen will overtake LPG as most promising alternative fuel. This is mainly due to the low greenhouse gas emissions and the high energy density of hydrogen.

4
Creating a Hydrogen Internal Combustion Engine

In order to create a hydrogen internal combustion engine by converting a conventional internal combustion engine, various challenges must be addressed. In this chapter, some of these challenges will be discussed, mainly those pertaining to injection, ignition and equivalence ratio. After this, some of the hydrogen specific changes that can be applied to an engine, to fix these problems, will be talked about. The information in this chapter was largely taken from the literature study that preceded this thesis work, where more extensive explanations on the subjects covered in this chapter can be found [4].

4.1. Abnormal Combustion Phenomena in Hydrogen Internal Combustion Engines

Several abnormal combustion phenomena can occur during the combustion of hydrogen inside an internal combustion engine. Three of these, preignition, knock and backfire are discussed in this section.

4.1.1. Preignition and Knock

Preignition and knock are both events where the mixture in the combustion chamber ignites without the presence of a spark from the spark plug. Some sources use the two terms interchangeably [18–21], while others make clear distinctions between the two [22]. White et al. acknowledge that the difference between preignition and knock is almost indistinguishable, but that they should nevertheless be separated, because the 'controlling phenomena' are different. In this study, the two will also be treated separately in their respective explanations, but might be used interchangeably after.

Preignition describes the event where the mixture in the combustion chamber ignites prior to spark discharge. This ignition usually occurs on a hot spot in the engine, such as a spark plug or a valve surface. Hydrogen has a very high autoignition temperature in air of 858 K [22]. However, a hydrogen-air mixture also has a much lower minimum ignition energy than hydrocarbon-air mixtures. This means that, although hydrogen is not well suited to be used in a compression ignition engine because of the high auto-ignition temperature, some preignition can be expected based on the low minimum ignition energy.

When preignition occurs, combustion is advanced and there will be an increased chemical heat release rate. This will result in a rapid pressure rise, higher peak cylinder pressure and higher in-cylinder temperatures. These higher temperatures can advance the start of combustion even more, resulting in a runaway effect, which could lead to engine failure.

As can be seen from Figure 4.1, the minimum ignition energy of a hydrogen-air mixture is highly dependent on the equivalence ratio of that mixture. It can be seen that approaching a stoichiometric mixture ($\phi = 1$) from the lean side, the curve is quite steep, resulting in the lowest minimum ignition energy right around that stoichiometric condition. This means that it is very hard to operate a hydrogen internal combustion engine at stoichiometric conditions without experiencing preignition.

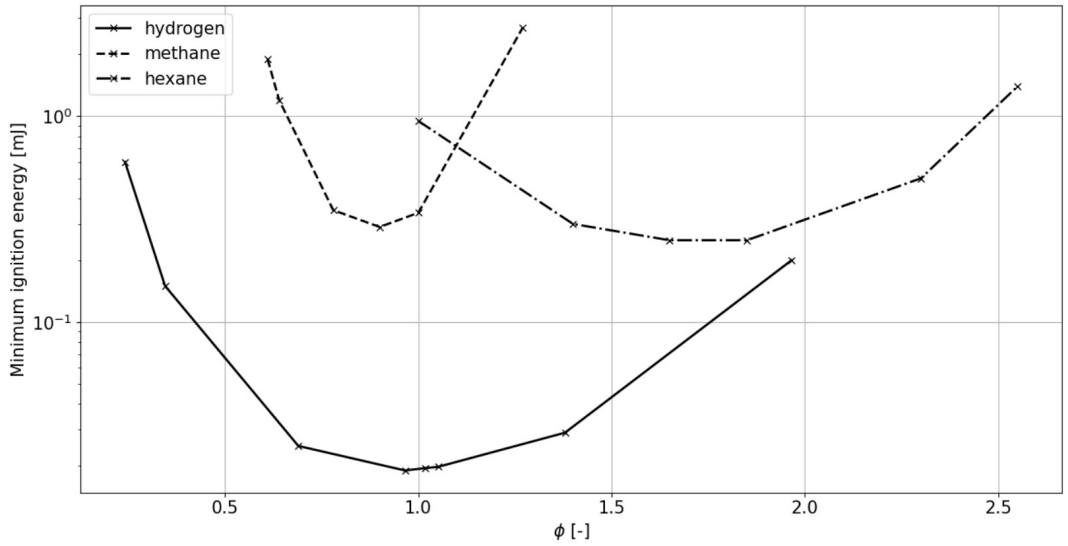

Figure 4.1: Minimum ignition energies for hydrogen-air, methane-air and hexane-air vs. the equivalence ratio [23]

Knocking can in a way be seen as a form of preignition, but where preignition is just defined as any event where the mixture in the combustion chamber ignites prior to spark discharge, knock is actually the autoignition of the mixture ahead of the flame front that originated from the spark. Knock can be somewhat controlled by retarding the spark timing [19], but is mostly a function of the compression ratio and as such puts a limit on the maximum compression ratio of the cylinder.

Experiments have been done to show the effects that various engine parameters have on the presence of knock in hydrogen internal combustion engines [21]. Figure 4.2 shows an example of the lean and rich knocking limits for a hydrogen internal combustion engine. In this work, the focus is put on the lean limit. The rich side of the spectrum might also have a knock-free zone, but is not beneficial for other factors that will be discussed later in this report. On the lean side, it can be seen that with increasing compression ratio, the highest knock-free equivalence ratio decreases. A higher intake temperature also decreases the knock limit. This makes sense, as a higher intake temperature will increase the combustion chamber temperature, which means that the mixture is more prone to autoignite.

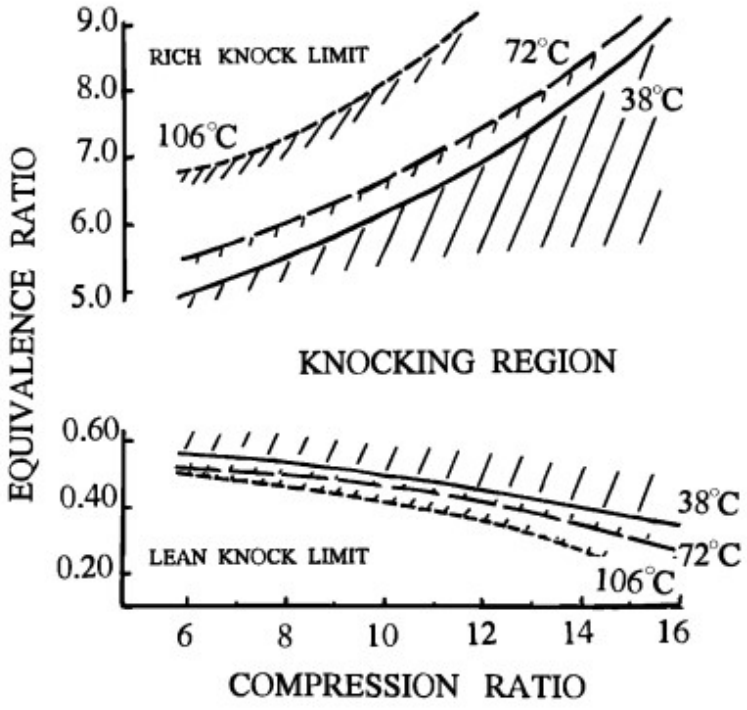

Figure 4.2: An example of the experimentally determined rich and lean knock limits for unthrottled hydrogen operation, at three different intake temperatures and at 900 RPM [21]

At this point it has to be noted the knocking limit is a very engine specific characteristic. To illustrate this point, let's look at the results from a different experiment shown in Figure 4.3 and Figure 4.4. These results were found by Sadiq Al-Baghdad [18] using a computer model of a hydrogen internal combustion engine.

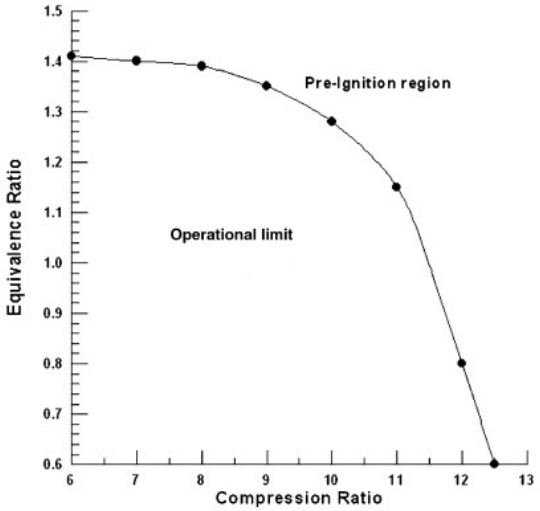

Figure 4.3: Example of the preignition/knocking limit for the combination of equivalence ratio and compression ratio [18]

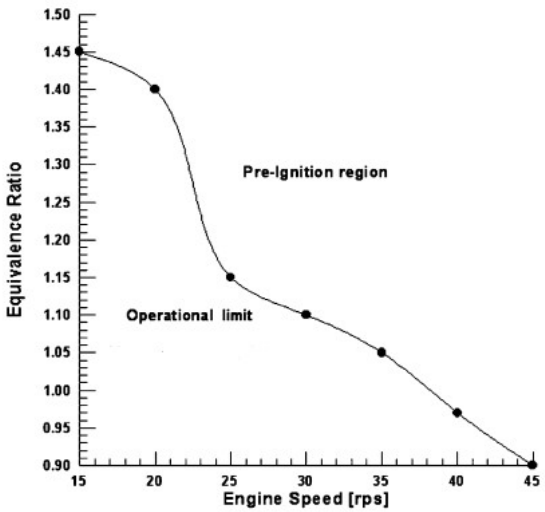

Figure 4.4: Example of the preignition/knocking limit for the combination of equivalence ratio and engine speed [18]

In the left figure, the same trend can be seen as in Figure 4.2, where and increase in compression ratio means a decrease in equivalence ratio. However, although the trend is similar, the values are quite different. In Figure 4.3, the maximum equivalence ratio is about 1.4, where it is only 0.6 in Figure 4.2. There are several reasons why this could be the case. First of all, these are two different engines with two different lay-outs. As stated before, knock is an engine specific phenomenon, so even if all other parameters were the same, two different engines would still display different knocking behaviours. Secondly, as we have seen from Figure 4.2, the intake temperature has quite some influence on the knocking limit. The intake

temperature is not stated for Figure 4.3, but it could well be much lower than for the other engine, especially if the hydrogen has been stored in cryogenic tanks. Lastly, we have to look at what the knocking limit even means in both of these graphs. The results that lead to Figure 4.2 were found experimentally, where the knocking limit was found by observation. The engine would start out in the knock-free region, from which point either the equivalence ratio or the compression ratio was increased until knock started to occur. The onset of knock would be marked by high frequency pressure oscillations, or by the characteristic knocking sound. In Figure 4.3 however, no such explanation is given of how the 'pre-ignition limit', as they call it, is found. Because the results were found using a model, there will of course not be any knocking sounds to listen for. Given that other sources also give an equivalence ratio of about 0.6 as the limit for knock and preignition [19, 24], it must be concluded that although the behaviour shown in Figure 4.3 makes sense, it underestimates the onset of knocking for typical smaller hydrogen internal combustion engines that are looked at in this report.

This brings us to Figure 4.4. This graph originates from the same report that was just concluded to underestimate the onset of knock, but it does show a very interesting relation between knock and the engine speed. Disregarding the actual numbers, Figure 4.4 shows that increasing the engine speed will also increase the chance of knock occurring in the engine. This means that even if the engine is running at an equivalence ratio and compression rate that should not warrant knock, a high engine speed could still bring the engine into knocking territory.

4.1.2. Backfire

Backfire or backflash is a premature auto-ignition event, where the flame propagates back into the intake manifold. When a carburettor or inlet manifold injector is used, a flammable mixture is already formed before it enters the combustion chamber. Once the intake valve is open, there will be a point in time when some of the fuel mixture is in the combustion chamber, and some of it is still in the intake manifold. If at this point the fuel mixture in the combustion chamber auto-ignites, the flame might travel back into the intake manifold as well. Because hydrogen has a small ignition delay and a high flame speed compared to fuels such as gasoline and diesel [20], the chances of a backfire event happening, increase when converting an internal combustion engine to run on hydrogen. This is because the intake valve now has a shorter time to close before the flame reaches the intake manifold. Another reason backfire is more likely to happen in a hydrogen internal combustion engine is the small quenching distance of hydrogen. This small quenching distance means effectively that the flame gets closer to the wall of the combustion chamber, which means an increased heat transfer to the walls, which results in higher wall temperatures. This increases the chance of auto-ignition happening at the combustion chamber wall and thus increases the chance of backfire happening.

Because backfire happens when the fuel in the combustion chamber auto-ignites, it is interesting to know at which conditions the mixtures auto-ignites. If these conditions are known, measures can be taken to prevent backfire from happening. Surface ignition is the most likely source for auto-ignition, and it is advised to keep the temperatures of hot spots in the combustion chamber below 900 $^{\circ}C$ [25] during the intake stroke. The two hottest components in the combustion chamber during the intake stroke are the spark plug and the exhaust valve. Possible ways to keep the temperatures of these two components below 900 $^{\circ}C$ is using cold-rated spark plugs and cooled exhaust valves.

Backfire depends on the geometry of the engine, so not only on the geometry of the combustion chamber, but also the geometry of the inlet manifold. It also depends on the equivalence ratio, the type of fuel, the compression ratio and the engine speed. Because the fuel has been mixed with the air before the inlet valve opens in engines with a carburettor and in engines with inlet manifold fuel injection, these two engine types are most susceptible to backfire. Port injection is less susceptible to backfire, because the hydrogen and air are not mixed as much before they reach the combustion chamber. Therefore, the amount of combustible mixture in the inlet manifold is much less, reducing the probability that backfire will occur. There is however only one way to fully eliminate the chance of backfire from happening, which is using direct injection. With direct injection, the inlet valve is closed when the fuel is injected, so even if the hydrogen-air mixture auto-ignites, there is no chance of the flame reaching the inlet manifold.

4.2. Hydrogen Specific Changes

One of the objectives of this work is to identify potential changes that need to be made in order to convert an aviation gasoline internal combustion engine to a hydrogen internal combustion engine. As such, a literature study has been performed to assess what areas of the engine need to be looked at [4]. Parts of that literature study have been used to create this section.

4.2.1. Injectors

One of the most important parts of the conversion of an internal combustion engine to run on hydrogen, but also one of the most researched parts, is the injection process. As discussed before, there are three main options for adding the fuel to the air; a carburettor, a port injector and a direct injector. In this section, only injection is considered, so the use of a carburettor is not discussed. Subsection 3.1.1 already discussed the basic workings of fuel injectors and this section will go into the hydrogen specific changes that need to be made to the fuel injectors to run the engine on hydrogen.

If one thing is clear from literature, it is that the engine can not be run on a standard, non-modified aviation gasoline injector. At least, it can not be run effectively and for longer periods of time. This is because of two properties of hydrogen; it's low volumetric energy density and the fact that hydrogen does not lubricate. As a result of hydrogen's low volumetric energy density, a lot of hydrogen, volume wise, needs to be injected into the combustion chamber. This means that the injector needs to be able to deal with this larger volume of fuel. The non-lubricant qualities of hydrogen mean that components will wear down sooner and as a result will break or stop functioning sooner. Both these problems need to be addressed when selecting an injector for a hydrogen internal combustion engine.

In this discussion, two types of injectors have to be distinguished; port injectors and direct injectors. Although the two challenges discussed above hold for both these types of injectors, the solutions might be different because of the two main differences between these two injectors; the fuel pressure and the maximum temperature that they have to endure.

A port injector is located in the inlet manifold of a cylinder, just outside the intake valve. Because of this location, the hydrogen can be injected at pressures between 3 and 6 bar [26] and the temperatures that the injector is subjected to are relatively low. With direct injection, injection will often happen late in the compression stroke. At this point, the pressure in the combustion chamber has risen significantly, which means that the fuel will have to be injected at a much higher pressure. Not only is the pressure of the air in the combustion chamber higher, but because of the late injection, the fuel has a lot less time to mix with the air. Therefore, a higher pressure is necessary, to still ensure adequate mixing. This can be seen very nicely in Figure 4.5 and Figure 4.6. These figures show the injection of hydrogen at the start of injection (SOI), 3 degrees after SOI and 17 degrees after SOI.

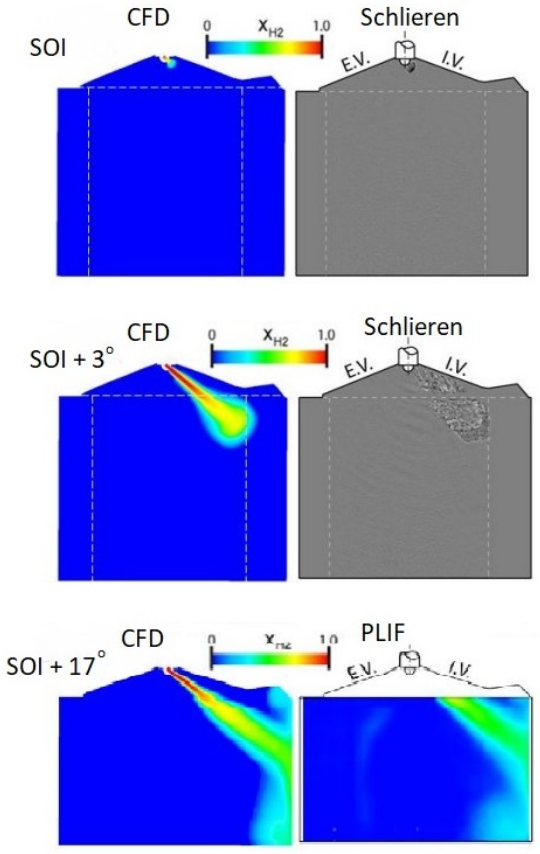

Figure 4.5: CFD, Schlieren and PLIF images of the combustion chamber at SOI, SOI + 3° and SOI + 17° at 25 bar [27]

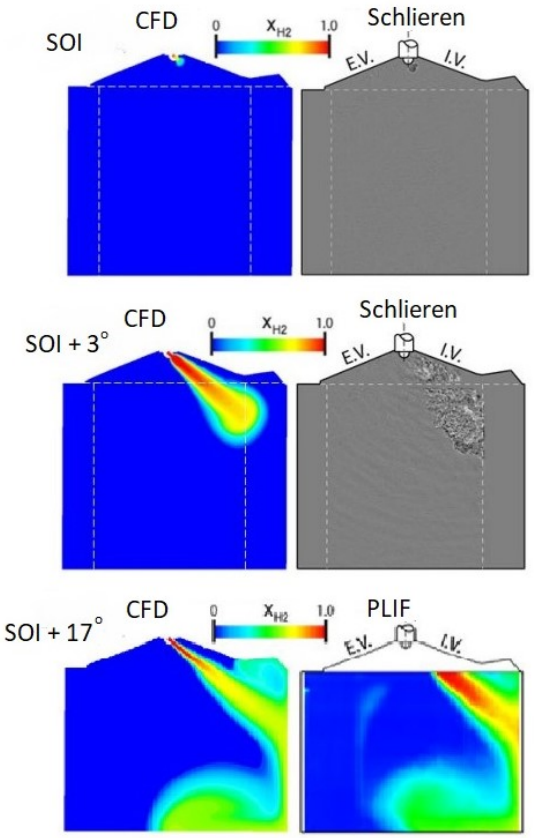

Figure 4.6: CFD, Schlieren and PLIF images of the combustion chamber at SOI, SOI + 3° and SOI + 17° at 100 bar [27]

Looking at the CFD pictures, it is clear that at 3 degrees after SOI, the hydrogen has advanced more into the combustion chamber in the 100 bar case than in the 25 bar case. The difference is even larger looking at 17 degrees after SOI. Figure 4.5 and Figure 4.6 not only show CFD results, they also show Schlieren and PLIF images. These images were obtained using an optical engine, an engine that has been altered such that the combustion chamber can be accessed by laser- and photographic equipment [27]. The exact methods behind obtaining the Schlieren images are not important for the purpose of this report and are very well documented elsewhere [28], but the technique is able to visualise the different densities of a transparent medium. For this reason, the otherwise transparent hydrogen can be visualised, because it has a different density than the air. As the hydrogen and air are mixed more and more, a homogeneous mixture results with similar densities everywhere, which is why the Schlieren technique only produces an interesting result at the start of injection, when you can still clearly see the boundaries between the injected hydrogen and the air. It can be seen that there is quite some resemblance between the CFD image and the Schlieren image.

The technique used to get the images at 17 degrees after SOI is the planar laser-induced fluorescence (PLIF) technique. In this technique, gaseous acetone is added to the hydrogen as a tracer. A laser is then used to excite the acetone that is mixed with the hydrogen. This will make the acetone fluoresce, which is then captured by a camera. It can again be seen that the flow pattern of the hydrogen in the CFD images resembles the flow pattern in the PLIF images quite well.

Depending on the air to fuel ratio of the hydrogen-air mixture, the adiabatic flame temperature of the hydrogen-air mixture ranges from 1300 to 2400 Kelvin [22]. As a result, the part of the direct injector that is inside the combustion chamber will have to be able to endure very high temperatures, something that the port injector does not have to do.

Fuel Flow Criteria

To show the volumetric problem that arises when trying to inject enough hydrogen, let's look at the chemical process of combusting hydrogen. Equation 4.1 shows the reaction equation for hydrogen with oxygen.

$$2H_2 + O_2 = 2H_2O \tag{4.1}$$

2 mole hydrogen react with 1 mole of oxygen and since air consists for 21% of O_2, to have a stoichiometric reaction with 2 mole of H_2, you need 4.762 mole of air. This means that the volumetric air to fuel ratio of a hydrogen-air mixture for stoichiometric reaction is 2.381:1. This means that in a stoichiometric hydrogen-air mixture, 29.57% of the volume is taken up by hydrogen. In contrast, for gasoline vapour, this value is about 2% [22]. Although a hydrogen internal combustion engine is usually run leaner than a gasoline internal combustion engine, to prevent knock and reduce NO_x emissions, the hydrogen that has to be injected still takes up a much larger volume than gasoline does.

Fortunately, hydrogen is not the only fuel with this problem. At stoichiometric conditions, compressed natural gas (CNG) takes up about 10% of the total volume of the fuel mixture. This is still less than for hydrogen, but it is so much more than gasoline, that special CNG injectors have been developed. Tests have been run to evaluate whether these CNG injectors can be used to inject hydrogen, and it was concluded that such injectors can indeed move a large enough quantity of hydrogen to be used in hydrogen internal combustion engines [29]. However, the injectors evaluated in this particular study were all port injectors, with injection pressures ranging from 1.7 to 13.7 bar. Because of these low injection pressures, these injectors are not suitable to be used in a direct injection engine. Port injection CNG injectors are readily available, but this is not the case for direct injection CNG injectors.

In literature, several experiments with a direct injection hydrogen internal combustion engine can be found. Throughout these experiments, several different approaches have been taken when it comes to the injector that is used. The only high pressure hydrogen injector that is being manufactured as of now is made by Westport Fuel Systems. The injector they developed [7] is used in multiple research papers [27, 30, 31], but it is still a work in progress and the injector itself is not yet commercially available. For other experiments, gasoline direct injectors were used, some without any modification [32], whereas others modified the injectors by removing the swirlers [33, 34].

External Injector Durability

As mentioned before, some durability issues may arise during operation of the injectors on hydrogen that should be taken into account. Hydrogen has no lubricating effect, which means that the parts of the injector that interact with hydrogen have no protection for when they touch other parts. When injecting gasoline, a small layer of oil will form on each of the surfaces it touches, which protects the surfaces and acts as a kind of buffer when two surfaces touch each other. Even with CNG, a small amount of compressor oil will be present, which is enough to also provide such a protective film. An example of the parts that need protection are the needle and the nozzle. Each time the injector is activated, which happens many times per second when the engine is running, the needle slides up and down the nozzle. With no protective film to keep the surfaces from touching, wear and tear will start to happen almost immediately, causing leakage of hydrogen and eventually causes the injector to stop working. For this reason, a standard gasoline or CNG injector can not be used in a hydrogen internal combustion engine for a longer duration without making modifications to it. Aleiferis and Rosati did in fact use an unmodified gasoline injector, but as they state themselves, it was "only due to the short running periods involved with optical engine operation that it was possible to adopt safely such a solution" [32]. The engine they used had modifications that allowed optical measurements to be taken in the combustion chamber. Because they did not run the engine for longer periods of time and not a large number of times, they could get away with using an unmodified gasoline injector, but for experiments with longer run-times and especially for real world applications, this is not an option.

Kabat and Heffel [35] have run tests on four different external hydrogen injectors, specifically looking at the durability of each of them. The experiment uses four different types of injectors and also tests four

different surface treatment on one of those injectors. Of the four different injectors, two will be discussed here; the one with four different surface treatments and a prototype injector that has no internal component rubbing/sliding.

The first injector is shown in Figure 4.7. This injector features a ball valve. The ball closes off the orifice that leads to the nozzle and is held in place by a spring, so that if the injector is not activated, the injector is closed. When the injector is activated, the armature is moved down by the magnetic field induced by the solenoid coil, moving the drive pin down and forcing the ball down as well. This will open the orifice and the hydrogen will flow through.

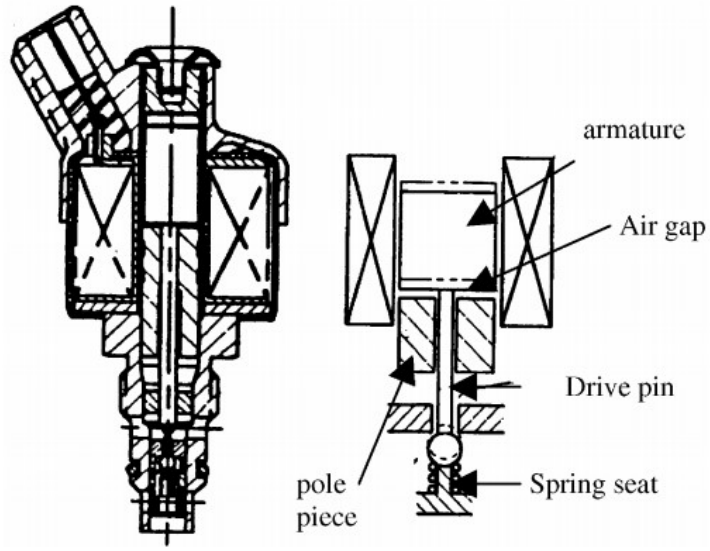

Figure 4.7: Ball valve injector used for durability testing [35]

In a CNG or gasoline internal combustion engine, the drive pin, ball and spring seat would all be lubricated by the respective fuel. However, in a hydrogen internal combustion engine, these components will touch each other without anything in between them to offer any protection. For this reason, four different variants of the injector shown in Figure 4.7 were created, each with its own surface treatment. The following four surface treatments were used:

1. A dry film lubricant containing the solid lubricants; molybdenum disulfide, graphite, and hexagonal boron nitride in a high temperature epoxy resin is sprayed on to the drivepin and seats.
2. A high temperature (800 K) silicon containing amorphous hydrogenated carbon was applied through a chemical vapour.
3. A two layer system was applied, consisting of silicon as a bottom layer with a carbon enriched layer on top.
4. Not a coating like the other three, but instead a surface treatment where nitrogen, carbon and oxygen are chemically diffused into the surface of the metals to create a case hardened compound layer.

One of the four injectors tested in the experiment by Kabat and Heffel was a prototype injector that can be seen in Figure 4.8. Where Figure 4.7 uses a ball to close the orifice, this injector uses a reed valve. This sounds trivial, but it is actually crucial here. Because of this reed, no moving parts are used in areas where there is hydrogen, which means no parts that can wear and tear due to the lack of lubricity of the hydrogen-air mixture.

In this injector, the flow path of the hydrogen is closed off by the reed. This reed is kept in place by the spring. When the injector is activated, the armature is lifted up by the magnetic field induced by the solenoid coil. The armature is connected to the reed, so when the armature is lifted, the reed is too. This opens up the flow path for the hydrogen. The hydrogen comes in contact with the reed, but the reed does not slide against anything. Instead, it closes off the flow annulus by laying flat on top of it.

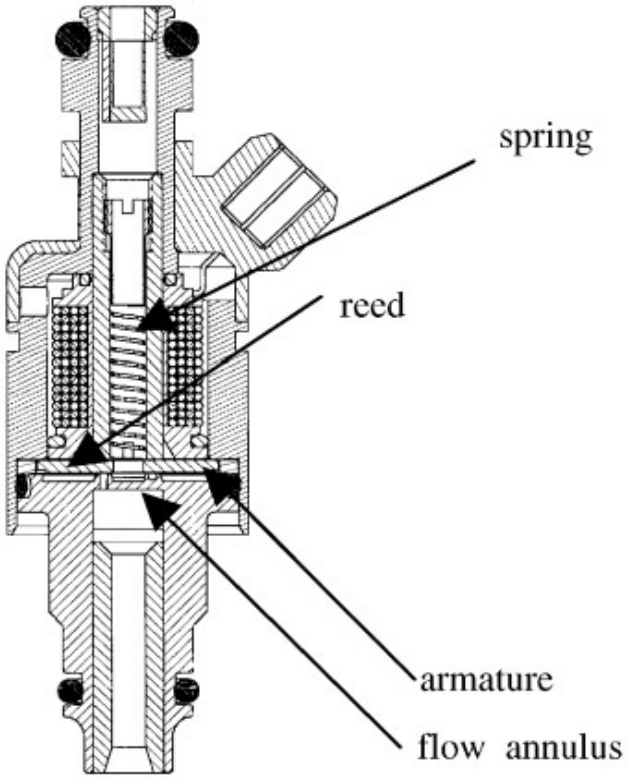

Figure 4.8: Reed valve injector used for durability testing [35]

All injectors were put through a series of tests with varying injection frequencies until they either failed or until they had run for 800 hours. The test with the unmodified ball valve injector was stopped after 75 hours, when five irregular injections had occurred. After examination, it was found that the curvature in the bottom of the drive pin was completely worn away. This is a great example of why just plugging in a regular CNG or gasoline injector will not work; an unmodified CNG injector that could have run for thousands of hours on CNG became defective after running only 75 hours on hydrogen. The first modification allowed the injector to complete the 800 hours of testing, which is already a huge improvement over the unmodified injector. However, upon inspection, the coating had worn away on most of the surfaces, which had already altered the injection behaviour of the injector. The third modification fared slightly better, but also here some wear could be spotted after 800 hours of running. Modifications 2. and 4. did not show any signs of wear and allowed the injector to run unaltered for 800 hours. This shows that coating certain parts of the injector can increase the lifespan of the injector dramatically and that all four surface treatments did so. It is, however, worth to note that not all surface treatments are created equal and that it is very beneficial for the performance of the injector to choose the type of surface treatment carefully. It should also be noted that the surface treatments did not significantly alter the flow performance of the injector.

During the 800 hours that the reed valve injector ran, no wear was introduced and the injector functioned flawlessly for the entire run-time. That no wear was introduced makes sense of course, because there are no parts to slide against each other or touch each other. It seems like the perfect solution; if you don't want parts to wear, have them not slide across other parts. Although this is of course true in theory, it has to be seen if this is actually the best solution. Although the injector performed well during this test, it is only a prototype injector without a proven record. It is also not readily available to buy. Therefore, it might be more feasible for now to modify injectors that are readily available and have been proven to work, also for longer periods of time.

Internal Injectors Durability

The injectors used in the experiments by Kabat and Heffel were all external injectors, meaning that the fuel is injected at relatively low pressures and that the injectors are exposed to only relatively low temperatures. For internal injection, both the injection pressure and the temperatures will be a lot higher. The problem presented here is that where there are many CNG injectors available for external injection, this is not the case for internal injectors. For internal injection, three options seem to be available in literature. The first option is to develop a high pressure hydrogen injector yourself [7, 36]. This requires a lot of prior knowledge, let alone a large amount of resources and time. However, the advantage is that developing an injector from the ground up lets you design an injector with the specific problems of high pressure hydrogen injection in mind, instead of trying to modify an existing injector. A nice example of this is the reed valve injector shown in Figure 4.8. The second option is to source a gasoline injector that is able to move enough volume to be used as a gas injector [33, 34]. The nice thing here is that there are many direct injection gasoline injectors available which are already designed for the conditions in the combustion engine. However, the injector will have to be modified to handle the durability issues that hydrogen presents. The last option is to source one of the very few high pressure hydrogen injectors that are available [27, 30, 31].

Both Welch et al. [7] and Yamane et al. [36] have developed high pressure hydrogen injectors. These injectors can be seen in Figure 4.9 and Figure 4.10 and will be called the Westport injector and the Yamane injector respectively from now on.

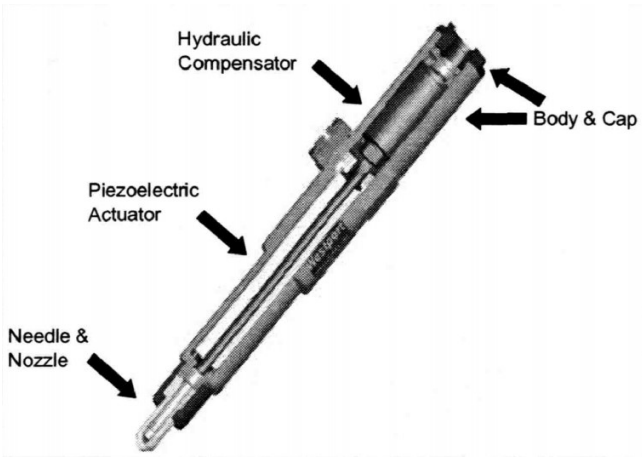

Figure 4.9: High pressure needle valve injector with a piezoelectric actuator (the Westport injector) [7]

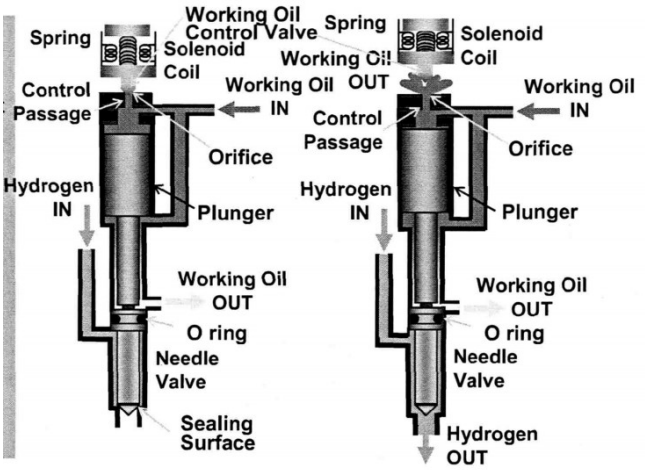

Figure 4.10: High pressure needle valve injector with a solenoid actuator (the Yamane injector) [36]

Both the differences and the similarities between these two injectors are very interesting. Both employ a needle valve, so both of these injectors will have to deal with the lack of lubrication provided by hydrogen at the needle seating. The injector in Figure 4.10 uses a solenoid actuator to move a plunger up and down. This plunger will then move the needle up and down using the working oil and the O ring. The injector in Figure 4.9 uses the piezoelectric actuator to move the hydraulic compensator, which in turn lifts the needle. In a way, the plunger, working oil and O ring in the Yamane injector have been replaced by the hydraulic compensator in the Westport injector. In both injectors these parts lift the needle, but they also passively adjust for any tolerances during assembly, variation in heat during operation and wear over the lifespan of the injector.

The O ring in the Yamane injector presents some durability issues when running on high pressure hydrogen. First of all, the O ring slides up and down and is in contact with hydrogen, meaning that it will be poorly lubricated and might wear out. Secondly, because the hydrogen is at such a high pressure, the O ring sees a large pressure differential. On one side, there is hydrogen, which might be at pressures higher than 100 bar, while on the other side there is the working oil, which drains to ambient pressure and is therefore only at 1 bar. That this pressure difference can cause problems was demonstrated during the development of the Yamane injector, when the O ring that was originally installed was severely damaged after just 50 hours of service. An O ring with a higher hardness was installed which was able to withstand the pressure difference,

but after inspection it was found that this ring also had some damage, this time from sliding. For this O ring, the pressure was not an issue, as O rings can be manufactured that can withstand a pressure difference of over 300 bar [37]. However, sliding against the injectors wall without any lubrication will wear the O ring down eventually. Although no hydrogen leakage was observed, it still shows the durability problems that present themselves when using hydrogen as a fuel.

Both injectors use a needle valve, which means they both have to deal with wear on the needle seat and the needle shaft. During initial testing of the Westport injector, it was found that the needle seating actually deforms plastically as a result of the impact of the needle, until equilibrium is reached. Both injectors had damage to the needle seat and shaft after the experiment, but in both cases it was not very severe and no leaking was observed. Parts of both injectors had been treated with coatings beforehand, but as was concluded earlier, not all coatings are created equal and it is important to choose the correct one, especially in an injector with such high pressures.

Lastly, as the Westport injector uses a piezoelectric actuator, it is important to look how that actuator interacts with hydrogen. Because as it turns out, during operation, some hydrogen was diffused into the piezoelectric actuator. This can cause the actuator to stop working and is one of the largest problems with this type of injector. The research in this field is still ongoing, but it seems possible to use different materials in the actuator that can deal better with exposure to hydrogen [38].

Velocity Profiles

As was mentioned before, plastic deformation was seen during the break-in period of the Westport injector. This shows that the force with which the needle is stopped by the needle seating is significant. This force is increased by the following phenomenon: When the needle approaches the seating, the hydrogen between the two surface is squeezed out. This creates a local increase in pressure, which slows down the needle. This is called squeeze film and in gasoline engines this significantly reduces the impact of the needle on the seating. However, this effect is dependent on the density and the viscosity of the medium, which are both a lot lower for hydrogen than for gasoline. Because of this, the squeeze film effect is a lot weaker for the hydrogen than it is for gasoline. To account for this, having a proper velocity profile for the injector is crucial. This means that the actuator should not just be used to lift the needle, but also to slow the needle down on its descend.

4.2.2. Spark Plugs

The differences between compression ignition and spark ignition have been explained already in subsection 3.1.2. Usually, one would look at the high research octane number (RON) of hydrogen (RON > 120) [39] and conclude that hydrogen would not be a suitable candidate to be used in a compression ignition engine. And indeed, almost all research into hydrogen internal combustion engines has been done on spark ignition engines. However, as was discussed in subsection 4.1.1, a hydrogen internal combustion engine is quite susceptible to knock, which is counter intuitive given the high RON. Often, the RON is used as a predictor of how well the knock resistance of a fuel is. Hydrogen's knock resistance is, however, a lot lower than its RON would suggest, due to its low minimum ignition energy (Figure 4.1) and its small quenching distance, both of which make autoignition more likely to occur. A better way to indicate hydrogen's knocking resistance is to use the motor octane number (MON) instead of the RON. The MON of a fuel is retrieved in a similar fashion as the RON, but the tests are run at tougher conditions, to really stress the knocking resistance of the fuel. Usually, a fuel's MON is about 8 to 12 points lower than its RON, but the MON of hydrogen is 60 [40], so much lower than its RON of over 120. With such a low MON, hydrogen could in fact be considered for a compression ignition engine.

There has not been a lot of research into hydrogen compression ignition engines, but it turns out that it is actually possible to run such an engine, at least in the environment of a laboratory. The key is to pre-heat the intake air, anywhere in a range from 200 to 400 degrees Celsius. Aleiferis and Rosati [32] also employed double injection as a method to get the combustion stable. A lot more can be said on compression ignition of hydrogen, but most of that is not relevant for this report. Because the engines that will be used in this project are all spark ignition engines, compression ignition of hydrogen is not considered any further. The

changes that would have to be made to accommodate for the higher compression ratios (they might have to be as high as 20:1 in a compression ignition hydrogen engine), the pre-heated intake air and double injection make the conversion too complicated and outside the scope of this project.

Now that compression ignition has been discarded, spark plugs will be needed. Just like with the injectors, not any regular spark plug will do. The degree to which attention has been paid to the spark plug varies per experiment. There are three main things that can be discussed when it comes to spark plugs in combination with hydrogen, which are the materials used, the design of the spark plug and the spark timing.

Looking at the materials used for the spark plugs in a hydrogen internal combustion engine, one thing that most authors seem to agree on is that platinum should not be used [41][42][24]. This is because platinum acts as a catalyst in the reaction between hydrogen and oxygen. Therefore, if the spark plug were to be made out of platinum, chances are the hydrogen-air mixture would pre-ignite on the platinum surface of the spark plug. Natkin et al. [41] are the only authors to go deeper into the material choices for the spark plugs they used. They found that nickel spark plugs would erode very quickly, possibly because of the presence of atomic hydrogen during combustion, which would erode the nickel. As stated before, platinum can not be used on a spark plug in combination with hydrogen, so Natkin et al. opted for iridium spark plugs, as iridium does not act as a catalyst for hydrogen and is even more erosion resistant than platinum [43].

For the design of the spark plug, the most important consideration when it comes to hydrogen is its ability to dissipate heat quickly. Because of the low ignition energy of hydrogen, a hot spark plug has the danger of igniting the fuel mixture prematurely. The spark plug therefore has to cool down as fast as possible. In the world of spark plugs, a spark plug that dissipates heat quickly is known as 'cold rated', while a spark plug that does not dissipate heat quickly is called 'hot rated'. Figure 4.11 shows the heat range of spark plugs, with a hot rated spark plug on the left and a cold rated spark plug on the right.

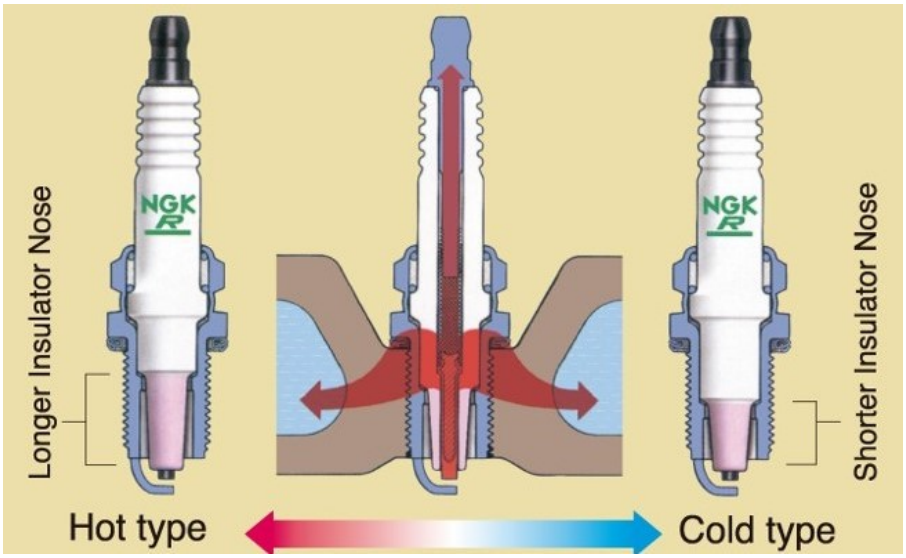

Figure 4.11: Heat range of spark plugs [1]

As can be seen in the picture, the hot rated spark plug has a longer insulator nose, while the cold rated spark plug has a shorter insulator nose. This insulator nose is the part of the spark plug that interacts with the hot environment of the combustion chamber, and having a longer nose means that more heat can be absorbed by the spark plug. A shorter nose will of course then absorb less heat, but it has another feature that makes it cold rated. Because it has a shorter nose, the area above the nose is bigger on a cold rated spark plug than on a hot one. Because of this larger area, the cold rated spark plug is able to dissipate more heat to the cylinder head in which it is mounted, resulting in a lower temperature of the spark plug itself.

Cold rated spark plugs can be used in hydrogen internal combustion engines because there are fewer deposits to burn off [44]. In gasoline engines, the combustion process will leave deposits on the spark plug.

[1] Source: https://www.ngk.com.au/technical_info/heat-range/, retrieved on 10-05-2021

A high spark plug temperature is needed to burn these deposits off and keep the spark plug functioning properly. With hydrogen, fewer of these deposits are present and as such, the spark plug does not have to get so hot.

The spark timing in a hydrogen internal combustion engine will be discussed later on in this report, as this is part of the CFD investigation that will be performed.

4.2.3. Miscellaneous

In this last section of the chapter, some smaller changes and considerations for hydrogen internal combustion engines are shown. Some of these will have to be implemented to have a successfully running hydrogen internal combustion engine, while others are just good to have in the back of the mind when working on this project.

Exhaust Gas Recirculation and Catalysts

It will be shown later in this report that decreasing the equivalence ratio also decreases the output power of the engine. This decreases the power density of the hydrogen internal combustion engine (the output power divided by the weight of the engine) which is especially important in aviation, where every gram counts. However, the equivalence ratio has to be kept low in order to have low NO_x emissions, something that is getting more and more important nowadays. That is, the equivalence ratio has to be kept low unless some measures are taken to reduce the NO_x emissions in the exhaust gas. Two of such measures are the use of exhaust gas recirculation (EGR) and a three way catalyst (TWC).

With EGR, part of the exhaust gasses are rerouted back into the engine during the intake stroke. This is effectively diluting the fuel mixture, but where diluting the fuel mixture with air would reduce the equivalence ratio, diluting the fuel mixture with exhaust gasses keeps the equivalence ratio the same. Salvi and Subramanian [45] found that adding EGR to a hydrogen fueled internal combustion engine could reduce the NO_x emissions by as much as 50%. In his experiments, Heffel [46, 47] ran an engine with exhaust gas recirculation, showing the effects on NO_x emissions, torque and brake thermal efficiency. These results are shown in Figure 4.12.

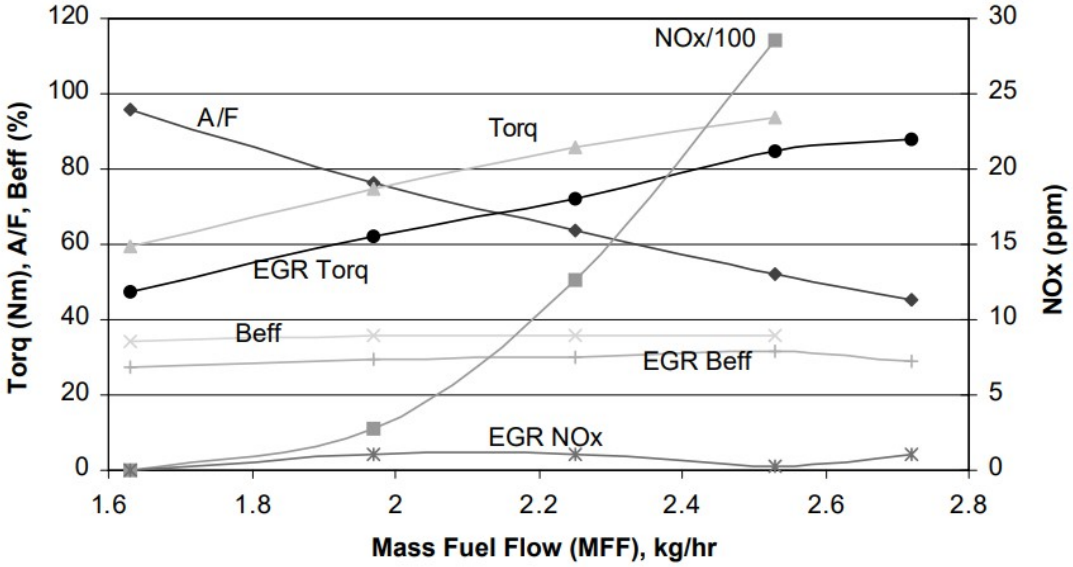

Figure 4.12: Mass fuel flow versus torque (Torq), air to fuel ratio (A/F), brake thermal efficiency (Beff) and NO_x emissions. The results for the EGR have 'EGR' as prefix and note that the non-EGR NO_x emissions have been divided by 100 to make them fit in the graph [46]

It can be seen that the torque produced by the EGR engine is always lower than that of the unmodified engine, which seems to defeat the whole purpose of the EGR, which was to increase the torque of the engine.

The maximum torque obtained by the unmodified engine here is 94 Nm, while the maximum torque for the EGR engine is 88 Nm. However, if we now look at the NO_x emissions, we can see that they rise very rapidly for the non-modified engine, but stay almost zero for the EGR engine. Taking near zero NO_x emissions as a constraint, the maximum torque obtained from the non-modified engine becomes about 55 Nm, while the EGR engine can still deliver 88 Nm. That is a 60% increase by adding EGR to the engine.

Although the NO_x-limited maximum torque is increased, the brake thermal efficiency is not; it actually drops a bit by adding EGR. It is thought that this is because of an increase in manifold temperature because of the hot exhaust gasses, which results in volumetric losses, and because of the extra work that the engine has to do to pump the exhaust gasses (mostly water) through the combustion chamber. This means that the unmodified engine can have low NO_x emissions and high brake thermal efficiency at the cost of low torque, while an EGR engine can have low NO_x emissions and high torque, but at the cost of lower brake thermal efficiency.

One limit to EGR, found by Berckmüller et al. [48], is that a maximum of 50% of the exhaust gasses can be recirculated while still keeping smooth engine operation.

Another way of reducing the NO_x emissions of the engine is by installing a three way catalyst (TWC). This TWC will break down the NO_x molecules (NO and NO_2) into N_2, thereby heavily reducing the NO_x emissions. This way, the engine can again be run at higher equivalence ratios without emitting much more NO_x. However, a TWC can only be used in a certain range of equivalence ratios, usually close to stoichiometric conditions. Therefore, the knocking behaviour of the engine at higher equivalence ratios has to be improved first before a TWC can be installed [42].

Pressure Boosting

Pressure boosting is not something that has been discussed before in this report. Thus far, it has been assumed that all the discussed engines were naturally aspirated, meaning that the pressure of the air that comes through the intake valve is equal to the pressure outside the engine, usually 1 bar. With pressure boosted engines, this pressure is increased, basically in an effort to fit more air into the combustion chamber, allowing for more fuel to be injected at the same equivalence ratio and thus have a higher power output. The two main ways to boost the pressure are supercharging and turbocharging. With supercharging, a compressor is attached to the crankshaft, which when rotated compresses the intake air. A turbocharger uses a turbine, powered by the exhaust gasses, to drive the compressor that in turn compresses the intake air. Both pressure boosters are used widely in all industries where internal combustion engines are used.

The appeal of using a pressure booster is clear; it allows hydrogen internal combustion engines to make up for the lower power density when compared to gasoline and CNG engines. This is especially the case for external injection hydrogen internal combustion engine, where the volumetric losses due to the low density of hydrogen result in an even lower power density than for internal injection engines. It is even thought that external injection hydrogen engines can only be made viable for real world applications if they are fitted with pressure boosters [22].

Nagalingam et al. [49], Berckmüller et al. [48] and Natkin et al. [41] all fitted superchargers to their respective hydrogen internal combustion engines to increase their power output. It was found that the specific power output could be increased by 30-35%. However, because of the higher pressure, the chance of pre-ignition increase and the NO_x emissions will go up. This means that the equivalence ratio will be limited, even more so than it already was. For Berckmüller et al., the maximum equivalence ratio for knock dropped from 1 to 0.6, while the limit equivalence ratio for NO_x was 0.45 when they increased the intake pressure, using a supercharger, from 1 to 1.85 bar. Nagalingam et al. increased the intake pressure from 1 to 2.6 bar and in doing so the maximum equivalence ratio for pre-ignition dropped from 1 to 0.5, while the limit equivalence ratio for NO_x emissions went down to 0.4.

Another aspect that has to be taken into account when using pressure boosters is that because of the higher pressures, the temperatures in the combustion chamber will also be higher. Nagalingam et al. mitigate this by using water injection, while Berckmüller et al. have designed the engine such that the exhaust valve and spark plugs are being cooled.

Valve-Seat Interaction

Not only the injectors have to deal with the poor lubricating qualities of hydrogen, so do the valves and the valve seats. For testing purposes, standard valves and valve seats can most likely be used, as the degradation of the materials does not seem to be too severe [41]. However, if the engine were to be developed for commercial use, the wear of the valves and valve seats should be investigated further. Natkin et al. [41] found that especially the exhaust valve is more prone to degradation.

Fuhurama et al. [50] found that the copper alloy used on the intake valve seat made the engine backfire violently. Replacing the valve seat with an iron alloy one solved the issue. This is the only instance found in literature where this occurs, but it is still important to keep this in mind and make sure that any engine that will be converted into a hydrogen internal combustion engine does not have copper valve seats.

Cooling the Hydrogen

So far, nothing has been said yet about the storage of hydrogen in this report. Because hydrogen is a gas at room temperature, it has a low density and giant tanks would be needed to store enough hydrogen to make it a viable alternative for carbon-based fuel in terms of range. Therefore, hydrogen is usually stored in one of two ways; compressed or cooled. Compressed storage is used more often than cryogenic (cooled) storage because cryogenic storage requires much more complex, heavy tanks and even then, the density of the hydrogen is still quite low. An advantage of cryogenic hydrogen storage is that the hydrogen will be injected into the combustion chamber cooled. This cool hydrogen will lower the temperature of the combustion chamber and reduce the chances of pre-ignition happening. It also reduces the emission of NO_x, as can be seen from Figure 4.13. Here, a hydrogen internal combustion engine is run both on cooled and uncooled hydrogen, where the cooled hydrogen is about -130 degrees Celsius.

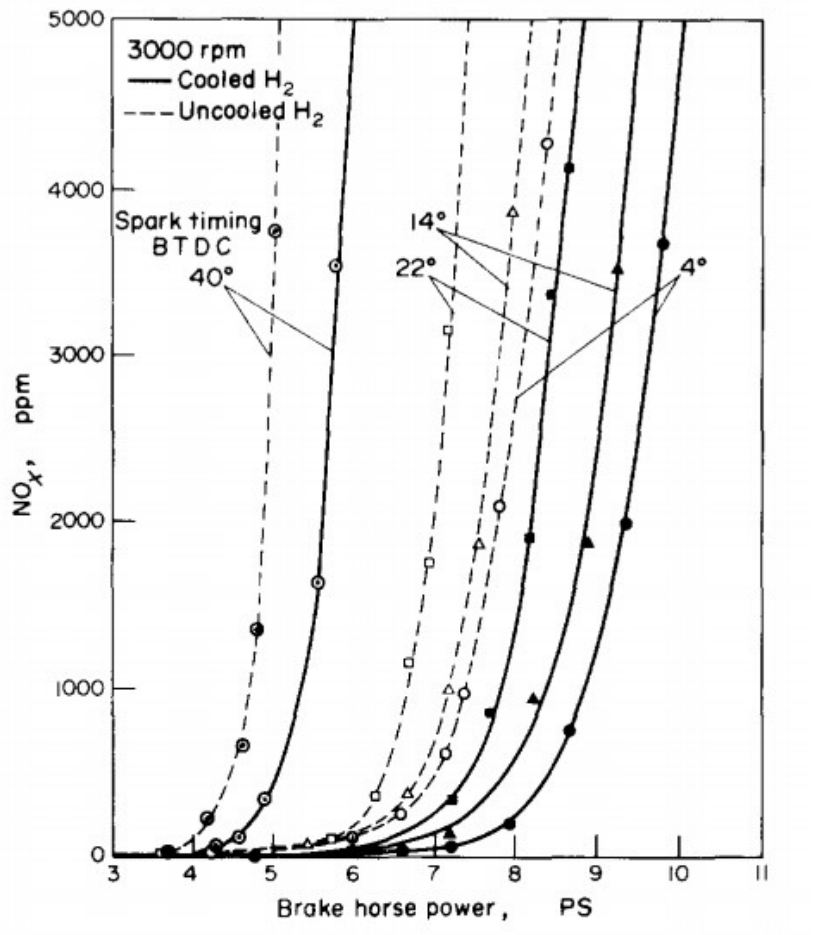

Figure 4.13: Brake horse power versus NO_x emissions for cooled and uncooled H_2 and different spark timings [50]

It is clear that for the same NO_x emission, the cooled hydrogen engine can produce more power.

5
CFD Set-Up

During research done prior to this thesis, it was found that there could be potential problems with pressure peaks in hydrogen internal combustion engines [51]. These pressure (and also temperature) peaks in the engine could potentially be so severe that it would not be safe to run such an engine. These results were from preliminary studies, so it was decided that performing CFD analyses would be a good way to find out if these safety concerns were valid. Apart from this safety concern, another reason to perform CFD simulations before starting the experiments that will follow the work in this thesis, was gaining a deeper understanding of the effects that certain parameters, such as injection timing, spark timing and equivalence ratio have on the engine performance. Running experiments can be expensive, so knowing, for instance, the range of injection timings in which the optimum engine performance lies beforehand, can save a lot of time and effort. This chapter will first describe the geometry of the engine model that was used in the simulations. After this, the models that are used in the CFD calculations are discussed. Finally, the meshing parameters and boundary and initial conditions that are used during the simulations are explained.

5.1. Engine geometry

Of course, to perform a simulation of an internal combustion engine, whether running on conventional fuels or on hydrogen, one first needs to have a digital model of such an internal combustion engine. The initial plan was to create such a model from scratch, exactly to the required specifications. However, this turned out to be more difficult than expected. Importing a geometry into Forte corrupted every geometry file that was tried and reaching out to ANSYS proved not very fruitful. The keep the project moving forward, it was decided to use an already existing and available model that is provided as a part of the Ansys Forte tutorials. This engine can be seen in Figure 5.1.

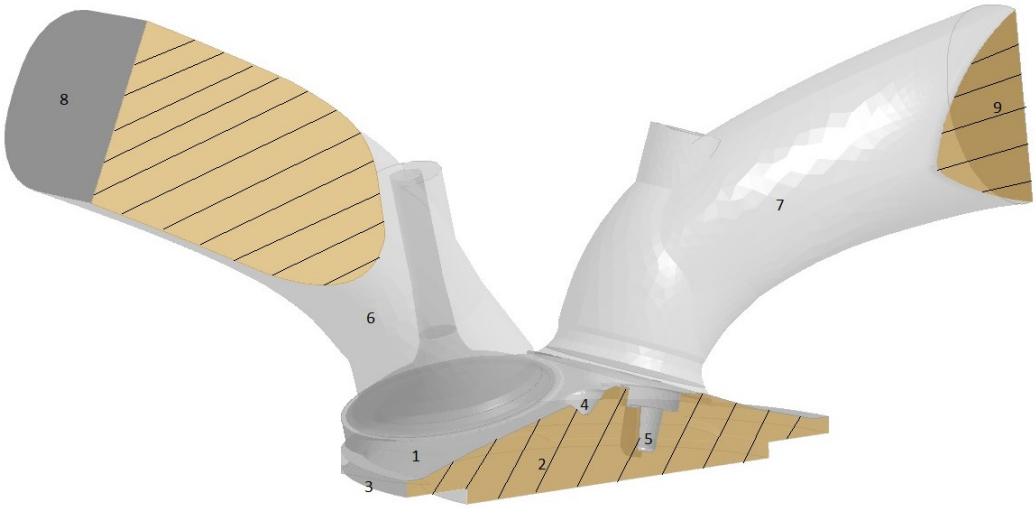

Figure 5.1: The engine used in the CFD analysis

Table 5.1 matches the engine part names to the numbers in the figure.

Also slightly visible in the figure is the inlet/intake valve. A similar valve is present in the exhaust, called the

Table 5.1: Names of the engine parts from Figure 5.1

Number	Part name
1	Cylinder head
2	Piston
3	Cylinder liner
4	Injector
5	Spark Plug
6	Intake
7	Exhaust
8	Inlet
9	Outlet

exhaust/outlet valve. The striped surfaces in the figure are the symmetry surfaces. If a number is present on this surface, the number is meant for the part behind it.

The engine in the figure was selected for several reasons. First of all, the desired engine has to be a direct injection engine. The reasons for this have been discussed in chapter 3, but simply put, direct injection can provide a higher power output for the engine than indirect injection does. It also allows for variable injection timing and removes the potential for backfire. Another reason to pick this engine is that the size of the engine is quite comparable to the engines used by Berckmüller et al. [48], Eichlseder et al. [52], Furuhama et al. [53], Ganesh et al. [26] and Welch et al. [7]. This means that potentially, the results of the simulation can be validated or verified using these sources.

As can be seen, the engine shown in the figure is only half of it. Since the engine is symmetric in the ZX-plane, only half the engine needs to be simulated. After the simulation has been completed, this one halve can be mirrored to obtain the other half. Figure 5.2 shows a drawing of the engine from the Ansys Tutorials.

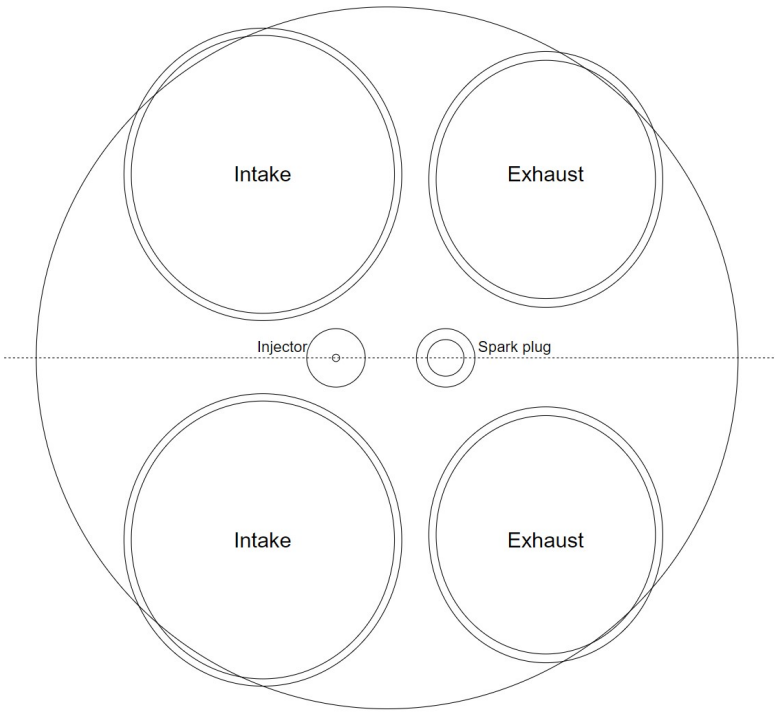

Figure 5.2: Drawing of the top view of the engine used in the CFD analysis

The engine is clearly symmetric along the dotted line, meaning that the completed engine has two intake ports and valves per cylinder and two exhaust ports and valves per cylinder. The engine consists of a single cylinder, with an injector and a spark plug. Some of the geometric features of the engine can be found in Table 5.2. Because the engine used in this simulation is a single cylinder engine, at some points during

this report, the engine will be referred to as the cylinder. Note that in this case, this does not just mean the cylindrical part of the single cylinder engine, but also includes the intakes and exhausts, the spark plug, the cylinder head and the fuel injector.

Table 5.2: Geometric features of the engine used in the CFD analysis

Engine bore [cm]	8.4
Engine stroke [cm]	9.0
Displacement Volume [cm^3]	498.8
Compression Ratio [-]	10.3

The engine bore of the model is a fixed value, as it follows directly from the geometry of the combustion chamber. The engine stroke can be altered in the set-up for the simulations. This effectively changes how far the piston moves down during the power and inlet strokes. Altering the engine stroke also influences the displacement volume and the compression ratio. Increasing the engine stroke will increase the displacement volume, because at bottom dead centre, the volume inside the combustion chamber will be larger. This larger volume will be compressed to the same volume at top dead centre and therefore, an increase in engine stroke also results in a higher compression ratio. It follows from this that a smaller engine stroke results in a smaller displacement volume and a lower compression ratio.

5.2. Models

One of the reasons that Ansys Forte was chosen to study the behaviour of a hydrogen internal combustion engine, is that this application was designed specifically to model internal combustion engines. The code used in Ansys Forte is based on the Reynolds Averaged Navier-Stokes (RANS) equations and uses the conservation of energy, mass and momentum as the primary governing equations. Usage of the RANS equations eliminate the need for resolving small-scale structures and fluctuations seen in individual flow realisations, while retaining the main effects of turbulence on the averaged flow and combustion characteristics. The main assumptions used in the derivation of the governing equations, are the use of the ideal gas law for the gas-phase thermodynamic equation of state, the use of Fick's law for mass diffusion, the assumption that all fluids in the simulation are Newtonian and lastly, Fourier's law is used for thermal diffusion.

The ideal gas law states that the gas in question behaves like an ideal gas, and as such adheres to the following assumptions. The molecules in the gas do not lose energy, so their motion is frictionless and any collisions that occur are completely elastic. The volume of the individual molecules in the gas is magnitudes smaller than the total volume of the gas. There are no forces between the molecules in the gas or between the molecules and their surroundings. Finally, the molecules in the gas are constantly in motion in random directions and the distance between two molecules is much larger than the size of an individual molecule. With these assumptions, the gas-phase thermodynamic equation of state can be written as:

$$PV = nRT \tag{5.1}$$

Where P is the pressure, V the volume, n the number of moles of the gas, R the gas constant and T the absolute temperature.

Fick's law for mass diffusion and Fourier's law for thermal diffusion are very similar. Fick's law for mass diffusion is given by:

$$\mathbf{J} = -D\nabla\phi \tag{5.2}$$

Here, **J** is the diffusion flux vector, D is the diffusion coefficient and $\nabla\phi$ is the gradient of the concentration of the mass. Fourier's law is given by:

$$\mathbf{q} = -k\nabla T \tag{5.3}$$

Where **q** is the local heat flux density vector, k is the conductivity of the material and ∇T is the temperature gradient. Lastly, a fluid is considered Newtonian if the viscosity of the fluid is independent of shear rate.

In a RANS approach, instantaneous quantities from the Navier-Stokes equations are decomposed into a mean or time-averaged component and a fluctuating part. In Forte, the Favre average is used. If we take the flow velocity vector **u** as an example, this can be decomposed into an ensemble average $\tilde{\mathbf{u}}$ and a fluctuating part **u**", such that $\mathbf{u} = \tilde{\mathbf{u}} + \mathbf{u}"$. Here, $\tilde{\mathbf{u}}$ is defined as a conventional density-weighted average: $\tilde{\mathbf{u}} = \overline{\rho \mathbf{u}}/\overline{\rho}$ and **u**" is defined to satisfy $\overline{\rho \mathbf{u}"} = \mathbf{0}$. In this notation, the over-bar represents an averaging operator.

In this section, some of the models that are used in the simulations will be explained and some of their limitations will be discussed. The information on the models and equations as stated in this section was taken from the Ansys Forte theory manual [54].

5.2.1. Species conservation

The contents of the internal combustion engine in Forte are modelled as a mixture of individual gas components or species. The composition of these contents change during the engine cycle due to things like flow convection, molecular diffusion and combustion. Equation 5.4 shows the equation for conservation of mass of species **k**.

$$\frac{\partial \bar{\rho}_k}{\partial t} + \nabla \cdot \left(\bar{\rho}_k \tilde{\mathbf{u}}\right) = \nabla \cdot \left[\bar{\rho} D \nabla \tilde{y}_k\right] + \nabla \cdot \Phi + \dot{\bar{\rho}}_k^c + \dot{\bar{\rho}}_k^s (k = 1, \cdots, K) \tag{5.4}$$

In this equation, ρ is the density, k is the species index, K is the total number of species, **u** is the flow velocity vector, y_k is the mass fraction of species k, D is the mixture-averaged molecular diffusion coefficient that follows from the use of Fick's law of diffusion and Φ accounts for the filtering of the convection term and is defined as $\Phi = \overline{\rho_k}\tilde{\mathbf{u}} - \overline{\rho_\mathbf{k}\mathbf{u}}$. Finally, there are two source terms present. One due to chemical reaction, $\dot{\bar{\rho}}_k^c$, and one due to spray evaporation, $\dot{\bar{\rho}}_k^s$.

5.2.2. Fluid continuity

Summing Equation 5.4 over all of the species gives the continuity equation for the total gas-phase fluid, as can be seen in Equation 5.5.

$$\frac{\partial \bar{\rho}}{\partial t} + \nabla \cdot (\bar{\rho} \tilde{\mathbf{u}}) = \dot{\bar{\rho}}^s \tag{5.5}$$

5.2.3. Momentum conservation

In the momentum equation used in Forte, the effects of convection, pressure force, viscous stress, turbulent transport, liquid sprays and body force are considered. This culminates in Equation 5.6.

$$\frac{\partial \bar{\rho} \tilde{\mathbf{u}}}{\partial t} + \nabla \cdot (\bar{\rho} \tilde{\mathbf{u}} \tilde{\mathbf{u}}) = -\nabla \bar{p} + \nabla \cdot \overline{\boldsymbol{\sigma}} - \nabla \cdot \boldsymbol{\Gamma} + \overline{\mathbf{F}}^s + \overline{\rho \mathbf{g}} \tag{5.6}$$

In this equation, p is the pressure, **u** is the velocity vector, ρ is the density, g is the specific body force $\tilde{\sigma}$ is the viscous shear stress which is given by $\overline{\boldsymbol{\sigma}} = \bar{\rho} \nu \left[\nabla \tilde{\mathbf{u}} + (\nabla \tilde{\mathbf{u}})^{\mathrm{T}} - \frac{2}{3}(\nabla \cdot \tilde{\mathbf{u}})\mathbf{I}\right]$, in which ν is the laminar kinematic viscosity, **I** the identity tensor and T means that the transpose of a vector is taken. $\overline{\mathbf{F}}^s$ is the rate of momentum gain per unit volume due to spray, but as no spray models are used in these simulations, this will not have any effect. Lastly, Γ accounts for the filtering of the nonlinear convection term and is called the Reynolds stress. It is defined as $\Gamma = \bar{\rho}(\widetilde{\mathbf{u}\mathbf{u}} - \tilde{\mathbf{u}}\tilde{\mathbf{u}})$, but will be talked more about in subsection 5.2.5, as these will be necessary to provide closure.

5.2.4. Energy conservation

From the first law of thermodynamics we know that any change in internal energy should be balanced by the pressure work and heat transfer. For an internal combustion engine, this means that the effects of

convection, turbulent transport, turbulent dissipation, sprays, chemical reactions and enthalpy diffusion of a multi-component flow should be considered. The internal energy transport equation then becomes:

$$\frac{\partial \bar{\rho}\tilde{l}}{\partial t} + \nabla\cdot(\bar{\rho}\tilde{\mathbf{u}}\tilde{l}) = -\bar{p}\nabla\cdot\tilde{\mathbf{u}} - \nabla\cdot\bar{\mathbf{J}} - \nabla\cdot\mathbf{H} + \bar{\rho}\bar{\varepsilon} + \dot{\overline{Q}}^{C} + \dot{\overline{Q}}^{S} \tag{5.7}$$

In Equation 5.7, l is the specific internal energy, J is the heat flux vector accounting for contributions due to heat conduction and enthalpy diffusion and is defined as $\bar{\mathbf{J}} = -\lambda\nabla\bar{T} - \bar{\rho}D\sum_k \widetilde{h}_k\nabla\bar{y}_k$, where λ is the thermal conductivity, T is the fluid temperature and h_k is the specific enthalpy of species k. Continuing in Equation 5.7, $\bar{\epsilon}$ is the dissipation rate of the turbulent kinetic energy, which will be defined in subsection 5.2.5. Source terms due to chemical heat release, $\dot{Q}_c$ and spray interactions, $\dot{Q}_s$ are added. The effects of filtering of the convection term are taken into account using $\mathbf{H}$, where $\mathbf{H} = \overline{\rho}(\mathbf{u}\widetilde{i} - \tilde{\mathbf{u}}\tilde{l})$. Here, $\mathbf{H}$ also needs to properly modelled using a turbulent model, as will be discussed in subsection 5.2.5.

5.2.5. Turbulence models

The equations found in this section provide closure to the undetermined terms from the sections above, according to the RANS methods.

The Reynolds stress tensor, as used in Equation 5.6, is defined as:

$$\mathbf{\Gamma} = -\bar{\rho}\nu_T\left[\nabla\tilde{\mathbf{u}} + (\nabla\tilde{\mathbf{U}})^T - \frac{2}{3}(\nabla\cdot\tilde{\mathbf{u}})\mathbf{I}\right] + \frac{2}{3}\bar{\rho}\tilde{k}\mathbf{I} \tag{5.8}$$

where ν_T is the turbulent kinematic viscosity and $\tilde{k}$ is the turbulent kinetic energy, defined by $\widetilde{k} = \frac{1}{2\bar{\rho}}\,\mathrm{trace}(\mathbf{\Gamma}) = \frac{1}{2}\widetilde{\mathbf{u}''\cdot\mathbf{u}''}$. ν_T is related to $\tilde{k}$ and the dissipation rate $\tilde{\epsilon}$ by $\nu_T = c_\mu\frac{\tilde{k}^2}{\tilde{\epsilon}}$.

The turbulent flux term Φ from Equation 5.4 is modelled as:

$$\mathbf{\Phi} = \bar{\rho}D_T\nabla\bar{y}_k, \tag{5.9}$$

in which D_T is the turbulent diffusivity. Turbulent flux term $\mathbf{H}$ from Equation 5.7 is modelled as:

$$\mathbf{H} = -\lambda_T\nabla\bar{T} - \bar{\rho}D_T\sum_k \widetilde{h}_k\nabla\bar{y}_k, \tag{5.10}$$

where λ_T is the turbulent thermal conductivity, which can be related to the turbulent thermal diffusivity α_T and the heat capacity c_p by $\lambda_T = \overline{\rho}c_p\alpha_T$. Furthermore, D_T and α_T can be related to the turbulent viscosity ν_T by $D_T = \frac{\nu_T}{Sc_T}$ and $\alpha_T = \frac{\nu_T}{Pr_T}$ respectively. Here, Sc_T and Pr_T are the turbulent Schmidt and Prandtl numbers.

It was shown before that in order to obtain the turbulent kinematic viscosity ν_T, the turbulent kinetic energy $\tilde{k}$ and dissipation rate $\tilde{\epsilon}$ should be modelled. In Ansys Forte, the choice can be made between the standard $k-\epsilon$ model or the Re-Normalized Group Theory (RNG) $k-\epsilon$ model.

The standard Favre-averaged equations for k and ϵ are given in Equation 5.11 and Equation 5.12.

$$\frac{\partial \bar{\rho}\widetilde{k}}{\partial t} + \nabla\cdot(\bar{\rho}\tilde{\mathbf{u}}\widetilde{k}) = -\frac{2}{3}\bar{\rho}\widetilde{k}\nabla\cdot\tilde{\mathbf{u}} + (\overline{\sigma} - \mathbf{\Gamma}) : \nabla\tilde{\mathbf{u}} + \nabla\cdot\left[\frac{(\mu+\mu_T)}{Pr_k}\nabla\widetilde{k}\right] - \bar{\rho}\widetilde{\varepsilon} + \dot{\overline{W}}^{s} \tag{5.11}$$

$$\begin{aligned}\frac{\partial \bar{\rho}\widetilde{\varepsilon}}{\partial t} + \nabla\cdot(\bar{\rho}\tilde{\mathbf{u}}\widetilde{\varepsilon}) &= -\left(\frac{2}{3}c_{\varepsilon 1} - c_{\varepsilon 3}\right)\bar{\rho}\widetilde{\varepsilon}\nabla\cdot\tilde{\mathbf{u}} + \nabla\cdot\left[\frac{(\nu+\nu_T)}{Pr_\varepsilon}\nabla\widetilde{\epsilon}\right] \\ &+ \frac{\tilde{\varepsilon}}{\tilde{k}}\left(c_{\varepsilon 1}(\boldsymbol{\sigma} - \mathbf{\Gamma}) : \nabla\tilde{\mathbf{u}} - c_{\varepsilon 2}\bar{\rho}\widetilde{\varepsilon} + c_s\dot{\overline{W}}^{s}\right)\end{aligned} \tag{5.12}$$

In these two equations, Pr_k, Pr_ϵ, $c_{\epsilon 1}$, $c_{\epsilon 2}$ and $c_{\epsilon 3}$ are model constants, for which the values are given in Table 5.3. The source terms involving $\dot{\bar{W}}^s$ are calculated based on the droplet probability distribution [55]. Amsden [55] suggested c_s=1.5, based on the postulate of length scale conservation in spray/turbulence interactions.

In the simulations done for this report, the RNG k-ϵ method was used, as it is the recommended method. This method was first proposed by Yakhot and Orszag [56] and replaces the ϵ equation by Equation 5.13.

$$\begin{aligned}\frac{\partial \bar{\rho}\tilde{\varepsilon}}{\partial t} + \nabla\cdot(\bar{\rho}\tilde{\mathbf{u}}\tilde{\varepsilon}) &= -\left(\frac{2}{3}c_{\varepsilon 1} - c_{\varepsilon 3}\right)\bar{\rho}\tilde{\varepsilon}\nabla\cdot\tilde{\mathbf{u}} + \nabla\cdot\left[\frac{(\upsilon+\upsilon_T)}{Pr_\varepsilon}\nabla\tilde{\varepsilon}\right] \\ &+ \frac{\tilde{\varepsilon}}{\tilde{k}}\left[c_{\varepsilon 1}(\boldsymbol{\sigma}-\boldsymbol{\Gamma}):\nabla\tilde{\mathbf{u}} - c_\varepsilon\bar{2}\tilde{\epsilon} + c_s\dot{\bar{W}}^s\right] - \bar{\rho}R\end{aligned} \tag{5.13}$$

where R is defined as:

$$R = \frac{c_\mu\eta^3\left(1-\eta/\eta_0\right)}{1+\beta\eta^3}\frac{\tilde{\varepsilon}^2}{\tilde{k}}, \tag{5.14}$$

with

$$\eta = S\frac{\tilde{k}}{\tilde{\epsilon}} \tag{5.15}$$

and

$$S = (2\bar{\mathbf{S}}:\bar{\mathbf{S}})^{1/2} \tag{5.16}$$

Here $\bar{\mathbf{S}}$ is the mean strain tensor $\bar{\mathbf{S}} = \frac{1}{2}\left(\nabla\tilde{\mathbf{u}} + (\nabla\tilde{\mathbf{u}})^T\right)$.

In Ansys Forte, the RNG value for $c_{\epsilon 3}$ is calculated as shown in Equation 5.17, based on the work of Han and Reitz [57].

$$c_{\varepsilon 3} = \frac{-1+2c_{\varepsilon 2}-3m(n-1)+(-1)^\delta\sqrt{6}c_\mu c_\eta\eta}{3} \tag{5.17}$$

In this equation, m=0.5 and n=1.4, based on the assumptions that we are dealing with an ideal gas. c_η is given by:

$$c_\eta = \frac{\eta\left(1-\eta/\eta_o\right)}{1+\beta\eta^3} \tag{5.18}$$

and δ is either 1 or 0, based on:

$$\delta = \begin{cases} 1, \text{ if } \nabla\cdot\tilde{\mathbf{u}} < 0 \\ 0, \text{ if } \nabla\cdot\tilde{\mathbf{u}} > 0 \end{cases} \tag{5.19}$$

$c_{\epsilon 3}$ is calculated automatically in Ansys Forte, based on the flow conditions and model constants η_0 and β. These and other constants are shown in Table 5.3, together with the values used in the simulation, both for the standard $k-\epsilon$ and RNG $k=\epsilon$ methods.

Table 5.3: Constants in the standard k-ϵ and RNG k-ϵ models

	c_μ	$c_{\varepsilon 1}$	$c_{\varepsilon 2}$	$c_{\varepsilon 3}$	$1/Pr_k$	$1/Pr$	η_o	β
Standard $k-\varepsilon$	0.09	1.44	1.92	−1.0	1.0	0.769		
RNG $k-\varepsilon$	0.0845	1.42	1.68	Equation 5.17	1.39	1.39	4.38	0.012

5.2.6. Ignition-kernel flame model

In this report, only spark ignition is considered as an ignition method. In a spark ignition engine, a spark is created that ignites the fuel mixture in the combustion chamber. This spark is created by a spark plug, which has two electrodes between which a high electric potential difference is created. An ignition-kernel flame is created that first expands on its own before the combustion reaction takes over. This ignition-kernel flame

is typically smaller than the average grid size of the mesh and as such has to be tracked differently before the flame becomes big enough to be tracked by the G-equation model that will be discussed after this.

In Ansys Forte, the growth of the ignition-kernel is tracked by using the Discrete Particle Ignition Kernel (DPIK) model by Fan, Tan and Reitz [58][59]. In this model, a spherical shaped kernel is assumed, where the flame front position is marked by Lagrangian particles. The flame surface density is then obtained from the density of these particles in each computational cell. The kernel growth rate can be found using Equation 5.20, assuming that the temperature inside the kernel is uniform.

$$\frac{dr_k}{dt} = \frac{\rho_u}{\rho_k}(S_{plasma} + S_r) \tag{5.20}$$

Here, r_k is the kernel radius, ρ_u is the local unburned gas density, ρ_k is the gas density inside the kernel region and S_T is the turbulent flame speed. The plasma velocity S_{plasma} can be found using:

$$S_{plasma} = \frac{\dot{Q}_{spk}\eta_{\dot{e}ff}}{4\pi r_k^2[\rho_u(u_k - h_u) + P\frac{\rho_u}{\rho_k}]} \tag{5.21}$$

Here ρ_u and h_u are the density and enthalpy of the unburned mixture, ρ_k and u_k are the density and internal energy of the mixture inside the kernel. $\dot{Q}_{spk}$ is the electrical energy discharge rate, η_{eff} is the electrical transfer efficiency due to the heat loss to the spark plug.

5.2.7. G-equation

Once the flame is large enough, Forte switches from the DPIK model to the usage of the G-equation to predict in-cylinder turbulent flame combustion, without including chemistry source terms in the transport equations. The G-equation is based on the turbulent premixed combustion flamelet theory by Peters [60] and was further developed by Tan and Reitz [59], Liang and Reitz [61] and Liang et al. [62].

The G-equation model consists of a set of Favre-averaged level-set equations, which include the equations for the Favre mean, $\widetilde{\mathbf{G}}$, and its variance, $\widetilde{\mathbf{G}}$"^{2}. The G-term is the scalar distance between the instantaneous and the mean flame front. The G-equation model uses Equation 5.22 and Equation 5.23 and the Favre averaging method to output the turbulent flame front location and flame brush thickness, respectively:

$$\frac{\partial \widetilde{G}}{\partial t} + \left(\widetilde{\vec{u}} - \vec{u}_{\text{vertex}}\right)\cdot\nabla\widetilde{G} = \frac{\bar{\rho}_u}{\bar{\rho}_b}S_T^0|\nabla\widetilde{G}| - D_T\widetilde{\kappa}|\nabla\widetilde{G}| \tag{5.22}$$

$$\frac{\partial \widetilde{G''^2}}{\partial t} + \widetilde{\vec{u}}\cdot\nabla\widetilde{G''^2} = \nabla_|\cdot\left(\frac{\bar{\rho}_u}{\bar{\rho}_b}D_T\nabla_|\widetilde{G''^2}\right) + 2D_T(\nabla\widetilde{G})^2 - c_s\frac{\widetilde{\varepsilon}}{\widetilde{k}}\widetilde{G''^2} \tag{5.23}$$

Here $\nabla_|$ denotes the tangential gradient operator, $\vec{u}$ is the fluid velocity, $\vec{u}_{vertex}$ is the velocity of the moving vertex, ρ_u and ρ_b are the average densities of the unburned and burned mixtures respectively, D_T is the turbulent diffusivity, $\widetilde{\kappa}$ is the Favre mean flame front curvature, c_S, a_4, b_1 and b_3 are modeling constants, $\widetilde{k}$ and $\widetilde{\epsilon}$ are the Favre mean turbulent kinetic energy and its dissipation rate from the RNG k-ϵ model and finally, S_T^0 is the turbulent flame speed.

Using these equations, the flamefront can be found using $\widetilde{\mathbf{G}}(\mathbf{x},\mathbf{t}) = \mathbf{0}$. From there, the flow field can be divided into the unburned region, where $\widetilde{\mathbf{G}}$<0 and the burned region, where $\widetilde{\mathbf{G}}$>0. It is assumed that the instantaneous flame front always falls within the those computational cells where the mean flame front is located. A schematic overview of the situation described above can be found in Figure 5.3

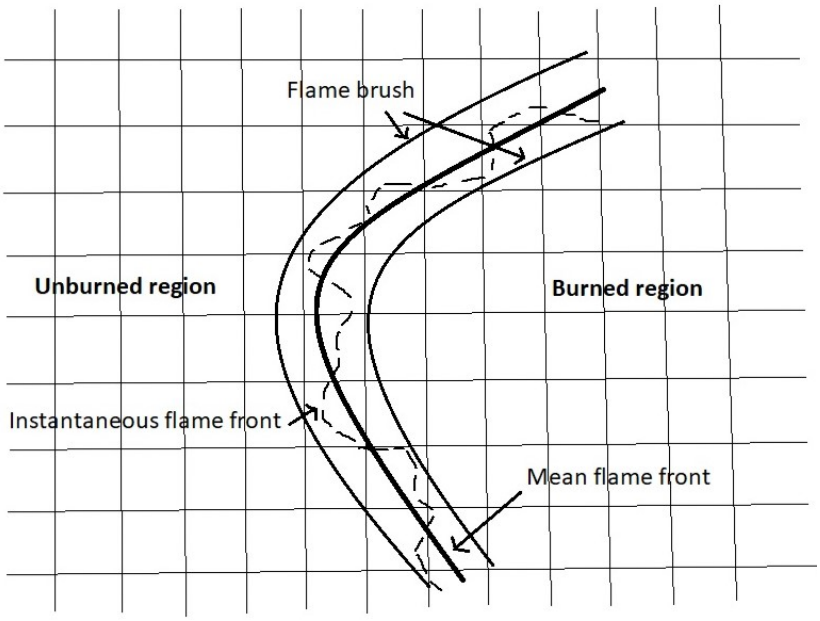

Figure 5.3: Schematic overview of the flame front

5.3. Meshing

The Ansys Forte program allows the user to select a global mesh size for the meshing of the geometry and then allows for local and temporal refinement. For this simulation the global mesh size was set to 0.3 cm, which should be fine enough to give valid results, but not so fine that the computational times become unworkable. A study on the mesh refinement can be found in subsection 7.1.1. Within that global mesh size, some refinements are applied. Some of these refinements are prescribed for a certain region and time interval, while others are actually dependent on the solution of the field at that time in the simulation (solution adaptive meshing). With this solution adaptive meshing, a certain solution variable is considered and if the value of that variable in a cell differs from the average value beyond a certain threshold, that cell will be refined in the next mesh update. This refinement can continue up to a set limit and once the variable in a cell does not differ enough from the average any more, the mesh will be coarsened in that location. In this simulation, two instances of solution adaptive meshing are used, one for the velocity, which is active for the duration of the entire simulation and one for the temperature, which is only active between crank angles of 700 and 800 degrees. The other mesh refinements are as follows:

Table 5.4: Mesh refinements

Location	Size as fraction of global mesh size	Active crank angles
All walls - 1 layer	1/2	All
Inlet and outlet - 2 layers	1/2	All
Spark location - sphere with 0.6 cm radius	1/4	All
Inlet and outlet valves - 2 layers	1/4	All
Walls in combustion chamber - 2 layers	1/4	340 - 380
Walls in combustion chamber - 2 layers	1/4	700 - 740
Full volume of combustion chamber	1/2	All
Injection location	1/8	Dependent on injection timing

During the course of the simulation, several parts of the engine are moving, meaning that there will not just be one mesh, but several different meshes. Fortunately, this is all taken care of by Forte automatically. The moving parts are the inlet valve, the exhaust valve and the piston. The mesh is automatically adapted to incorporate the movement of these parts.

5.4. Boundary and Initial Conditions

All surfaces of the engine that interact with the flow need to be assigned a boundary condition, as they are literally boundaries that the flow may not cross. In this simulation, four kinds of boundaries are used; inlets, outlets, walls and symmetries. The table below shows the boundary conditions that were set as a wall condition. These walls were all given a constant temperature, as shown in the table.

Table 5.5: Wall boundary conditions

Boundary name	Wall temperature
Piston	485 K
Intake	313 K
Exhaust	485 K
Head	485 K
Intake-valve	400 K
Exhaust-valve	777 K
Liner	500 K

Besides these seven boundary conditions, there are four more, namely the inlet, the outlet, the symmetry and the injection point. The symmetry consists of all the symmetry planes, as they can be seen in Figure 5.1. The outlet is defined as a static pressure outlet, with a pressure of 100,000 Pa. The inlet is defined as a static pressure inlet with a pressure of 80,000 Pa, but here also the composition of the fluid that enters the model is defined. In case of direct fuel injection, only air is taken in, with a composition of 76.7% N_2 and 23.3 O_2. With indirect injection, the fuel is added to the air before arrives at the inlet valve. In this work, this is simulated by adding the fuel (hydrogen or gasoline) to the inlet mixture. The percentage of the mixture that the fuel takes up depends on the desired equivalence ratio. Finally, there is the injection point boundary condition. With the indirect injection, this boundary condition is of course not necessary. With direct injection however, this boundary condition is necessary to inject the hydrogen into the combustion chamber. Ansys Forte has a spray model included, that can be used to model a liquid fuel spray into the engine. Unfortunately, this does not work for a gaseous fuel like hydrogen. Therefore, a replacement for the spray model needed to be found. In the end, it was decided to use a inlet boundary condition, as developed by Rahman [63]. The surface at the tip of the injector was separated from the rest of the injector and this surface was used for the inlet boundary condition. Forte allows the user to use a 'velocity time varying' option, where the user can specify a velocity profile for the inlet condition. In this way, the user can control the rate at which the hydrogen is injected and the moment at which this happens. The angle under which the fuel is injected can also be chosen, by specifying a direction vector. A drawback of this method is that the exact amount of hydrogen that is injected can not be specified. Therefore, the settings that correspond to certain amounts of hydrogen and certain equivalence ratios had to be found by trial and error. Another drawback is that the shape of the injection cone can not be controlled directly. This shape is depended on the injection pressure, velocity and the pressure in the combustion chamber at the moment of injection. Lastly, where the spray in the Forte spray model and in reality often consists of multiple cones, all pointed in their own distinct direction, with the inlet boundary condition method, only one cone can be created.

Apart from the boundaries, also the initial conditions of the simulation have to be specified. The initial conditions form a first kind of 'solution', that will be used as a starting point for the calculations. The cylinder consists of three main volumes, each of which is assigned an initial temperature, pressure and species composition. These three main volumes consist of the combustion chamber, the inlet volume and the exhaust volume. The intake composition consists of the air that is taken into the engine and consists of 76.7% N_2 and 23.3 O_2. Its pressure is 80,000 Pa and the temperature is 313 K. The mixtures in the combustion chamber and in the exhaust volume at the start of the engine cycle are the same and are the result of the combustion process in the previous engine cycle. Ansys Forte has a feature that lets the user calculate the resulting composition of the combustion products, given the mixture of air and fuel that is combusted. This composition was then inserted as an initial condition for both the combustion chamber and the exhaust volume, together with a temperature of 1070 K and a pressure of 100,000 Pa.

6
CFD Results

Once a CFD model had been chosen and had been set up, the first simulations could be run and the first results could be gathered. The results that were found using the CFD simulations are presented in this chapter. The chapter starts out with the first steps that were taken in the simulation campaign. Beforehand, it was not known which simulations were going to be run. There were plans to look at varying the equivalence ratio, the spark timing and the injection timing, but as no simulations had been run before, it was unknown which of these might prove doable, or even useful. Once the initial simulations had been run and the simulation process had been optimised, different combustion processes were observed and it was found that the injection of hydrogen could be optimised to ensure better engine performance. This will be discussed in detail, as it might prove very useful in the future development of internal combustion engines. After this, the effect of the equivalence ratio and spark timing on the engine performance will be discussed. It is also important to compare the combustion of hydrogen with the combustion of gasoline, to see if the power output of hydrogen can get close to that of gasoline and to compare the combustive processes, to potentially discover changes that need to be made to the engine. Lastly, the pressure peaks of hydrogen combustion are discussed. This was a major safety concern before this simulation campaign, which is why it was attempted to lower the pressure peak and investigate how problematic these pressure peaks are.

6.1. Optimised Injection

In this section, the phenomenon of 'optimised hydrogen injection' is described. Firstly, it is explained how this optimised injection was discovered, after which the differences with 'normal' combustion are discussed. Finally, the effects of incomplete combustion due to attempted optimised injection are explained.

6.1.1. Initial Investigation

As stated before, there was no list of simulations beforehand that had to be run in order to get the desired results. Part of the reason for this was that the amount of fuel that is injected into the engine can not be set directly, but is determined by a number of factors, such as the velocity profile of the fuel at the inlet boundary condition, the pressure and temperature of the fuel and the pressure and temperature of the combustion chamber. Therefore, these parameters had to be varied in the first simulations to find a relation between these parameters and the equivalence ratio in the combustion chamber. It took some time to get this right, but once it was, the next steps could be taken.

Those next steps were to evaluate the influence of both different equivalence ratios and different injection timings on the performance of the engine. That initial investigation consisted of thirty simulations, varying between six different equivalence ratios (0.47, 0.6, 0.72, 0.89, 1.06, 1.28) and five different injection timings (40, 60, 80, 100 and 120 degrees BTDC). This injection timing marks the start of injection, after which all injections lasted for 20 degrees. So if the injection timing was 60 degrees BTDC, the injection lasted from 60 degrees BTDC to 40 degrees BTDC. The equivalence ratio is defined as the ratio of the actual fuel to air ratio, to the stoichiometric fuel to air ratio. It was shown in section 4.2.1 that the volumetric fuel to air mixture for hydrogen is 2.38:1. However, for the equivalence ratio, the fuel to air ratio in terms of mass is needed. This can be calculated in a similar way to be 34.33:1. This means that in stoichiometric conditions, hydrogen has a mass fraction of 0.0291 of the total mass in the combustion chamber. The equivalence ratio per engine cycle is then calculated by dividing the mass fraction of hydrogen inside the combustion chamber by the stoichiometric hydrogen mass fraction. The range of equivalence ratios that is chosen for

the initial investigation might seem on the higher side, considering that abnormal combustion phenomena may occur at higher equivalence ratios, as was explained in chapter 4. It would therefore make sense to choose lower equivalence ratios, to avoid any of these abnormal combustion phenomena. However, the eventual application for a hydrogen internal combustion engine in this project is a high power application, namely as an aircraft engine. It was therefore decided to look at somewhat higher equivalence ratios, as these are expected to deliver more power.

Another parameter that can be varied is the engine speed. This engine speed is measured in revolutions per minute (RPM), where one revolution is one full rotation of the crank shaft. It can be imagined that the engine speed influences the flow inside the combustion chamber and therefore influences the performance of the engine. When looking at engine performance figures for aircraft piston engines, it can be noticed that the engine is usually rated for one single engine speed. This is because, contrary to a car engine, an aircraft engine spends most of its life running at one single engine speed, as it does not have to slow down and accelerate again at traffic lights or roundabouts. As such, it was decided that varying the engine speed, even though it can greatly influence the engine performance, was not a priority. Therefore, all of the simulations performed in this work, were performed at an engine speed of 2000 RPM. Different engine speeds will have to be evaluated at a later stage in the project. Because even though an aircraft engine spends most of its time at one engine speed, it still needs to be able to perform at all engine speeds between idle and full throttle.

The performance results of all of these simulations were evaluated and plotted against each other. One of the graphs that was examined can be seen in Figure 6.1.

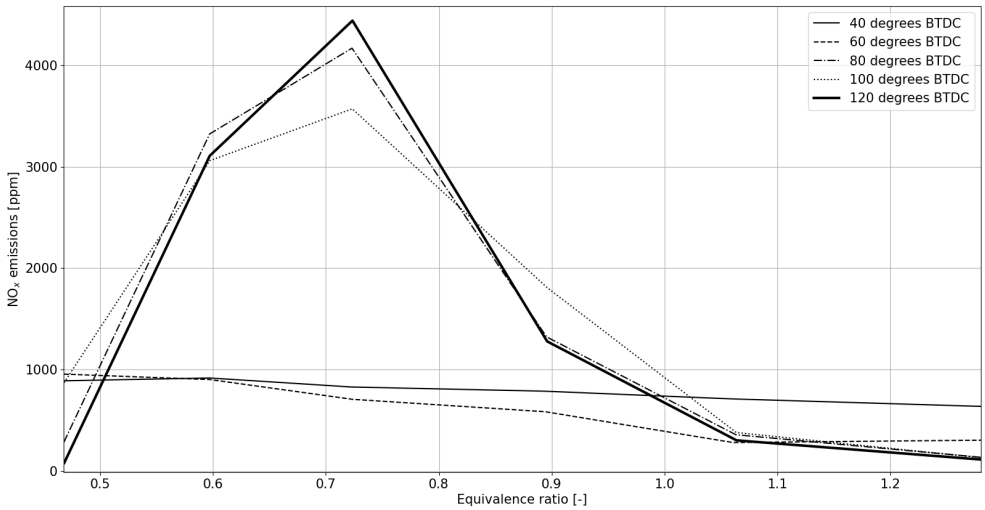

Figure 6.1: NO_x emissions vs. equivalence ratio for different injection timings

In this graph, the NO_x emissions are plotted against the equivalence ratios for different injection timings. The first thing, and as it turns out also the most important thing, that can be seen from this figure is the difference between the group of 40 and 60 degrees BTDC and the group of 80, 100 and 120 degrees BTDC. In the latter group, a parabolic relationship can be seen between the equivalence ratio and the NO_x emissions. As the equivalence ratio increases from 0.5, so do the NO_x emissions, until there is a peak around an equivalence ratio of 0.7. From there, the emissions decline again, until they seem to level out. The emission lines for the last two injection timings look quite different. They start out at higher NO_x emissions, but where the other lines go up, these lines slope down slightly, in a more or less straight line.

The difference between the two groups of lines is clearly the largest at an equivalence ratio of 0.71. Therefore, Figure 6.2 shows the NO_x emissions versus the start of injection at an equivalence ratio of 0.71.

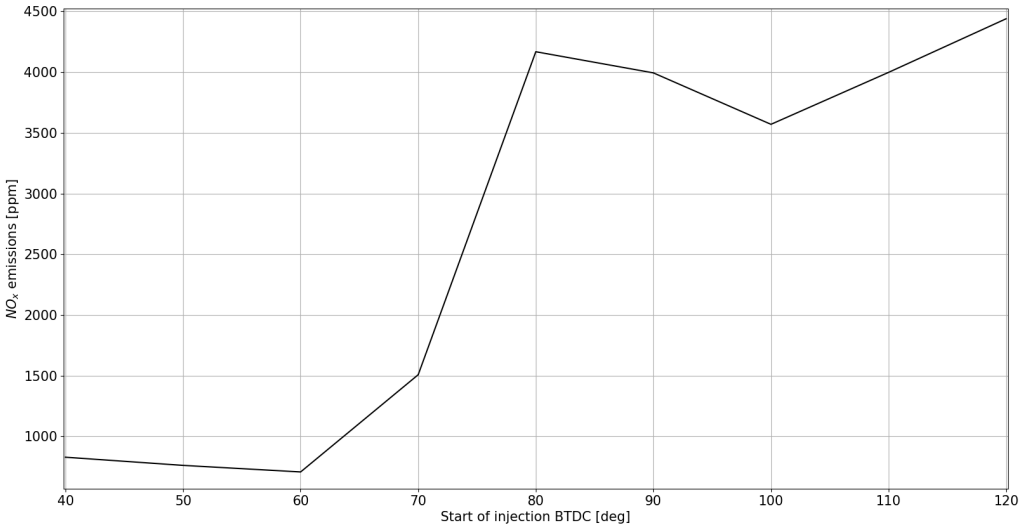

Figure 6.2: NO_x emissions vs. start of injection BTDC, with ϕ=0.71

It can clearly be seen from this figure that there are indeed two groups of injection timings, one with early injections that result in high NO_x emissions and one with later injections that result in lower NO_x emissions.

At first, no explanation could be found for this phenomenon, so further investigations had to be performed to find out what is causing these differences in NO_x emissions.

6.1.2. Different types of combustion

The first step that was taken, was to look at the pressure curves of these different injection timings, to see if any difference could be seen there. And indeed, quite a significant difference could be observed. Figure 6.3 shows the pressure curves of an early hydrogen injection engine cycle (start of injection (SOI) at 160 degrees BTDC) and, what in this report will be called, an optimised hydrogen injection engine cycle (SOI at 40 degrees BTDC).

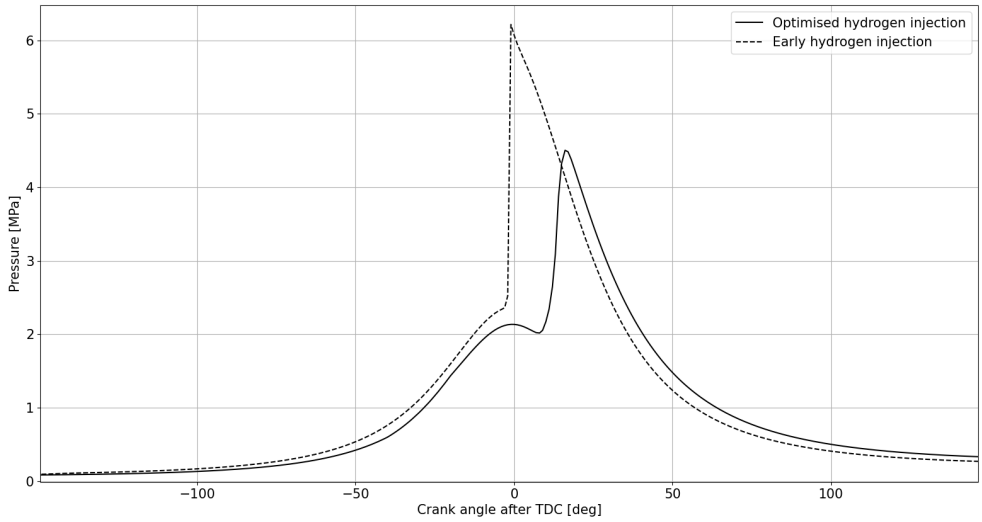

Figure 6.3: Pressure plots of early and optimised hydrogen injections, both at ϕ=0.7

It is immediately clear that these two engine cycles are very different. First of all, it can be seen that the pressure in the early injection cycle is higher in the build-up to TDC than in the optimised case. This has

to do with the moment of injection in the cycle. Take the point at 50 degrees BTDC. At this point, all of the hydrogen has been injected into the combustion chamber for the early injection cycle. This is done at high pressure, into a closed chamber. Because of this, the pressure in the combustion chamber will rise. But in the optimised case, no hydrogen has been injected at 50 degrees BTDC, so therefore the pressure is lower. The next difference that can be seen in the graph is the difference in combustion timing between the early and the optimised cycle. In both engine cycles, a spark is fired 5 degrees BTDC, so the difference is not due to different spark timings. The reason for this ignition delay will be discussed later in this section, but also in section 6.2. The third and last difference, and probably the most obvious one, is the difference in shape between the two pressure peaks. Not only is the pressure peak in the early injection cycle significantly higher, the peak itself is also steeper, meaning that the combustion is faster.

To understand these differences in pressure curves, the processes inside the combustion chamber must be examined in detail. This will be done by looking at the hydrogen and temperature distributions within the combustion chamber. First of all, let's take a look at the hydrogen injection and distribution for the optimised hydrogen injection cycle. Figure 6.4 to 6.6 show three points along the injection timeline. The first image shows the hydrogen injection 5 degrees after it has started, so at 35 degrees BTDC. It can be seen that the piston has already moved quite far up and the volume inside the combustion chamber is already very small. As we go to the second image, which was taken 20 degrees after the first image, it can be seen that the hydrogen has hit the piston and is now moving upwards again in a ring shape. Finally, the third image shows the hydrogen at TDC.

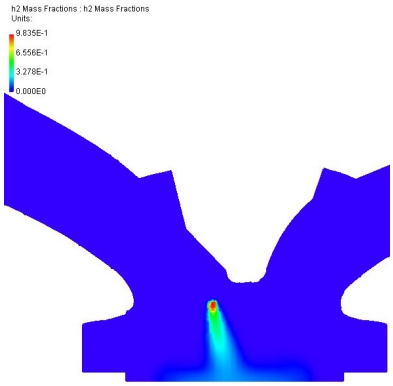

Figure 6.4: Optimised hydrogen injection at 35 degrees BTDC

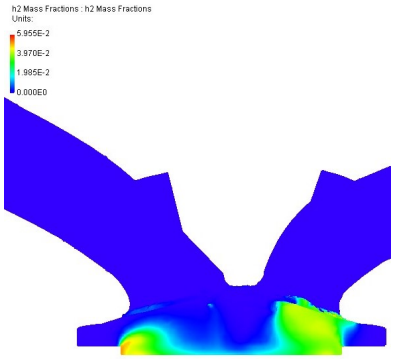

Figure 6.5: Optimised hydrogen injection at 15 degrees BTDC

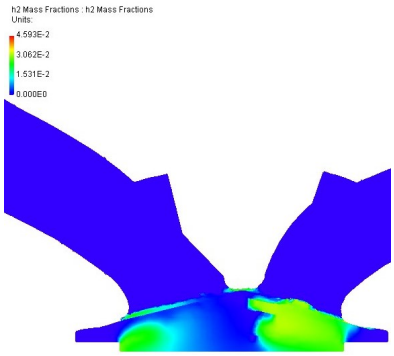

Figure 6.6: Optimised hydrogen injection at TDC

It was stated above that the hydrogen hits the piston and then moves up in a ring shape, but this was not really visible in the images. It can however be seen very clearly in Figure 6.7. This is the same engine cycle as the three images above, but now the engine is shown from below and the hydrogen distribution on the piston bowl is visible. In the centre of the piston, where the hydrogen first hit the bowl, almost no hydrogen is left. Instead, it has curled up and to the side, leaving a ring of hydrogen.

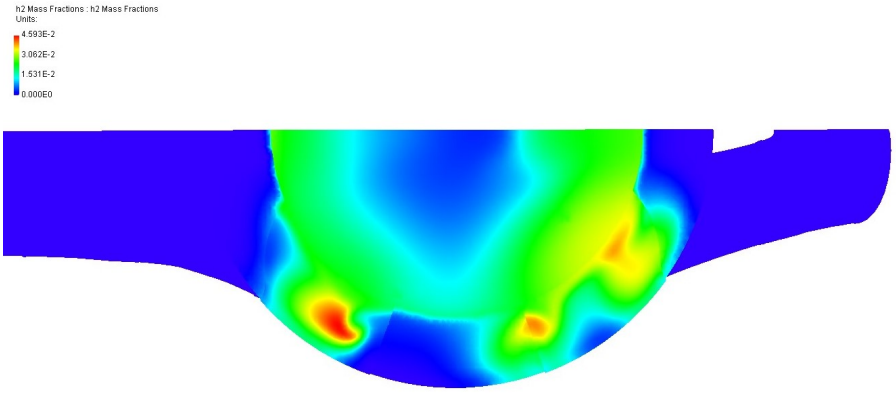

Figure 6.7: Bottom view of the hydrogen distribution at TDC, using optimised hydrogen injection

This ring of hydrogen in the optimised hydrogen injection case is in stark contrast with the hydrogen distribution in the early injection engine cycle, which can be seen in Figure 6.8. It is clear from this image that the hydrogen distribution is not homogeneous, but much more so than for the optimised injection.

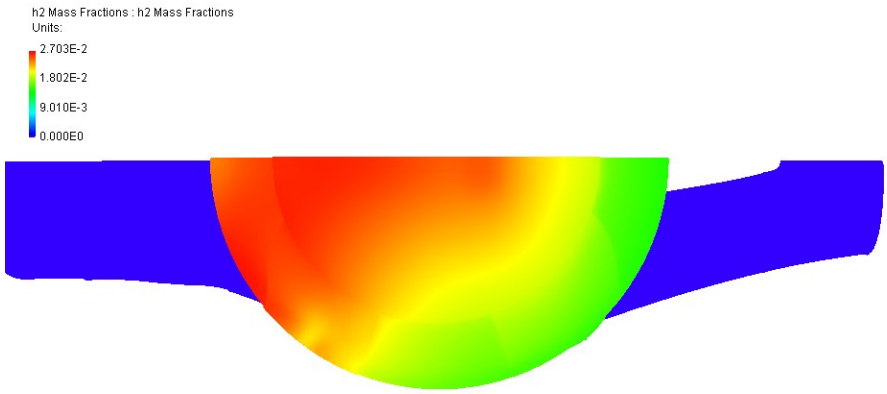

Figure 6.8: Bottom view of the hydrogen distribution at 5 degrees BTDC, using early hydrogen injection

With the clear difference in hydrogen distribution shown between the early and the optimised injection engine cycles, let's now look at how these differences influence the combustion phase of the engine cycles. Figure 6.9 to 6.20 show the development of the combustion inside the combustion chamber for the optimised hydrogen injection case. The spark is first lit at 5 degrees BTDC, but the flame only starts to develop after TDC, as can be seen in the images. The reason for this, is a combination of the distribution of the hydrogen and the location of the sparkplug. When the sparkplug is fired, the local equivalence ratio at the location of the spark is quite low. This low equivalence ratio results in a a slow flame propagation, as will be discussed further in section 6.2.

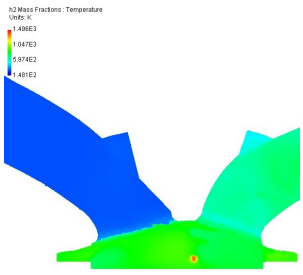

Figure 6.9: Temperature distribution inside the engine at TDC, using optimised hydrogen injection

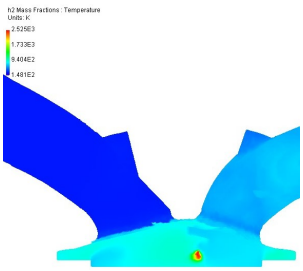

Figure 6.10: Temperature distribution inside the engine at 3 degrees after TDC, using optimised hydrogen injection

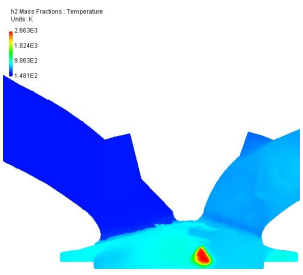

Figure 6.11: Temperature distribution inside the engine at 5 degrees after TDC, using optimised hydrogen injection

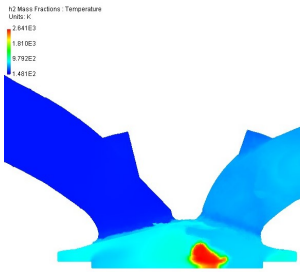

Figure 6.12: Temperature distribution inside the engine at 7 degrees after TDC, using optimised hydrogen injection

10 degrees after the spark was first fired, so at 5 degrees after TDC, the flame starts to first grow in size. But even once a flame has been developed, it still takes quite some time, another 10 to 15 degrees, before almost all of the hydrogen in the combustion chamber has reacted. This combustion sequence goes as follows. The first bit of hydrogen to combust is obviously the bit closest to the spark plug. As time goes on, this region of combusting hydrogen grows and reaches the pocket of higher density hydrogen that is located to the right of the sparkplug, as can be seen in Figure 6.6. This pocket of higher density hydrogen is part of the ring of hydrogen that was described earlier and can be seen in Figure 6.7. The combustion then 'moves' through this ring of hydrogen, until it reaches the left side of the the combustion chamber, as can just be seen in Figure 6.16.

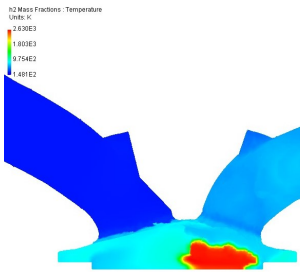

Figure 6.13: Temperature distribution inside the engine at 9 degrees after TDC, using optimised hydrogen injection

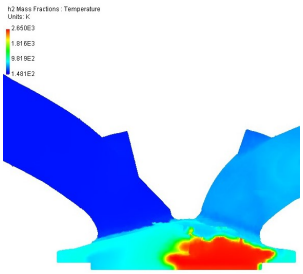

Figure 6.14: Temperature distribution inside the engine at 11 degrees after TDC, using optimised hydrogen injection

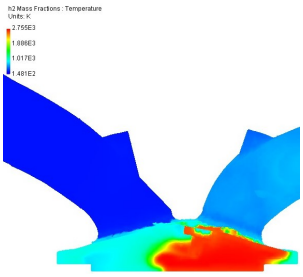

Figure 6.15: Temperature distribution inside the engine at 13 degrees after TDC, using optimised hydrogen injection

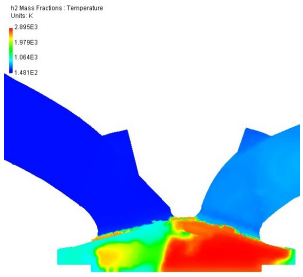

Figure 6.16: Temperature distribution inside the engine at 17 degrees after TDC, using optimised hydrogen injection

To show the movement of the combustive area through the combustion chamber even more clearly, let's look at the same sequence of temperature distributions from the bottom of the cylinder. In Figure 6.17 to 6.20, it can indeed be seen that the pocket of hydrogen on the right does indeed combust first. The flame then travels round the outside of the combustion chamber until it also reached the left side of the chamber. It must be noted that this is of course only half of the combustion chamber, so in reality, the flame will travel around the chamber both on the top and on the bottom side and the two will meet again on the left side of the cylinder.

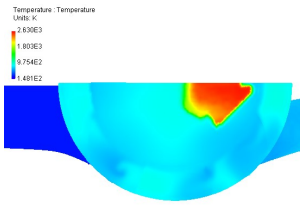

Figure 6.17: Bottom view of the temperature distribution inside the engine at 9 degrees after TDC, using optimised hydrogen injection

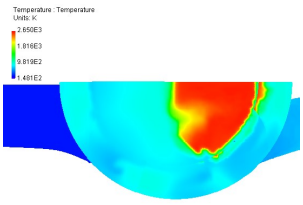

Figure 6.18: Bottom view of the temperature distribution inside the engine at 11 degrees after TDC, using optimised hydrogen injection

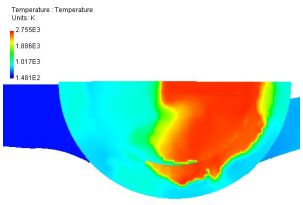

Figure 6.19: Bottom view of the temperature distribution inside the engine at 13 degrees after TDC, using optimised hydrogen injection

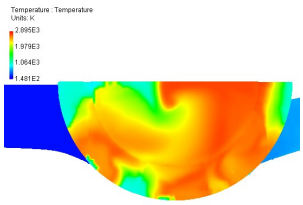

Figure 6.20: Bottom view of the temperature distribution inside the engine at 17 degrees after TDC, using optimised hydrogen injection

Now that we have seen the combustion process in the optimised hydrogen injection engine cycle, it is now time to look at the process in the early hydrogen injection engine cycle. Where the combustion in the previous cycle was quite complex, the combustion in the early injection case is quite simple, as can be seen in Figure 6.21 to 6.24.

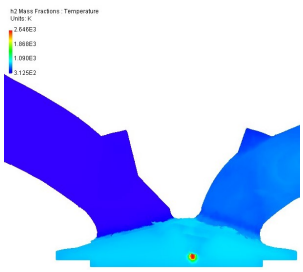

Figure 6.21: Temperature distribution inside the engine at 4 degrees BTDC, using early hydrogen injection

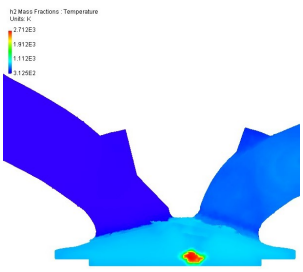

Figure 6.22: Temperature distribution inside the engine at 3 degrees BTDC, using early hydrogen injection

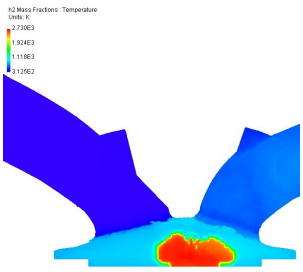

Figure 6.23: Temperature distribution inside the engine at 2 degrees BTDC, using early hydrogen injection

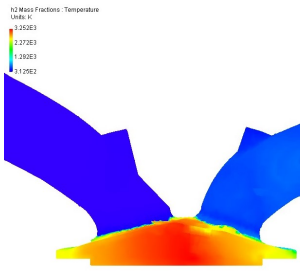

Figure 6.24: Temperature distribution inside the engine at 1 degrees BTDC, using early hydrogen injection

The first difference that can be noted is the duration of the combustion. In the optimised injection case, the combustion lasted more than 20 degrees between the moment the spark plug was fired and the moment that most of the hydrogen had been combusted. In the early injection case, this lasts about 4 degrees. Just 2 degrees after the spark plug has been fired, a clear flame development can already be seen in Figure 6.22. This difference in flame development is caused by the higher equivalence ratio at the location of the spark

plug in the early injection case. And where the flame had to find its way through the high density hydrogen pockets in the optimised injection combustion, it does not have to go through all that trouble here. The hydrogen distribution is quite even throughout the combustion chamber, so the flame can move in all directions simultaneously. And it does, as can be seen in Figure 6.23 and Figure 6.24.

Figure 6.3 already showed that the two hydrogen combustions occurred at different speeds, but after looking at the processes inside the combustion chamber, it is now also clear why this happens. The combustion in the optimised hydrogen injection engine cycle is slowed down by two factors. Firstly, the equivalence ratio at and near the location of the spark plug is low, which delays the development of the flame. But even after the flame has started to develop, it can't just travel in any direction like it does in the early injection case. Instead, it has to follow the ring of higher density hydrogen, which delays the combustion even more. So, now we know how it is that the two combustions are different, but what is the effect of that difference?

6.1.3. Effects on performance

So far, it has been concluded from Figure 6.1 and Figure 6.3 that there are two groups of engine cycles, each with a different type of combustion. It has also been shown where this difference in combustion comes from, but it has not been shown what the effect on the performance of engine of this difference is. In Figure 6.1, it was seen that the later or 'optimised' engine cycles result in lower NO_x emissions. One of the issues with internal hydrogen combustion is the resulting NO_x emissions. So for those emissions to be so much lower, is quite a big deal. Usually however, in hydrogen combustion, lower NO_x emissions come with a lower power output and a higher power output comes with higher NO_x emissions. With this in mind, the performance figures that are shown in Table 6.1 are quite counter-intuitive.

Table 6.1: Performance figures of early and optimised injection

	SOI BTDC [deg]	ϕ [-]	Gross indicated power [kW]	Max T [K]	NO_x emissions [ppm]
Early injection	160	0.7	4.60	2628.82	4164.39
Optimised injection	40	0.7	6.13	2367.06	1551.23

From Figure 6.1 it could already be seen that the NO_x emissions were much lower for later injection timings than for early ones, and this is confirmed by the table above. The NO_x emissions for the early injection case are more than twice that of the optimised hydrogen injection engine cycle. This difference is due to the difference in temperature that is reached within the combustion chamber, values that can also be seen in the table. From Figure 6.3, it was already concluded that the pressure peak was much higher and steeper for the early injection case. In Figure 6.25, it can be seen that this pressure peak is also reflected in the temperature inside the combustion chamber.

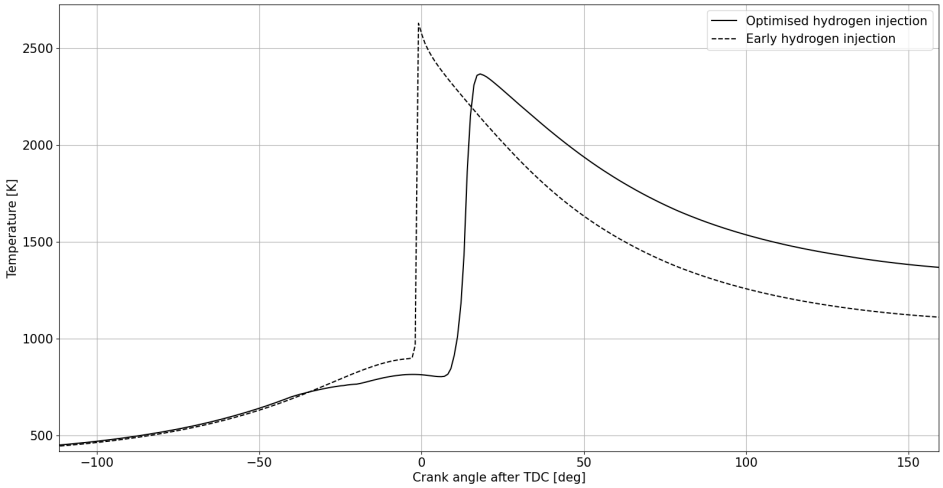

Figure 6.25: Temperature vs. crank angle of early and optimised hydrogen injection, both at ϕ=0.7

The temperature rise for the early injection case is much steeper and the peak is higher than that of the optimised injection. One reason for this, is that the combustion is much faster and and therefore also hotter. But an additional reason for this can be seen in the temperature diagram above. The hydrogen that is injected into the combustion chamber is injected at room temperature (293 K). At 40 degrees BTDC, the temperature inside the combustion chamber is about 750 K. When the hydrogen is injected at this point for the optimised hydrogen injection cycle, the hydrogen has a cooling-effect on the contents of the combustion chamber. This cooling-effect can clearly be seen in the graph, as the two lines are similar until the point where injection occurs in the optimised case. At that point, it can be seen that the temperature in the optimised injection case increases less than the temperature in the early injection engine cycle, which is because of this cooling effect. Because of this lower temperature at TDC, the maximum temperature in the combustion chamber is lower for the optimised injection engine cycle. The hydrogen in the early injection case is also injected at 293 K, but much earlier, where the temperature inside the combustion chamber is much lower (around 400 K) and the cooling effect is thus less pronounced. This lower peak temperature results in lower NO_x emissions. The relationship between peak temperature and NO_x emissions is exemplified by Figure 6.26.

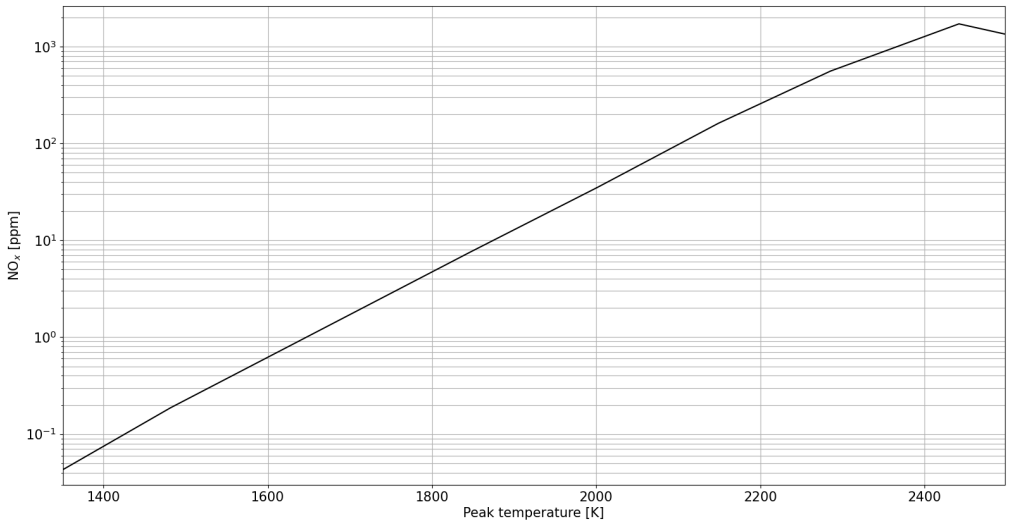

Figure 6.26: NO_x emissions vs. peak temperatures for indirect hydrogen injection

The lower NO_x emissions of the optimised hydrogen injection case have now been explained, but the higher power output has not. Figure 6.3 shows that the early injection case has a higher pressure peak and intuitively, this translates to a higher power output. However, judging from Table 6.1, this is not the case. So what is going on?

To answer this question, we must look at where the power that the engine produces comes from. For this analysis, instead of the power output, the work will be considered, but since power is just work per time, these two are interchangeable as long as you consider both cycles for the same amount of time. The work W [J] done by the engine is the force F [N] enacted on the piston, times the displacement S [m] of the piston:

$$W = FS \tag{6.1}$$

However, the force on the piston is not constant during the engine cycle, so instead, the following equation will be used:

$$W = \int F dx \tag{6.2}$$

Here, the force is integrated over the piston displacement. The next step is to realise that force equals pressure per area, so we can replace F with pA_p. Filling this into Equation 6.2, we encounter the term $A_p dx$, which is equal to the differential volume dV. The resulting equation therefore becomes:

$$W = \int pdV \tag{6.3}$$

This means that if we have a pressure-volume (pV) diagram, we will be able to find the work performed by the engine in a cycle. Figure 6.27 is such a pV diagram , where the pressure-volume curves of the early and optimised hydrogen injection engine cycles are shown.

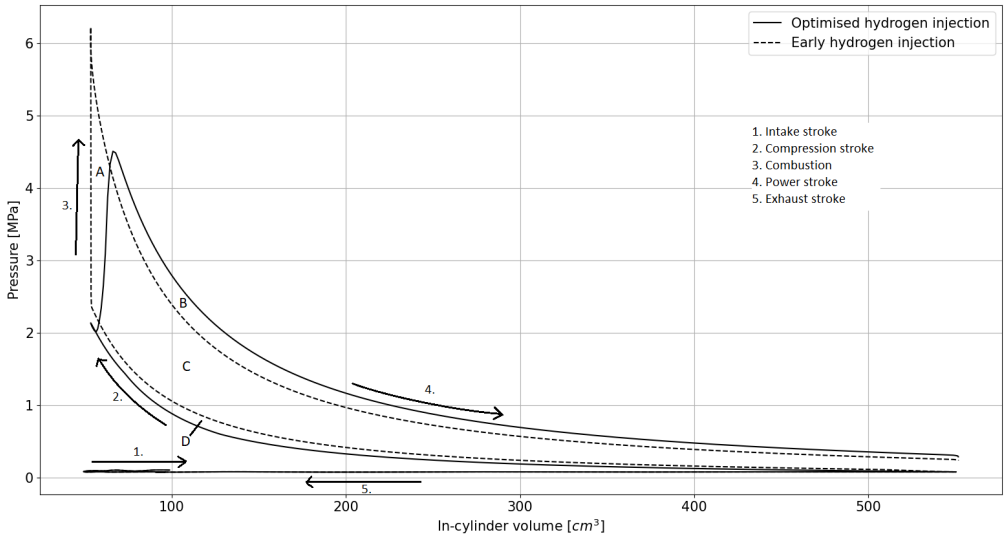

Figure 6.27: Pressure-volume diagrams for early and optimised hydrogen injection, both at ϕ=0.7

In this graph, there are four areas that are of importance, labelled A through D. The work done by the early injection case can be found by adding areas A and C, while the work done by the optimised case can be found by adding areas B, C and D. It can therefore be seen that the early injection case does indeed do more work during its pressure peak, but the optimised cycle makes up for that in two areas. The first one is area D, which is there because during compression, the early injection case has a higher pressure, due to the hydrogen that has already been injected into the closed-off combustion chamber. The second area is area B. which stems from the slower, but longer-sustained combustion of the optimised cycle. Together, areas B and D are larger than area A, which is why the work and power outputs of the optimised hydrogen injection cycle are higher than those of the early injection case.

One way to think of this is as follows; by spreading the combustion over a longer period of time, the conversion of chemical heat to kinetic energy is more efficient in the optimised injection cycle. In the early injection case, the combustion process is so sudden, that less of the energy can be transferred to the piston, and therefore less work is done on the piston.

6.1.4. Incomplete combustion

One of the goals of designing or running an internal combustion engine is what is called 'stable combustion'. This means that each of the engine cycles is virtually identical and that no misfiring or backfiring occurs. With direct injection, there is almost no chance backfire occurring. However, the occurrence of a misfire in an optimised hydrogen injection engine cycle is quite a real possibility. To understand this, one simply has to look at Figure 6.6, where the density of hydrogen close to the spark plug is so low that is slows down the flame propagation significantly. This is of course a balancing act, where the middle needs to be found between a density that is too high and results in a flame that moves too fast, and a density that is too low, where no flame is formed or the flame is quenched. During the optimisation of the hydrogen injection in this work, both these conditions were found. Where a density close to the spark plug that is too high will still lead to combustion of the hydrogen-air mixture, this will not occur if the density is too low. This section investigates what happens when such a misfire occurs and what the consequences are for the following combustion cycle.

Figure 6.28 shows the pressure plots for four consecutive engine cycles. It also shows the amount of hydrogen that is present inside the combustion chamber along these four engine cycles.

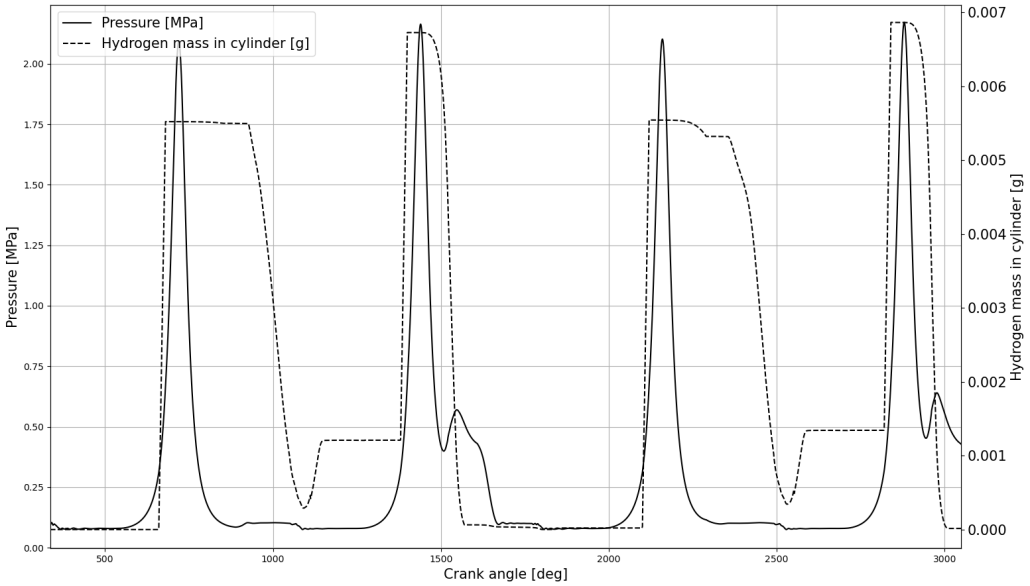

Figure 6.28: Pressure and hydrogen mass vs. crank angle, for ϕ=0.5 and SOI at 60 degrees BTDC

Looking at the first cycle, with TDC at 720 degrees, it can be seen that hydrogen is injected during the compression stroke, but that almost none of the hydrogen is burnt. Next, the exhaust stroke can be seen, where most of the hydrogen is expelled from the engine into the exhaust. A bounce-back in the amount of hydrogen inside the combustion chamber can be seen around a crank angle of 1100 degrees. At this point, the inlet valve is opened. The pressure inside the combustion chamber is still slightly higher than the pressure in the inlet, so some of the contents of the combustion chamber flow into the inlet, including some of the hydrogen that remained in the combustion chamber. As the intake stroke progresses, that hydrogen is sucked back into the combustion chamber and the amount of hydrogen inside the combustion chamber stays the same for a while, at just over 0.001 g. After the inlet stroke, the compression stroke follows, during which a new load of hydrogen is injected. Note that the amount of hydrogen inside the combustion chamber after injection is now higher than it was in the previous cycle. At first, it seems like no combustion occurs in this cycle either, but then, around a crank angle of 1500 degrees, the pressure increases slightly and most of the hydrogen is burnt. After this, basically the same thing repeats itself, although in the third cycle, slightly more hydrogen is burnt than in the first cycle and even more hydrogen is left inside the combustion chamber after the exhaust stroke, which explains why the pressure peak in the fourth cycle is slightly higher than in the second cycle.

Figure 6.29 and Figure 6.31 show the hydrogen distribution 5 degrees BTDC in the the second cycle, where Figure 6.30 and Figure 6.32 show the same moment in the cycle, but now for the third cycle. The difference in hydrogen distribution is subtle but still noticeable. The difference is basically that the hydrogen density is slightly higher throughout the whole combustion chamber in the second cycle than it is in the third cycle.

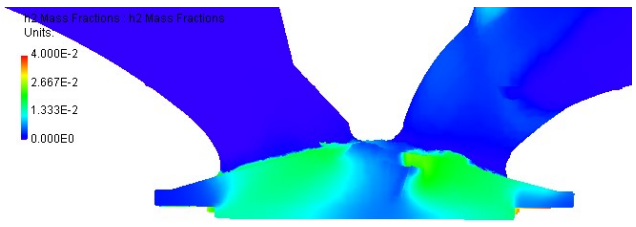

Figure 6.29: Hydrogen distribution in the combustion chamber at 5 degrees BTDC in the second cycle

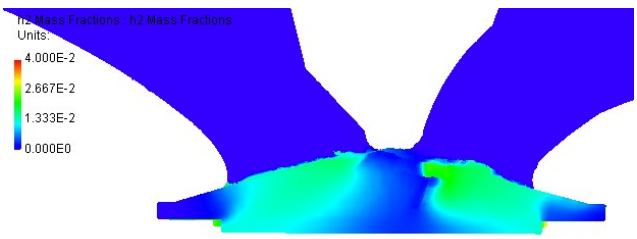

Figure 6.30: Hydrogen distribution in the combustion chamber at 5 degrees BTDC in the third cycle

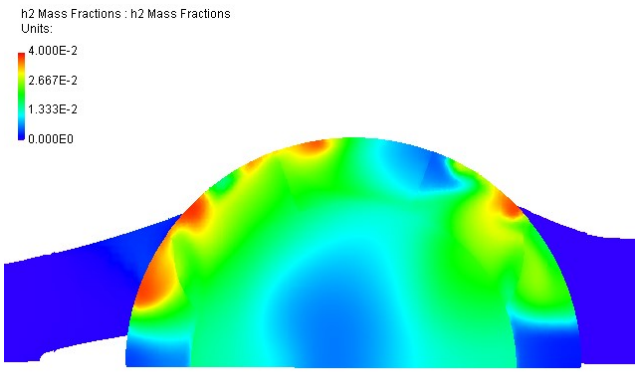

Figure 6.31: Hydrogen distribution in the combution chamber at 5 degrees BTDC in the second cycle, bottom view

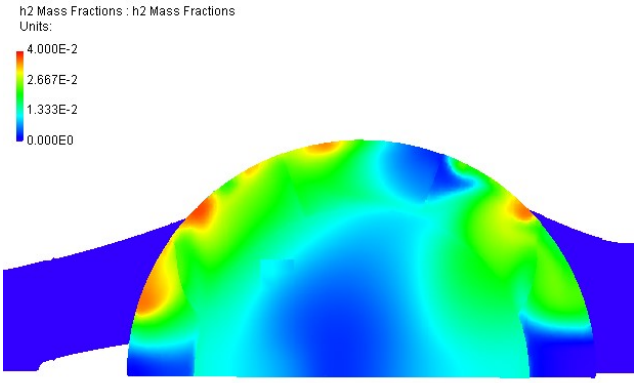

Figure 6.32: Hydrogen distribution in the combution chamber at 5 degrees BTDC in the third cycle, bottom view

Apparently, such a small difference in overall hydrogen density can mean the difference between a misfire and a full combustion, although it must be said that the combustions in the second and fourth cycle are very inefficient, as the combustion is so slow. So, how bad is it if the engine is tuned such that these are the resulting engine cycles? Well, in previous sections, the optimised injection cases were compared to the early injection cases, so let's do the same here (though 'optimised' might not be the correct term for these engine cycles). The gross indicated power produced by an engine cycle with direct injection, ϕ = 0.5 and an SOI at 160 degrees BTDC, is 4.3 kW. The total gross indicated power produced by the four engine cycles as shown in Figure 6.28, so with ϕ = 0.5 and an SOI at 60 degrees BTDC, is 3.5 kW. The average power per cycle would then be about 0.88 kW per cycle.

It is now clear that the difference between a successful combustion and a misfire is very small in the realm of optimised injections. Great care should therefore be taken when employing optimised injection, as it could lead to a great loss of power if implemented incorrectly.

One idea to limit the risk of a misfire for optimised injection, is to split the injection into two separate injection moments. By having part of the hydrogen injected early on in the engine cycle, a base layer of well-mixed hydrogen is created, on top of which more hydrogen is injected in strategic places. By doing so, combustion is almost guaranteed, but some optimisation in the second injection can still take place. More research into this area is needed, but to see if the concept works, the incomplete engine cycle that is shown above was modified to incorporate this idea. The amount of hydrogen was split evenly, with half being injected early, at 160 degrees BTDC and half injected at the original injection timing. Figure 6.33 shows the results of the split injection case compared to an early injection cycle.

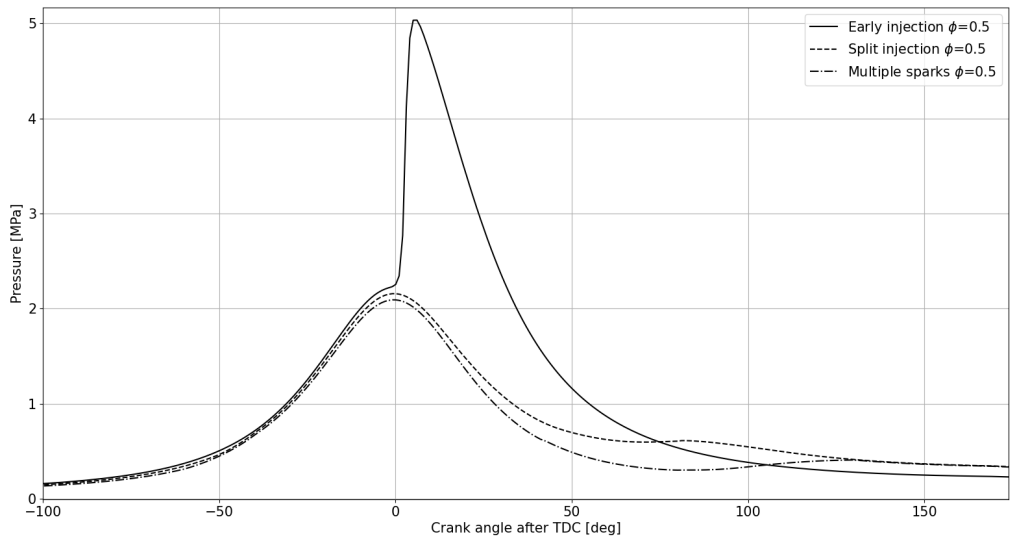

Figure 6.33: Pressure vs. crank angle for early and split injection and for multiple sparks engine cycles

It is clear that the split injection cycle combusts very late and very slowly. Almost all of the hydrogen is combusted, but because it happens so late in the cycle, the power output is much lower, at 2.4 kW vs. 4.3 kW for the early injection case. So, injecting part of the hydrogen early did prevent the misfire from occurring, but it would have been more efficient to inject all of the hydrogen early. This example of a split injection strategy is just that, one example out of the many possible combinations that there are for multiple injection engine cycles. It is therefore recommended that more research is done into this subject, to further explore the potential of this concept.

Another idea would be to fire multiple sparks at different timings, to try to force combustion, even if it is at a later stage in the engine cycle. Figure 6.33 also shows a pressure curve for an engine cycle in which such a tactic is employed. It can be seen that combustion does take place here, but only at a very late stage. In this figure, a spark is fired at four points in the engine cycle; at 5 degrees BTDC, 10 degrees after TDC, 25 degrees after TDC and 40 degrees after TDC. The major part of the combustion only occurs after the spark is fired for the fourth time, at which point the piston has moved down so far that a lot of potential work has been lost. In the end, this cycle produces 1.1 kW, compared to 4.3 kW for early injection with the same amount of hydrogen injected. This shows that even though this method can be used to make sure that most of the hydrogen is eventually burnt, the method can not make up for the main flaw in this engine cycle; the poor injection strategy. The multiple sparks method shown here was only tested for one engine cycle, so further research should be done to see if better results can be found for different engine cycles with different engine flows.

6.2. Equivalence Ratio

The equivalence ratio is probably the parameter, out of the ones discussed in this work, that has the most influence on the performance of the engine. In subsection 4.1.1, it was discussed that a higher equivalence ratio can lead to abnormal combustion phenomena such as knocking. On the other hand, an equivalence ratio that is too low can result in a misfire, where no combustion takes place. Clearly, a middle ground should be found between these two extremes. But apart from these extremes, what influence does the equivalence ratio have on the performance of a hydrogen internal combustion engine?

The first performance parameter that will be looked at in this section is the gross indicated power. The relation between this gross indicated power and the equivalence ratio can be seen in Figure 6.34.

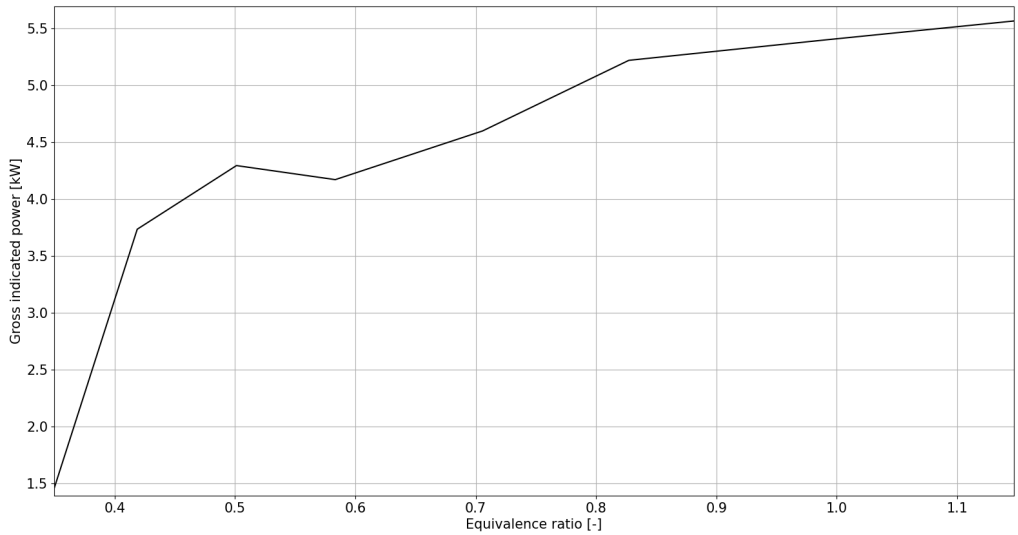

Figure 6.34: Gross indicated power vs. equivalence ratio for direct injection engine cycles, SOI at 160 degrees BTDC

The relationship between power and equivalence ratio is very clear from this graph. The higher the equivalence ratio, the higher the output power of the engine. This makes intuitive sense, as a higher equivalence ratio means that, for the same amount of intake air, more hydrogen is injected into the combustion cham-

ber, so there is more hydrogen to combust, which results in more power. However, looking at the relative increase in power with equivalence ratio, it can be seen that when the equivalence ratio is doubled from 0.5 to 1.0, the gross indicated power increases, but is far from doubled. In fact, from 4.3 kW to 5.4 kW (which corresponds to a doubling in equivalence ratio) is only a 25% increase. So even though the output power is increasing, the efficiency seems to be decreasing.

This is exactly what we see when looking at Figure 6.35.

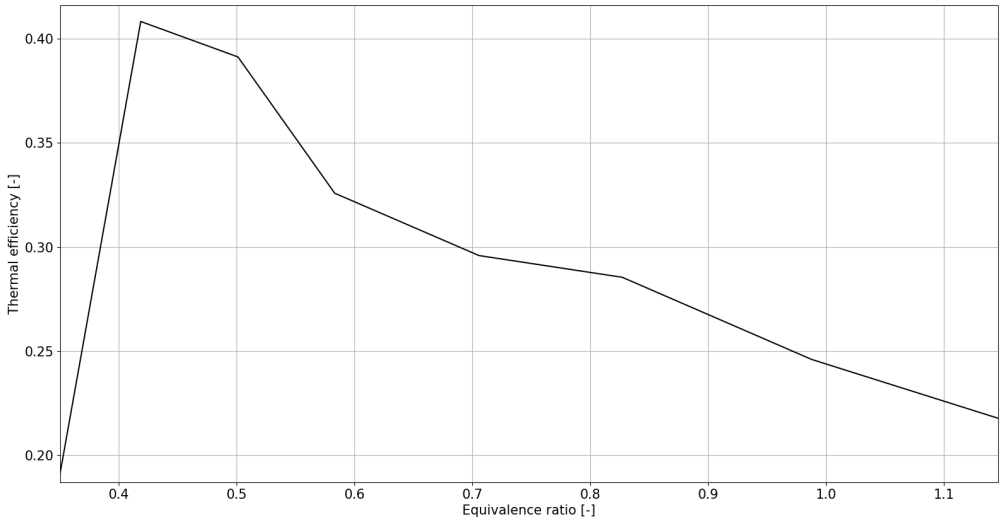

Figure 6.35: Thermal efficiency vs. equivalence ratio for direct injection engine cycles, SOI at 160 degrees BTDC

The thermal efficiency of a hydrogen internal combustion engine decreases dramatically as the equivalence ratio is increased. So even though the power increases as more hydrogen is combusted, the power output per unit of hydrogen decreases. However, a lower equivalence ratio does not always lead to a higher efficiency. Quite a drop in efficiency can be observed in the graph going from just over 0.4 to about 0.35. This is because at some point, the equivalence ratio becomes so low that incomplete combustion starts to occur. In this case, injection occurs early on in the engine cycle, so the hydrogen-air mixture is quite homogeneous. Some of the hydrogen is still combusted, but the combustion happens a lot slower, so there isn't enough time to combust all of the hydrogen and as the piston moves down again, the pressure inside the combustion chamber decreases, further decreasing the combustion rate.

That hydrogen combustion happens slower at lower equivalence ratios can be observed from Figure 6.36, where the pressure peaks for different equivalence ratios are shown.

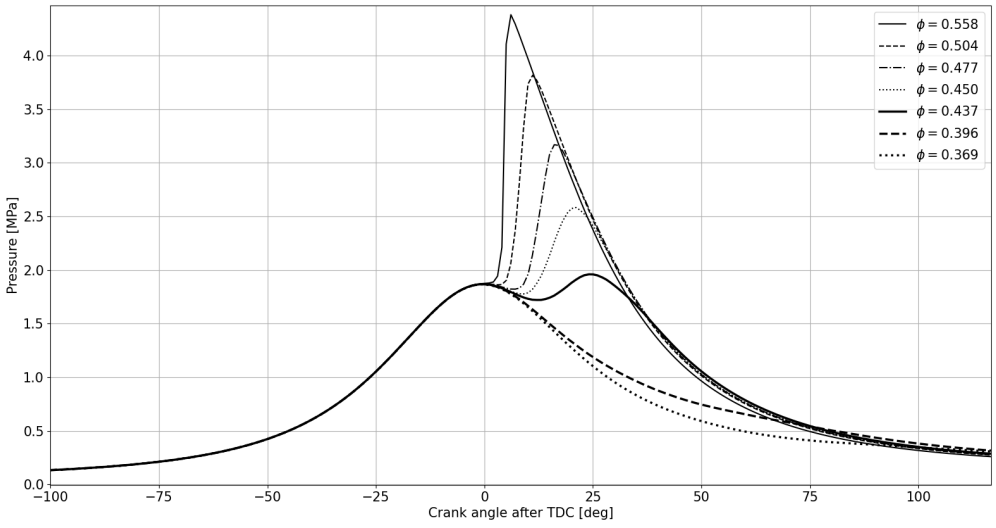

Figure 6.36: Pressure vs. crank angle for different equivalence ratios, indirect injection

Two major observations can be made from this graph. With decreasing equivalence ratio, the height of the pressure peaks decreases and the point of maximum pressure is delayed. This second point confirms that combustion occurs slower with decreasing equivalence ratio. It should be noted that the spark timing was the same for all of these engine cycles. The height of the pressure peaks is clearly influenced by the equivalence ratio. This was to be expected for two reasons. The first is that a lower equivalence ratio means less hydrogen inside the combustion chamber and therefore less energy to be released at combustion. The second reason has to do with the slower combustion. As combustion occurs later in the cycle, the pressure inside the combustion chamber has begun to decrease again, once the piston has passed TDC. The pressure at the moment of combustion is therefore lower, which results in a lower peak pressure.

But power is not everything. NO_x emissions are also a very important performance parameter for hydrogen internal combustion engines. Figure 6.37 shows the NO_x emissions as a function of equivalence ratio for early hydrogen injection engine cycles.

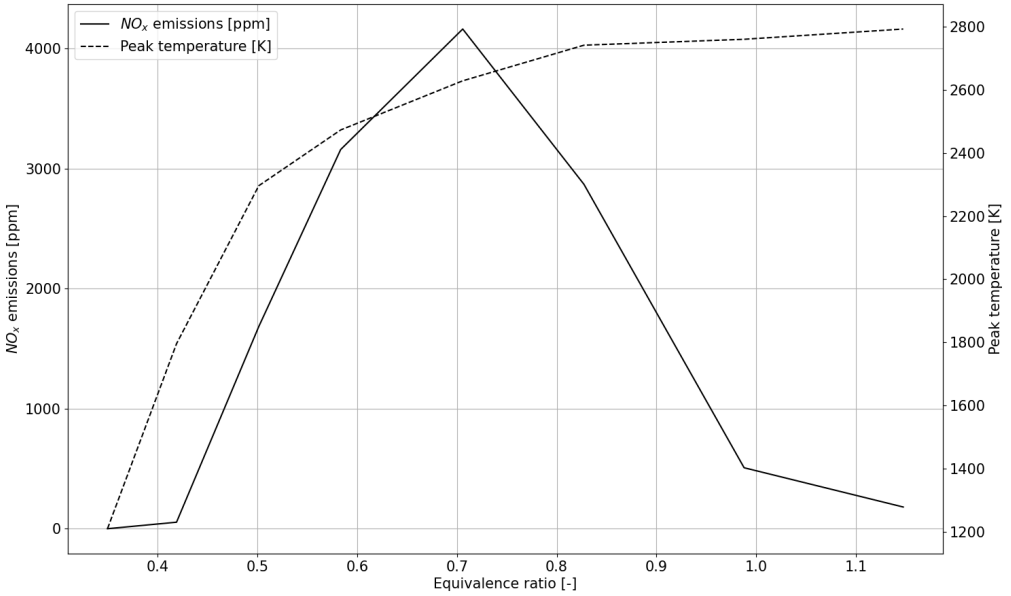

Figure 6.37: NO_x emissions and temperature vs. equivalence ratio for direct injection engine cycles, SOI at 160 degrees BTDC

Going from left to right in the graph, NO_x emissions start out low at lower equivalence ratios. Not only the pressure peaks are lower at lower equivalence ratios, but so are the maximum temperatures. The creation of NO_x typically occurs at higher temperatures and therefore the emissions at lower equivalence ratios are quite low as well. As the equivalence ratio goes up, so do the NO_x emissions. This trend can be explained by the higher peak temperatures inside the combustion chamber, which clearly go up. But as the equivalence ratios get to 0.7, 0.8, the NO_x emissions decrease again, where the temperatures remain high. This decrease in emissions has to do with the reduced amount of oxygen available to create NO_x. At an equivalence ratio of 1.0, the amount of hydrogen and oxygen should match such that both are used up completely during combustion. As the equivalence ratio approaches this stoichiometric point, the remaining amount of oxygen available for reaction with N_2 to create NO_x reduces, and thus the NO_x emissions reduce.

6.3. Spark Timing

One of the sub-questions of the research question of this work, asks how the spark timing influences the performance of a hydrogen internal combustion engine. The performance of a hydrogen internal combustion engine in this work is mainly judged by the output power of an engine cycle and the NO_x emissions during that engine cycle. Therefore, a diagram was created that shows exactly that, the power output and NO_x emissions as a function of the spark timing. This diagram can be seen in Figure 6.38.

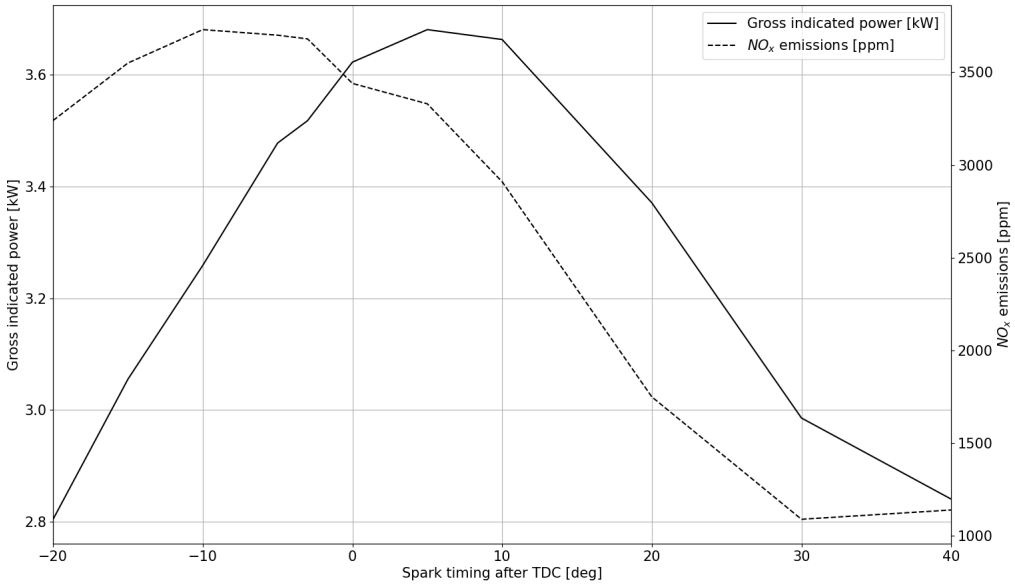

Figure 6.38: Gross indicated power and NO_x emissions vs. spark timing for ϕ=0.7

Both curves clearly have maximums at some spark timing, but interestingly enough, not at the same spark timing. The maximum power seems to be achieved at a spark timing of 5 degrees after TDC, while the maximum NO_x emissions occur at a spark timing of 10 degrees BTDC. The power curve is quite surprising, because this contradicts what we learn from conventional internal combustion engines. The theory in such engines behind the spark timing, is to time it such that the majority of the combustion occurs at or just after top dead centre. This way, force on the piston can be applied for the largest amount of distance and thus the highest efficiency is achieved. In order to achieve combustion at or just after TDC, the spark is often timed to be fired before TDC, because there is some delay between the firing of the spark and the combustion to occur (combustion delay). At 5 degrees after TDC, it can be seen from Figure 6.40 that the combustion delay is about 4 degrees, so the combustion does not occur until 9 degrees after TDC.

A reason for this difference in strategy for maximum power between a conventional internal combustion engine and a hydrogen internal combustion engine could have something to do with the phenomena that were described in section 6.1. Looking at Figure 6.39, it is clear that the height of the pressure peaks at combustion decrease with delayed spark timing, at least from a spark timing of 5 degrees BTDC onward.

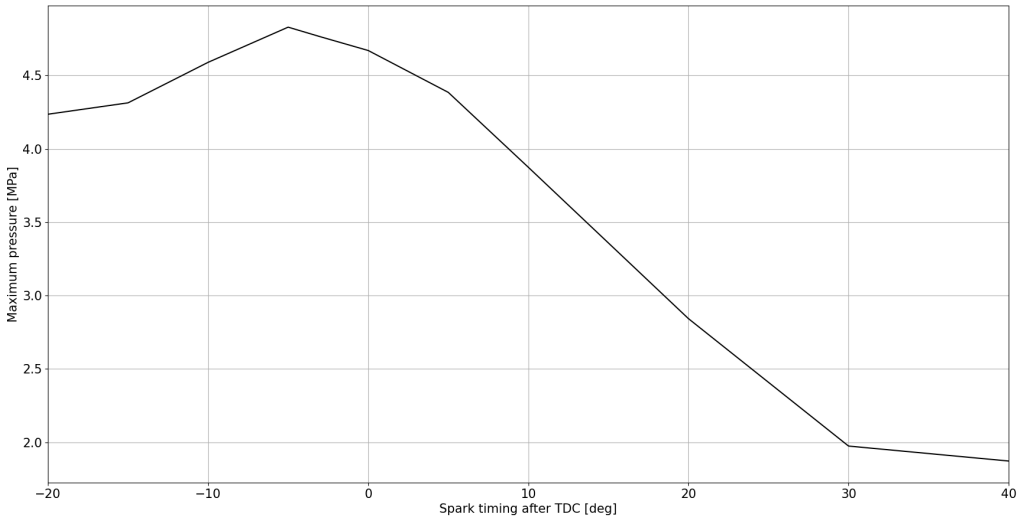

Figure 6.39: Maximum pressure vs. spark timing for ϕ=0.7 and indirect injection

This means that as the spark timing is retarded, the severity of the pressure peak goes down and the efficiency of the combustion increases. But while the efficiency due to slower combustion increases, the piston moves down further and further with retarding spark timing. This creates a maximum power output, after which the decrease in pressure in the combustion chamber due to the downward moving piston causes such a decline in potential work, that retarding the spark timing even further no longer increases the power output of the engine. For this particular engine and cycle conditions, this maximum lies at a spark timing of 5 degrees after TDC.

The NO_x emissions on the other hand, do have their maximum at a spark timing before TDC, because the NO_x emissions are dependent on the maximum temperature that is reached in the combustion chamber. It was shown before that the maximum temperature trend follows that of the pressure peaks and it does so again here.

Another interesting result of varying the spark timing, is a variable combustion delay. Figure 6.40 shows the combustion delay for different spark timings, both in degrees and in seconds. The combustion delay is measured as the time between the moment the spark is first fired and the moment when 2% of the total heat that will be released during combustion, is released.

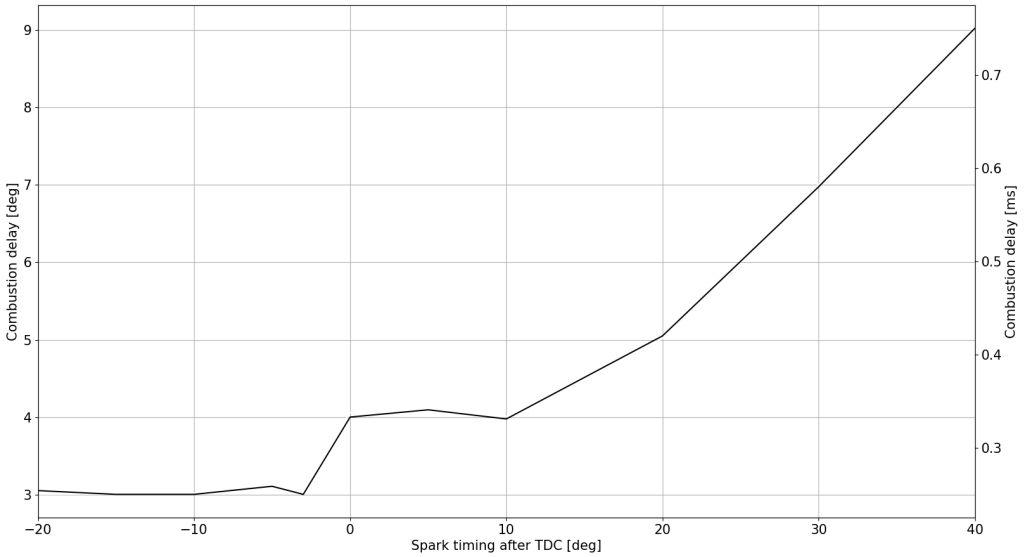

Figure 6.40: Combustion delay vs. spark timing for ϕ=0.7

A graph like this could be used to determine what spark timing should be used when performing experiments on a converted internal combustion engine. Because the combustion delay varies with spark timing, it can not simply be said that retarding the spark timing by 5 degrees will also retard the combustion by 5 degrees. This is dependent on the condition inside the combustion chamber. A later spark timing clearly results in a longer combustion delay, which is because at that later time, the pressure in the combustion chamber has reduced, which increases the combustion delay.

In the previous section on the equivalence ratio, it was shown that combustion occurs slower at lower equivalence ratios and therefore the pressure peaks are retarded for lower equivalence ratios (see Figure 6.36). In that case, the spark timing was kept constant. However, as the combustion timing varies with equivalence ratio, the optimum spark timing should vary with equivalence ratio too, to account for the different combustion velocities. The spark timing should therefore not only be optimised on an engine per engine basis, but also for each equivalence ratio. Furthermore, it is expected that the engine speed also greatly influences the optimum spark timing. It is therefore recommended that more research be done into the relation between engine speed and spark timing.

6.4. Indirect vs. Direct Injection

When the Lycoming engine that is part of this project is converted to run on hydrogen, a choice has to be made between direct and indirect injection. To aid in this decision, this section discusses the differences between these two types of injection that were found during the CFD investigation. It must be noted here once again, that in the indirect injection case, hydrogen and air are mixed outside the combustion chamber and the mixture that comes into the combustion chamber is a homogeneous mixture. In this regard, the indirect injection considered in this report more closely resembles an engine with a carburettor than for instance an engine with port injection.

To take out as much of the flow effects on the combustion process as possible, the direct injection cases considered in this section are all early injection engine cycles, where the start of injection occurs at 160 degrees BTDC. The aim of this strategy is to get a homogeneous mixture in both engine cycles. However, as could be seen before, the hydrogen-air mixture in the early injection case is not truly homogeneous. Figure 6.41 shows that although the hydrogen has spread throughout the combustion chamber, there is still a gradient in the hydrogen distribution.

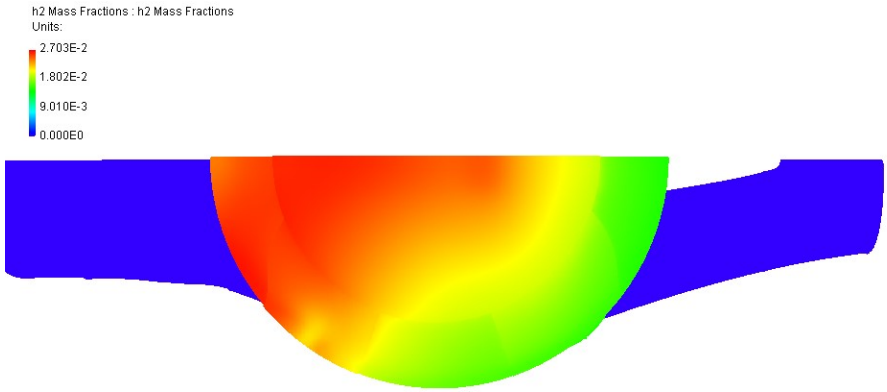

Figure 6.41: Bottom view of the hydrogen distribution at 5 degrees BTDC, using early hydrogen injection

In the indirect injection case on the other hand, the hydrogen-air mixture just before combustion is homogeneous, as can be seen in Figure 6.42.

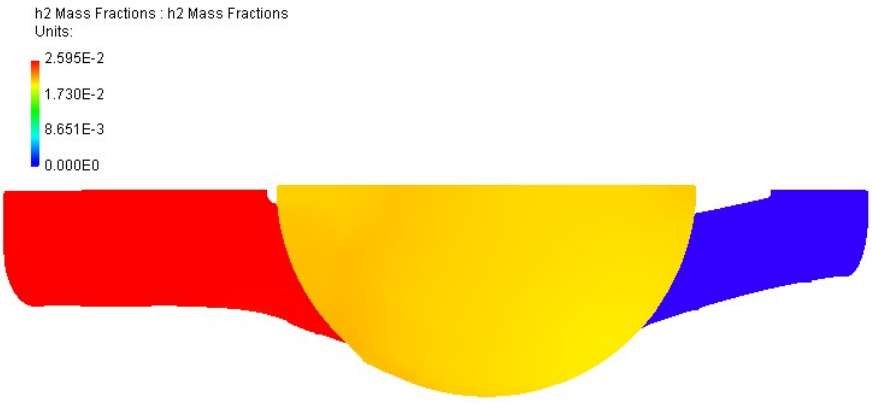

Figure 6.42: Bottom view of the hydrogen distribution at 5 degrees BTDC, using indirect hydrogen injection

Despite efforts to prevent it, the hydrogen distributions in the indirect and direct injection cases differ slightly, which might have an impact on the results. However, the difference is very slight, so it is judged to be acceptable for the comparison purposes in this section. The pressure plots for these two engine cycles can be seen in Figure 6.43.

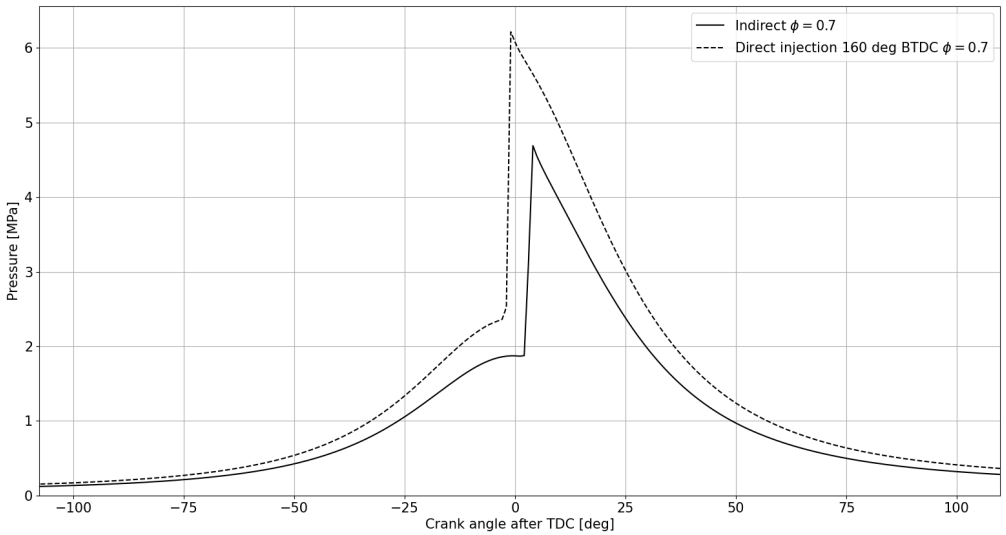

Figure 6.43: Pressure plots for early and indirect injection cycles

One obvious difference between these two pressure plots, is the much lower pressure during the compression stroke in the indirect injection case. This pressure loss is often called the volumetric loss and it is caused by the fact that the density of hydrogen is quite low, and therefore takes up a large part of the volume that is taken into the engine. In the indirect injection case, the hydrogen replaces air that would have otherwise been taken into the engine. In the direct injection case, there is more air and because of that, there is also more hydrogen, because the equivalence ratios in both of these engine cycles is the same. Simply put; there is more hydrogen-air mixture inside the combustion chamber during the compression stroke for the direct injection engine cycle. Because the combustion chamber volume is the same in both engine cycles, this means automatically that the pressure is higher in the direct injection case, as can be seen in the graph.

So, what is the result of this higher pressure? One of the results of this volumetric loss can be seen in Figure 6.44.

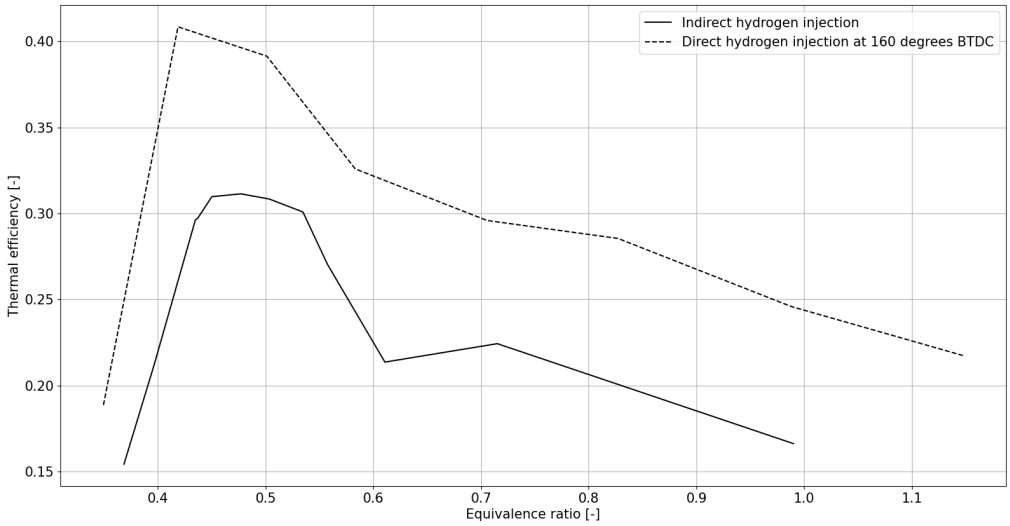

Figure 6.44: Thermal efficiency vs. equivalence ratio for direct and indirect hydrogen injection

The thermal efficiency of the engine cycles for the direct injection cases is higher than that for the indirect injection cases for every single equivalence ratio that was evaluated. This means that also the output power of the engine is higher for the direct injection cases, for every equivalence ratio. Since the application for hydrogen internal combustion engines in this project is to power a propeller on an aircraft, power is quite an important aspect of the performance. Another important aspect of the performance of the engine are the NO_x emissions. Figure 6.45 shows the NO_x emissions for both engine cycles.

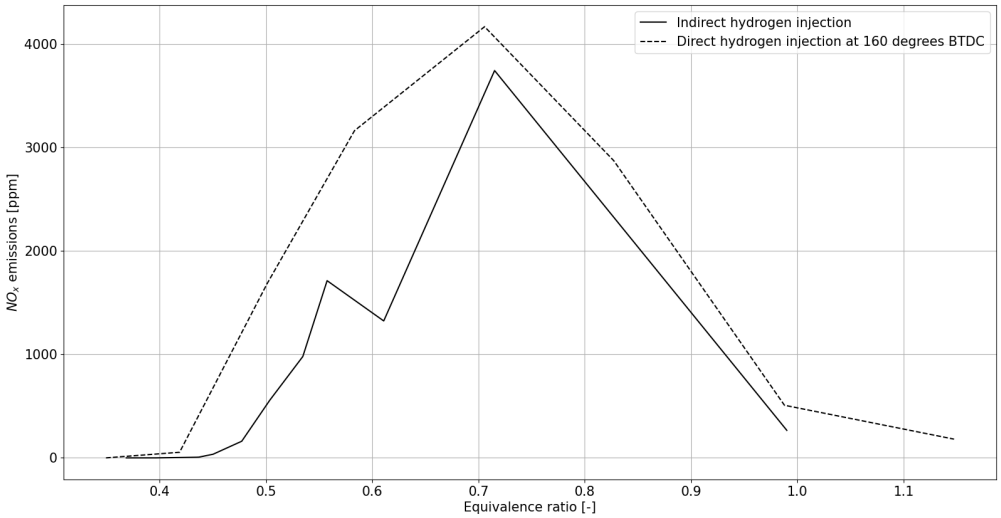

Figure 6.45: NO_x emissions vs. equivalence ratio for direct and indirect hydrogen injection

It is clear from this graph that the trend of higher NO_x emissions around an equivalence ratio of 0.7 holds for both direct and indirect injection. The NO_x emissions for the direct injection cases are higher than those of the indirect injection cases for all engine cycles, which is because of the higher peak temperatures inside the combustion chamber, which result in higher NO_x emissions.

6.5. Gasoline Combustion

In order to get an idea of the similarities and differences between hydrogen internal combustion engines and more conventional gasoline internal combustion engines, gasoline also had to be combusted in the same engine. Initially, it was attempted to inject gasoline in a similar manner as was done with hydrogen. However, this proved difficult, as gasoline is less flammable than hydrogen, so the window of conditions for which the air-fuel mixture will combust is narrower. In practice, this resulted in many simulations where the gasoline would not combust and the flame would be quenched, or where combustion would be very slow and inefficient.

As was stated before, the amount of fuel that is injected in this simulation is dependent on a great number of parameters, such as the velocity profile of the fuel at the inlet boundary condition, the pressure and temperature of the fuel and the pressure and temperature inside the combustion chamber. But those parameters do not only affect the amount of fuel that is injected, they also affect how the fuel is then distributed throughout the combustion chamber. Different pressures, temperatures and velocities may result in different shapes of the 'injection cone', and may also affect how fast the fuel mixes with the air inside the combustion chamber. But these are not the only parameters that influence how the fuel is distributed over the combustion chamber. There are also the injection angle (the direction in which the fuel is injected) and the injection timing.

Because hydrogen is more flammable, it will combust in more instances of combinations of these parameters than gasoline. This, combined with the fact that this research is focused on hydrogen internal combustion engines, led to the decision that getting the gasoline internal combustion engine simulation working would not be a top priority in this work. However, not having any gasoline simulation was not an option, as the hydrogen results need to be compared to gasoline, as one of the goals of this research is to assess the power potential of hydrogen internal combustion engines.

It was therefore decided to investigate the gasoline simulations that had been done up to that point, to see if a more stable form of combustion could be found that would lead to usable results, without the need for extensive optimisation. During this investigation, it would found, as could have been predicted, that a more homogeneous air-gasoline mixture will more easily combust. It was therefore decided to abandon direct gasoline injection and instead focus on indirect gasoline injection. It was shown before that for hydrogen, the difference between direct and indirect injection is very significant, due to the volumetric losses. For

gasoline however, the volumetric losses are a lot smaller. There will still be a difference in power output between direct and indirect injection for a gasoline internal combustion engine, but the difference will be much smaller than for a hydrogen internal combustion engine.

Therefore, in this section, indirect injection cycles are compared, of engine cycles with hydrogen and gasoline as a fuel. Figure 6.46 shows the pressure plots of four engine cycles, two hydrogen and two gasoline.

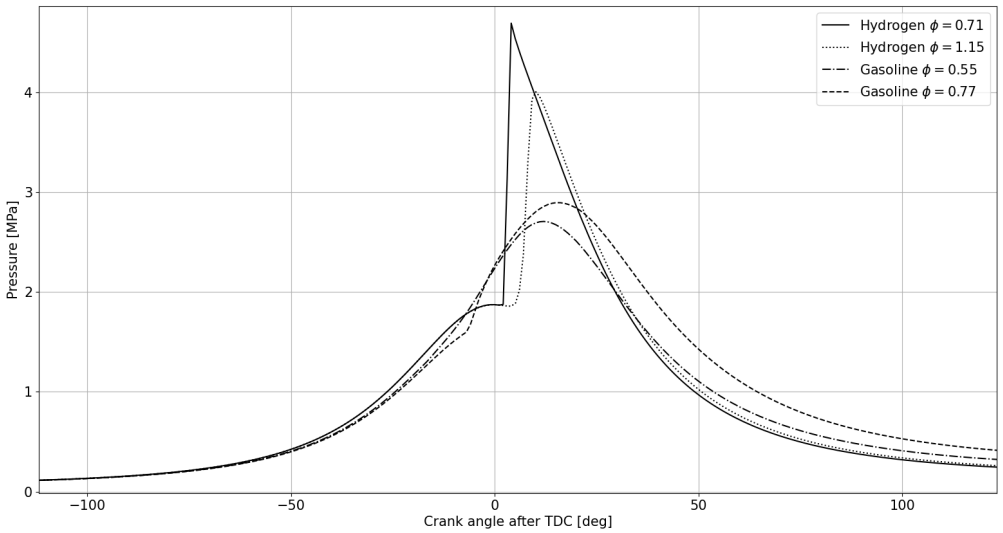

Figure 6.46: Pressure graph of indirect injection engine cycles of both gasoline and hydrogen

It is quite clear from this graph that the two different fuels have wildly different combustion characteristics. In the gasoline engine cycles, the difference between the compression and the combustion peaks can hardly be distinguished, because of how gradual the combustion of gasoline is. For hydrogen, we again see the steep and high pressure peaks that we have seen before.

The output power of all four engine cycles from the graph can be seen in Table 6.2, including three additional engine cycles, two early injection cases and one optimised injection cycle.

Table 6.2: Power outputs of various engine cycles, both gasoline and hydrogen

Cycle type	ϕ [-]	Gross Indicated Power [kW]
Gasoline indirect injection	0.77	5.80
Gasoline indirect injection	0.55	4.12
Hydrogen indirect injection	0.99	3.38
Hydrogen indirect injection	0.61	2.91
Hydrogen direct early injection	0.99	5.40
Hydrogen direct early injection	0.58	4.17
Hydrogen direct optimised injection	0.71	6.23

The first thing to note from this table is of course the higher power output for the gasoline cycles compared to the indirect hydrogen cycles. This was to be expected, as with indirect hydrogen injection, there are quite large pressure losses due to the low density of hydrogen. What is also interesting to note, is the difference in the relation between the equivalence ratio and the gross indicated power for hydrogen and gasoline. A 40% increase in gasoline equivalence ratio, from 0.55 to 0.77, results in a 41% increase in power. For hydrogen, a 62% increase in hydrogen equivalence ratio results in only a 16% increase in power. This has to do with the higher efficiency of hydrogen combustion at lower equivalence ratio, as was discussed in section 6.2.

Looking at the early direct injection engine cycles, it can once again be concluded that direct injection is necessary for the high power application of an aircraft piston engine. At an equivalence ratio of 0.58, direct hydrogen matches the power output of an indirect injection gasoline engine at an equivalence ratio of 0.55. At higher equivalence ratios, the hydrogen engine falls behind, due to the lower efficiency of a hydrogen

internal combustion engine at higher equivalence ratios. As was discussed above, the difference in power output between direct and indirect injection for gasoline internal combustion engines is limited. It can therefore be concluded that a hydrogen internal combustion engine with early direct injection can almost match the power output of a gasoline internal combustion engine. If we now look at the last row of the table, it can be seen that using optimised hydrogen injection, a higher power output can be achieved than using gasoline. Optimised hydrogen injection still needs a lot of research to be applied to an actual engine, but the prospects are very promising.

From this analysis, it can be concluded that, as expected, the combustion processes of gasoline and hydrogen are quite different. It can also be concluded that, just comparing indirect injection cases, gasoline combustion results in more power than hydrogen combustion. Including hydrogen direct injection cases, it can be seen that hydrogen comes close to matching the power output of a gasoline engine and might even exceed it using optimised injection. The analysis of gasoline internal combustion engines in this work has been very limited and it is therefore recommended that future investigations be launched into the differences between hydrogen and gasoline combustion, also taking into account direct gasoline injection.

6.6. Reducing the Pressure Peak

One of the concerns that was raised in the work of Hosking [51], was the potential danger of increased pressure peaks at the moment of combustion due to the conversion from gasoline to hydrogen. Because the work presented here is a prelude to actual engine tests, this concern has to be taken seriously and it must be investigated under which conditions these pressure peaks occur and how to potentially lower these peaks. To that end, three different parameters are discussed that affect the height of the pressure peaks.

6.6.1. Indirect vs. early vs. optimised injection

Figure 6.47 shows the pressure peaks for indirect, early and optimised injection, all for an equivalence ratio of 0.7.

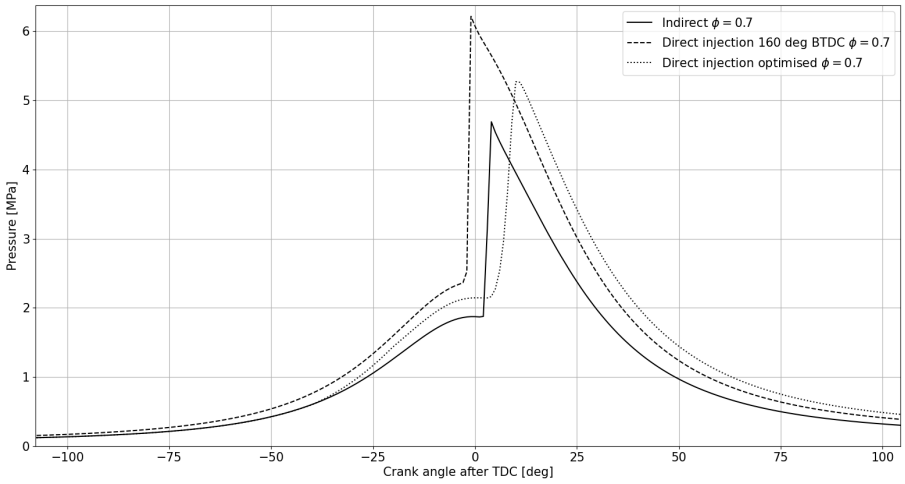

Figure 6.47: Pressure peaks for indirect injection, early injection and optimised injection

Comparing the indirect and early injections, it can be seen that the pressure peak is much higher for the early injection. Furthermore, it can be seen that both pressure peaks are very steep, indicating that combustion occurs very suddenly and very fast. The first instinct might therefore be to say that direct injection poses a risk in terms of the pressure peak that is produced during combustion. However, looking at the optimised pressure peak, it can be seen that this conclusion would be premature. The optimised pressure peak in this graph is still higher than the peak for indirect injection, but it is much less steep. Additionally, it must be kept in mind that this direct injection cycle was optimised for power and not for reducing the pressure peak. By varying the injection and spark timing, an optimised engine cycle could be devised that combines that power output of early injection with the lower pressure peak of indirect injection.

6.6.2. Equivalence ratio

It has already been discussed in section 6.2, but the height of the pressure peak can be influenced greatly by the equivalence ratio. This is shown again in Figure 6.48.

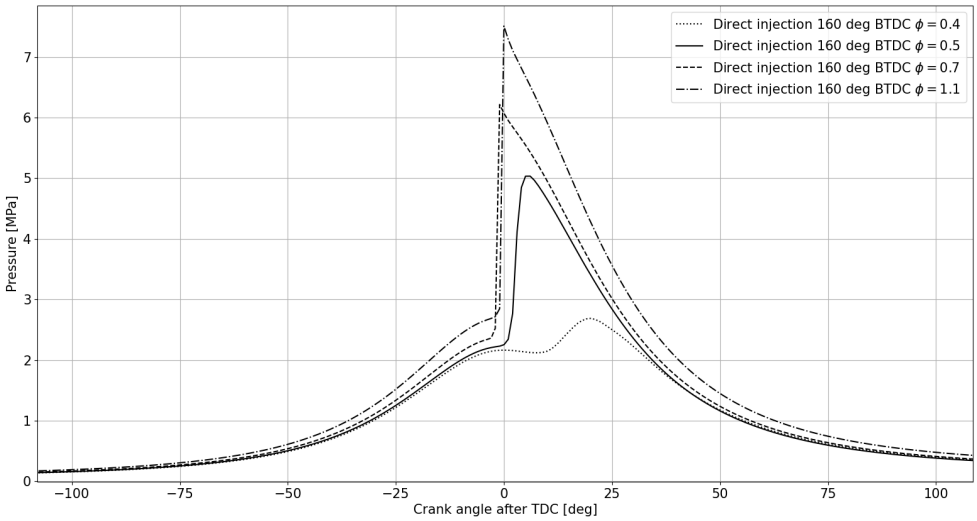

Figure 6.48: Pressure peaks for four different equivalence ratios

Not only the height of the pressure peak is influenced by the equivalence ratio, but so are the steepness of the pressure curve and the combustion delay. One easy way of ensuring safe operation would be to start testing at low equivalence ratios and to make sure that the pressures observed there are below the threshold, before moving to higher equivalence ratios.

6.6.3. Spark timing

Figure 6.49 was already shown before in the section on spark timing, but it perfectly demonstrates the effect of spark timing on the peak pressures inside the combustion chamber.

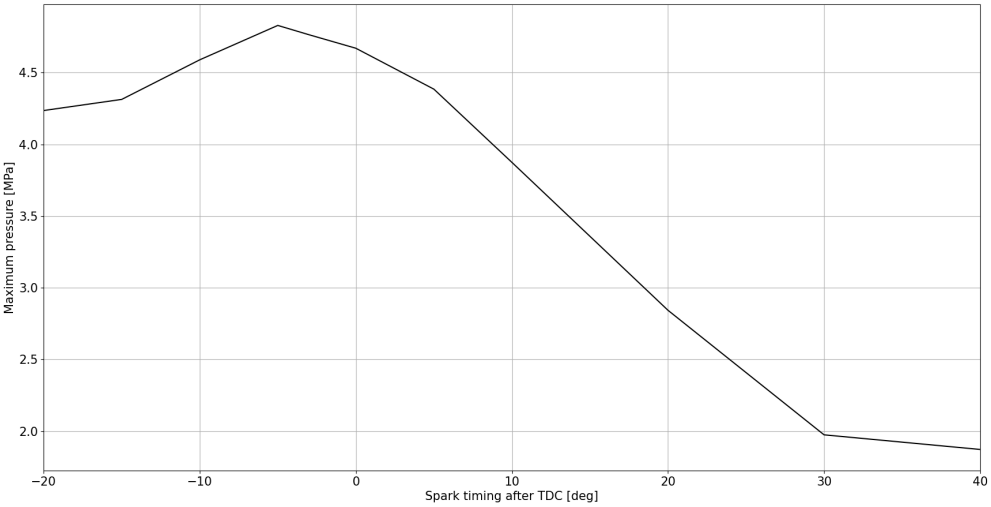

Figure 6.49: The maximum pressures in the combustion chamber for different spark timings, for indirect injection and ϕ=0.7

From this graph, it is very clear that retarding the spark timing greatly reduces the height of the pressure peak. Therefore, a strategy to ensure safe operation during testing could be to start with a retarded spark timing and advance the spark timing once the pressure peaks are found to be safe.

7
Verification and Validation

7.1. Verification

The verification efforts in this work are focused on two aspects; mesh refinement and multiple engine cycles. In any CFD-related work, looking at the mesh refinement that is used, is a must. The finer the mesh that is used is, the more accurate the results will be, but at a cost; the simulation will take longer to complete. A middle ground needs to be found. An additional point of interest in this particular CFD simulation, is that the desired result is not just one steady state image, but a full engine cycle, with between thirty and fourty thousand timesteps. This means that any small difference in mesh geometry will influence the final result of the simulation. These influences and what they mean for the usefulness of the results will be discussed in this section. The second aspect of the verification deals with single vs. multiple engine cycles. The simulations in this report all consist of one engine cycle. However, in reality, many engine cycles follow each other and each cycle is dependent on the results of the previous cycle. To compensate for this, initial conditions are set up to imitate a previous engine cycle. By running a simulation with multiple engine cycles, the accuracy and effect of these initial conditions can be evaluated.

7.1.1. Mesh refinement

As promised in section 5.3, a mesh refinement study was performed to evaluate the influence of the mesh geometry on the results of the simulations. As was discussed in that section, the meshing in Ansys Forte is done automatically and is based on a global mesh size, together with local or temporal mesh refinements. Simply put, the CFD calculation starts at the initial conditions that are specified by the user. It then goes a small timestep further, calculates the conditions there, and so on and so forth. As a result, the simulation of one engine cycle can, depending on factors like mesh size, injection timing and length, and combustion mechanics take between thirty and fourty thousand 'cycles' to complete. This not only means that the calculations can take a long time, it also means that a different mesh can lead to wildly different results. The difference between two different meshes for one calculation cycle might not be that big, but that small difference gets bigger and bigger, over thousands of cycles, until the two flows in the cylinder are completely different. It was already expected beforehand that the mesh would have an effect on the result of the simulations, but with the appearance of the optimised injection strategy, that largely depends on the flow of the hydrogen in the cylinder, this issue becomes even more pressing.

Here, two different scenarios are considered. The first one is a direct injection engine cycle, where the outcome of the simulation heavily depends on the hydrogen flow within the combustion chamber. After this, an indirect injection case is considered. Here, the flow before ignition is virtually the same for all of the different mesh refinements, but the results of the simulation still differ, as the flow after ignition differs quite significantly.

Mesh refinement for direct injection

As alluded to before, different mesh refinements greatly influence the flow of hydrogen in the combustion chamber. Therefore, also the results of optimised direct injection are influenced greatly by different mesh refinements, as the optimised injection is highly dependent on the location and spread of the hydrogen at the time of ignition. In order to show this, one run-case of an optimised injection simulation was selected and for this run-case, five different levels of mesh refinement were selected. This was done by setting the global mesh size to five different sizes; 0.225, 0.25, 0.275, 0.3 and 0.35 cm. In the selected run-case, hydrogen

is injected starting at 60 degrees BTDC and continues until 40 degrees BTDC. The equivalence ratio will be 0.7. Figure 7.1 to 7.5 show five bottom views of the engine, showing the hydrogen distribution at 10 degrees BTDC. The cell counts in the description of each of the five figures also corresponds to the cell count at 10 degrees BTDC.

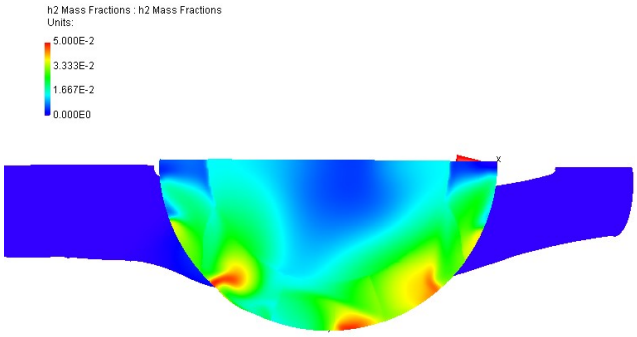

Figure 7.1: Bottom view of the hydrogen distribution 10 degrees BTDC, with a mesh size of 170,974 cells

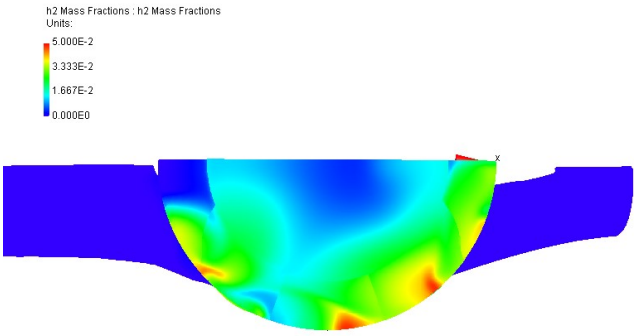

Figure 7.2: Bottom view of the hydrogen distribution 10 degrees BTDC, with a mesh size of 135,921 cells

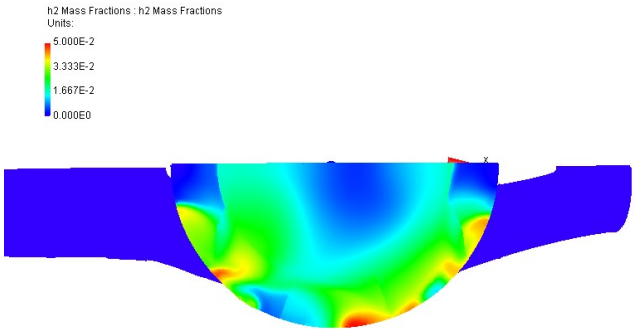

Figure 7.3: Bottom view of the hydrogen distribution 10 degrees BTDC, with a mesh size of 104,356 cells

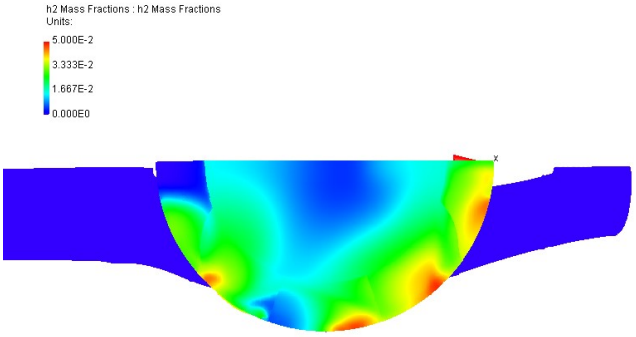

Figure 7.4: Bottom view of the hydrogen distribution 10 degrees BTDC, with a mesh size of 87,841 cells

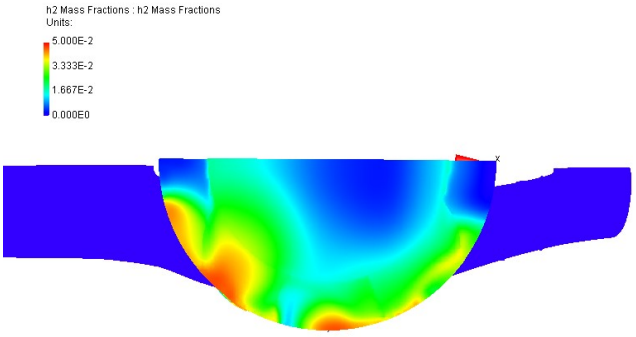

Figure 7.5: Bottom view of the hydrogen distribution 10 degrees BTDC, with a mesh size of 59,097 cells

It is quite clear from these images that a different mesh refinement will result in a different flow of the hydrogen in the combustion chamber. The two finest meshes have hydrogen hot-spots in the same locations, but their shapes and sizes differ. As the cell count drops, the differences become larger and for the last figure, where the cell count is approximately a third of the first image, the distribution of hydrogen is completely different. In the last image, the majority of the hydrogen is located on the left side of the combustion chamber, whereas in the first image, it is more evenly distributed, with a slightly higher concentration on the right. The differences in hydrogen flow also become apparent looking at the engine from the front, in Figure 7.6 to 7.10.

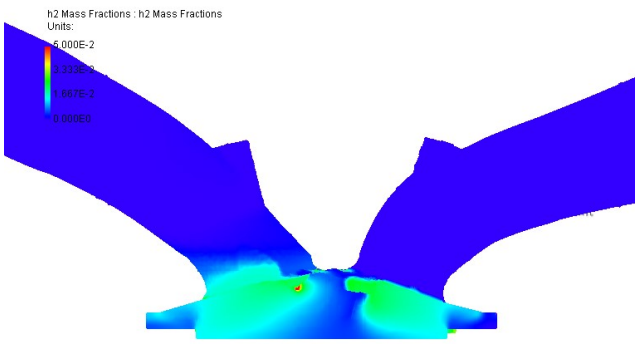

Figure 7.6: Front view of the hydrogen distribution 10 degrees BTDC, with a mesh size of 170,974 cells

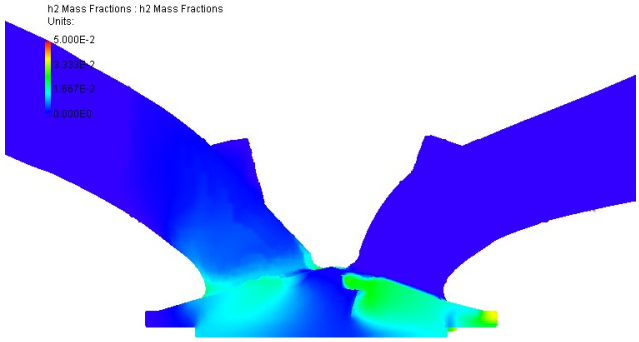

Figure 7.7: Front view of the hydrogen distribution 10 degrees BTDC, with a mesh size of 135,921 cells

An interesting observation that can be made looking at Figure 7.6 and Figure 7.7, is that the inlet valve apparently does not close off the inlet to the combustion chamber tight enough to prevent leakage, as some hydrogen can be seen leaking into the inlet. This is leakage can be due to either one of two things. Either it is due to a flaw in the geometric model of the engine, or due to a flaw in the meshing.

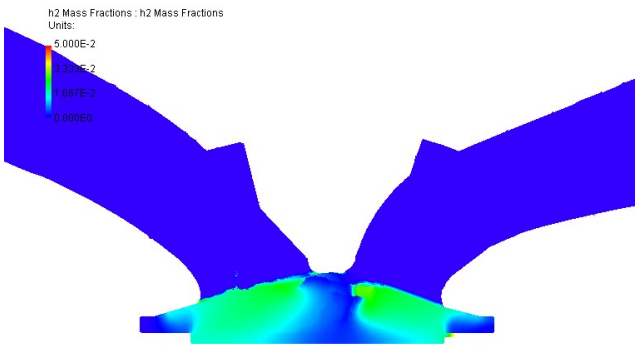

Figure 7.8: Front view of the hydrogen distribution 10 degrees BTDC, with a mesh size of 104,356 cells

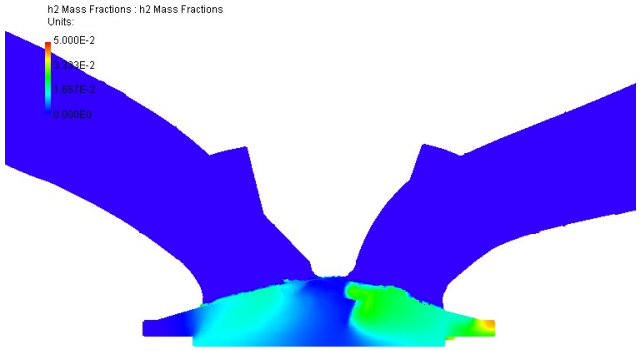

Figure 7.9: Front view of the hydrogen distribution 10 degrees BTDC, with a mesh size of 87,841 cells

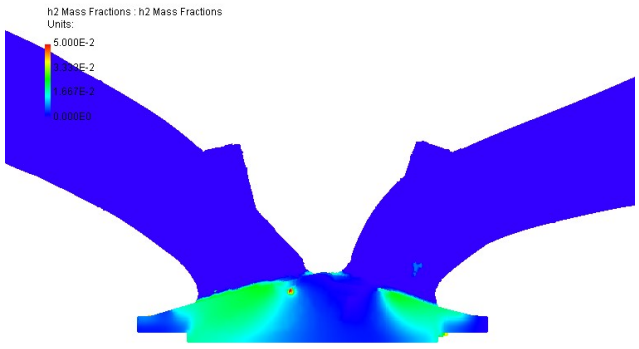

Figure 7.10: Front view of the hydrogen distribution 10 degrees BTDC, with a mesh size of 59,097 cells

Looking at the front view, again a clear difference in hydrogen distribution can be seen between the different levels of mesh refinement. If the mixture were to be ignited at this crank angle, the combustion processes would be wildly different between the different mesh refinements. In Figure 7.5, there is clearly no hydrogen anywhere near the location of the spark plug. A spark at this crank angle would have nothing to ignite and no combustion would take place.

Therefore, it must be concluded that, for direct injection, the mesh refinement and mesh geometry greatly influence the flow within the cylinder before ignition, and as such greatly influence the results of the simulation, to the extend where it even determines whether the hydrogen-air mixture combusts or whether

the flame is quenched. Because of this, the results in this report for direct injection can not be used to make any quantitative predictions for a real hydrogen internal combustion engine. They can, however, be used as a guide to say something about how the hydrogen flow inside the combustion chamber affects the performance of the engine.

Mesh refinement for indirect injection

Like with the direct injection mesh refinement investigation, five different mesh sizes are considered. These different mesh sizes are set by specifying five different global mesh sizes, one for each simulation. The global mesh sizes that were used here are 0.225, 0.25, 0.275, 0.3 and 0.35 cm. Instead of directly injecting the hydrogen in the combustion chamber, the hydrogen is mixed with the air before it enters the combustion chamber. It is mixed in such a way that the equivalence ratio is 0.7.

Figure 7.11 shows the pressure peaks of each of the five simulations.

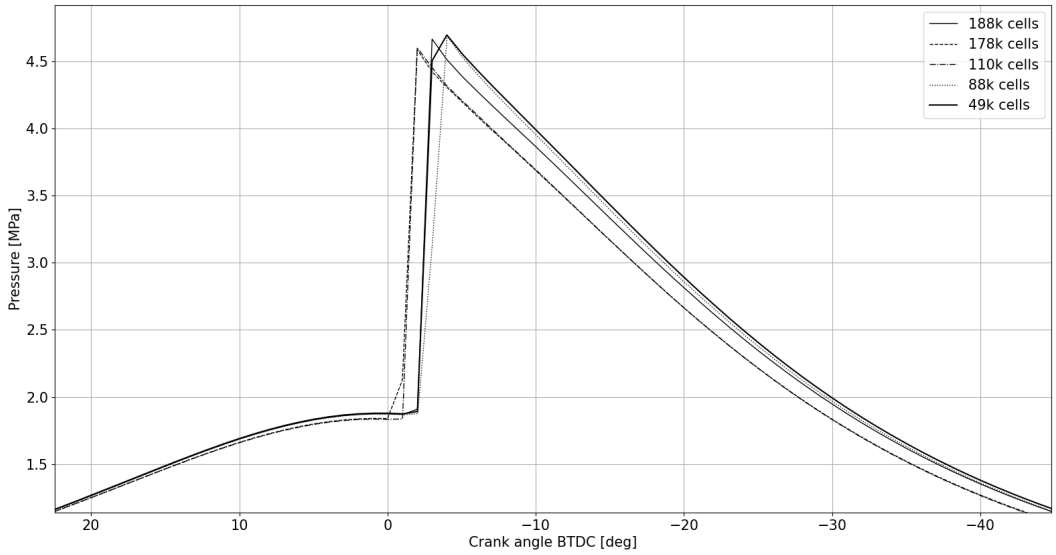

Figure 7.11: Crank angle versus pressure graph for the five different mesh refinements

First of all, it can be seen in this graph that the assumption of equal conditions in all five simulations before ignition, does not hold. There are clearly two groups of simulations. The group with 178k and 110k cells clearly has a lower pressure before ignition than the other simulations. An exact explanation for this difference can not be given, other than that a different cell-size in the mesh can also lead to a different mesh structure, a difference which reflects back in the flow inside the combustion chamber. The second difference that can be seen in this graph, is that the combustion timing of the hydrogen-air mixture also differs between the different mesh refinements. Again, the simulations seem to be split up in those same two groups, where group with 178k and 110k cells combusts well before other three simulations.

In Figure 7.12, where the temperatures during combustion are shown for the five mesh sizes, the same grouping can be seen, although it is harder to distinguish in this graph. What can however be distinguished, is that although the maximum temperatures that the various simulations reach are very similar, the engine temperatures post-combustion all level out to different values.

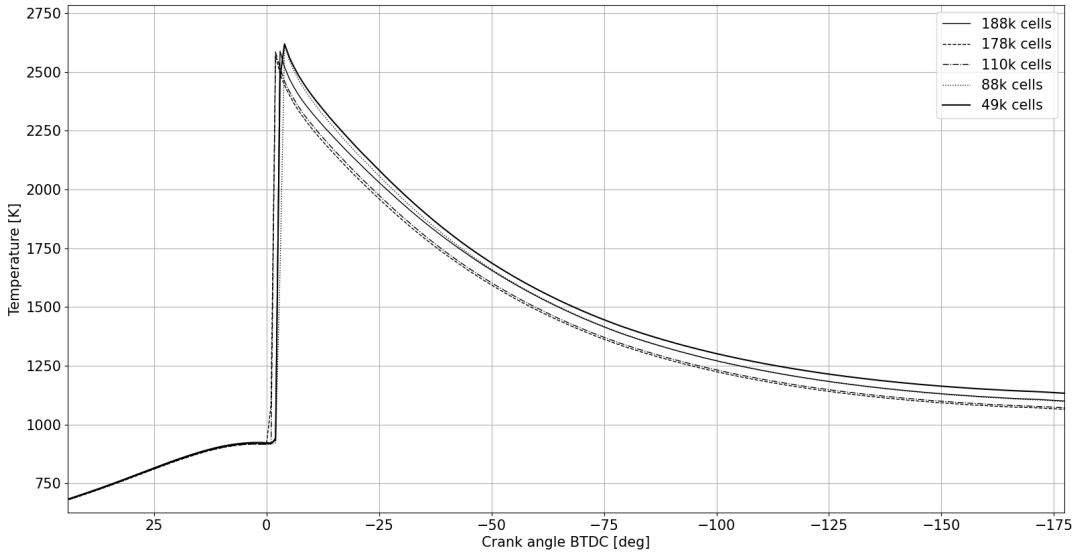

Figure 7.12: Crank angle versus temperature graph for the five different mesh refinements

Given these apparent differences in post-combustion temperatures, it is interesting to look and the temperature distributions for each of the mesh refinements at bottom dead centre (BTC), so 180 degrees after TDC and the combustion. These temperature distributions can be seen in Figure 7.13 to 7.17.

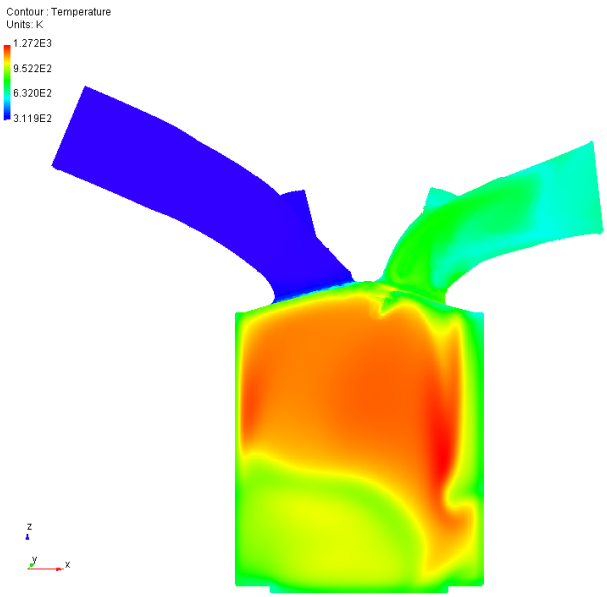

Figure 7.13: View of the temperature distribution at the symmetry plane of the engine, at bottom dead centre (BDC), with a mesh size of 188,294 cells

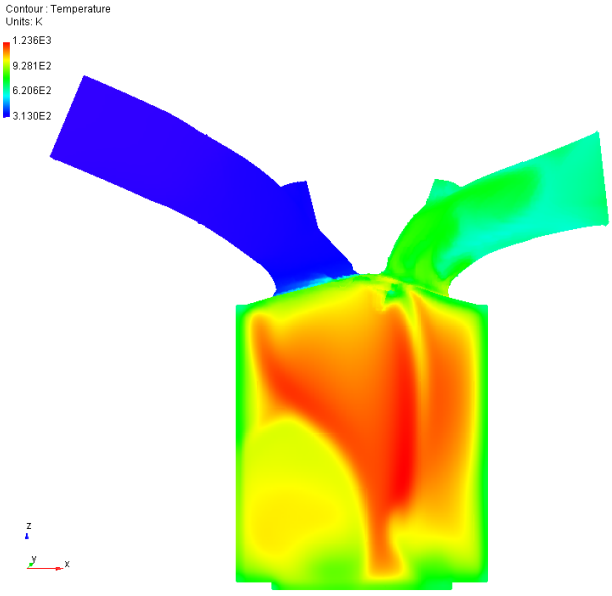

Figure 7.14: View of the temperature distribution at the symmetry plane of the engine, at bottom dead centre (BDC), with a mesh size of 177,556 cells

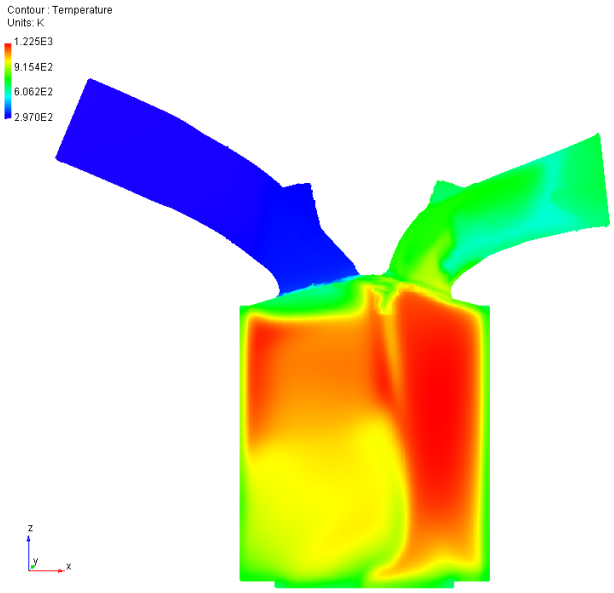

Figure 7.15: View of the temperature distribution at the symmetry plane of the engine, at bottom dead centre (BDC), with a mesh size of 110,258 cells

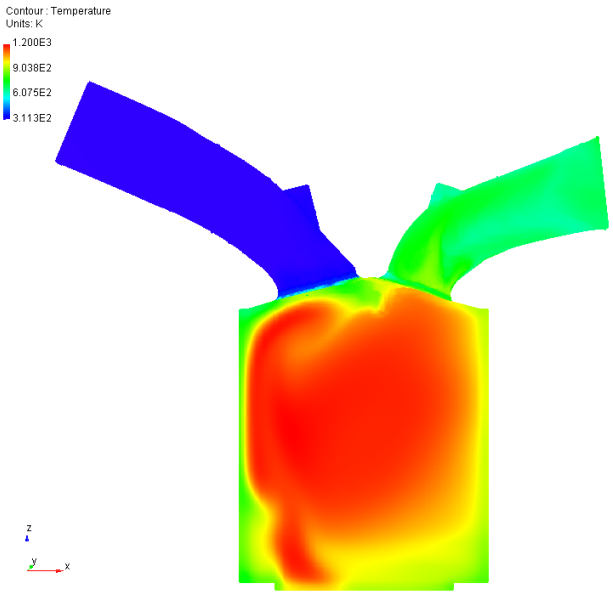

Figure 7.16: View of the temperature distribution at the symmetry plane of the engine, at bottom dead centre (BDC), with a mesh size of 87,684 cells

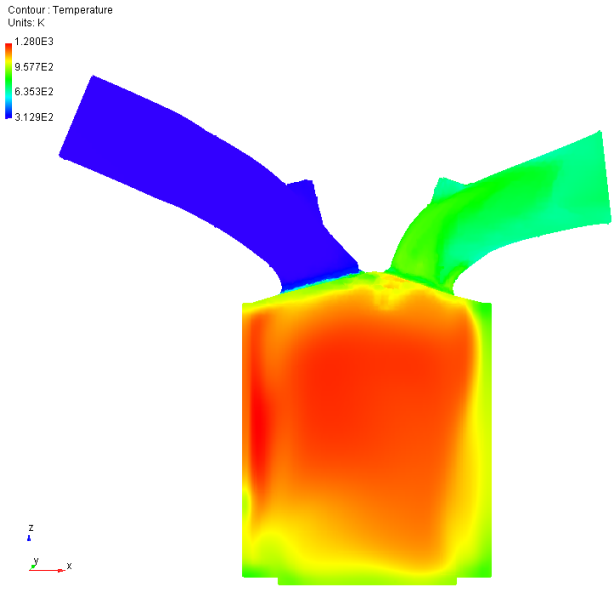

Figure 7.17: View of the temperature distribution at the symmetry plane of the engine, at bottom dead centre (BDC), with a mesh size of 49,263 cells

It can be seen that the areas of higher temperature seem to be larger in Figure 7.17 and Figure 7.16 than in the other simulations, and indeed, their temperatures are higher than those of Figure 7.14 and Figure 7.13. But the area of the higher temperature is not the only important aspect in these images. The other is the temperature of the areas of high temperature. Looking at the legends in each of the figures, it can be seen that the maximum temperatures are highest in Figure 7.13 and Figure 7.17, which indeed also corresponds with what can be seen in Figure 7.12. Furthermore, it can once again be seen that different mesh sizes and geometries will result in different flows within the combustion chamber. This is clearly shown by the wildly different temperature distributions that can be seen in these images.

Finally, we come to Table 7.1, where some of what was talked about before has been summarised, and also the thermal brake efficiency of each of the simulations is shown.

Table 7.1: Table showing the results of five different mesh refinements for an indirect injection cycle

Cell count	188,294	177,556	110,258	87,684	49,263
Thermal brake efficiency [-]	0.22277	0.20721	0.20762	0.22433	0.23106
Maximum temperature [K]	2588.91	2571.67	2585.63	2617.98	2619.73
Maximum pressure [MPa]	4.67	4.59	4.60	4.69	4.70

It is clear from this table once again that interestingly, the results for the thermal brake efficiency and the maximum pressure seem to break down into two distinct groups. Within these groups, the results are quite similar, but the differences between the two groups are quite large. There is about a 10% difference in thermal break efficiency between the two groups, which is of course quite significant. It was hoped beforehand that the results for the different mesh refinements for indirect injection would not be so different, as the conditions before ignition are almost identical. However, it has to be concluded that because of the different post-combustion flows in the different mesh refinement simulations, the results still differ greatly and that the results from these simulations can only be used as indications of how a real engine could behave and do not have any quantitative predictive value.

7.1.2. Multiple engine cycles

In section 5.4 it was explained that in order for the simulation to be run, initial conditions need to be set. The selected conditions will of course influence the results of the simulation and should thus be verified. This verification process is described in this section.

The results that are shown in this report have all been taken from simulations that only consider one single engine cycle. In this section, four consecutive engine cycles are considered. The pressure peaks of these four engine cycles can be seen in Figure 7.18.

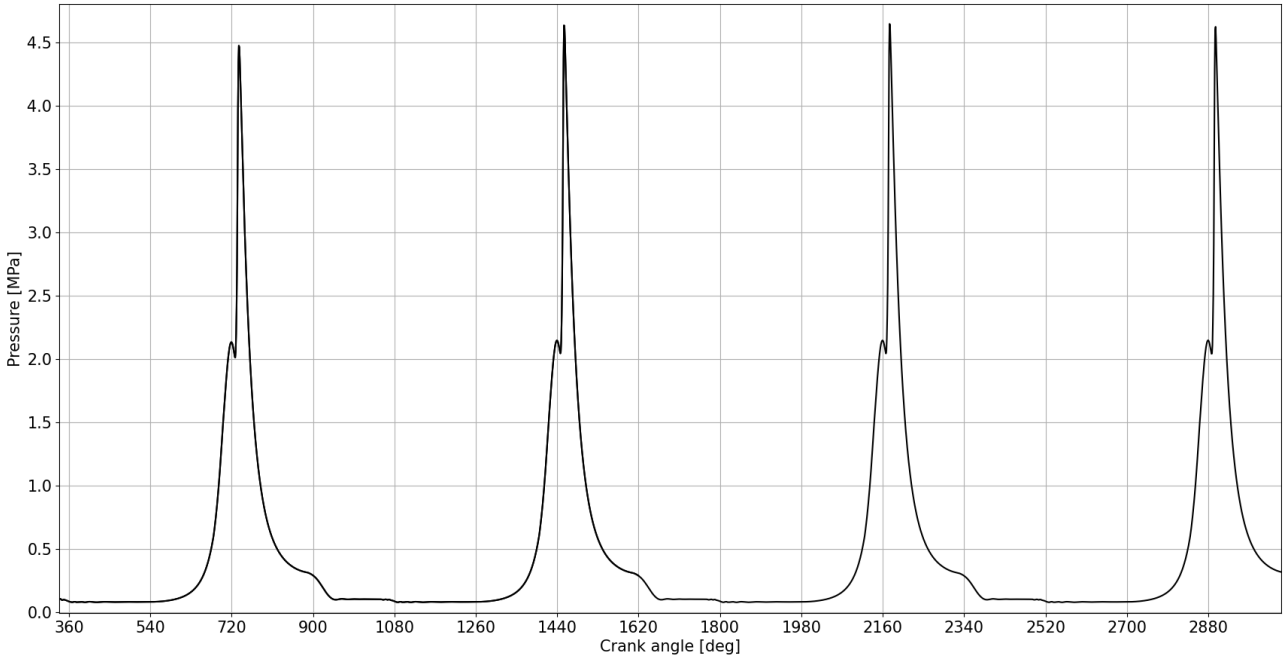

Figure 7.18: Crank angle versus pressure for four consecutive engine cycles

Looking at this graph, it is clear that the four engine cycles are very similar. The only discernible difference between them is that the first pressure peak is slightly lower than the following three. So apparently, the initial conditions are not fully correct, which result in a lower pressure peak for the first engine cycle. To verify this hypothesis, we will now look at the temperature distribution in the initial condition and compare it to the same crank angle in the fourth engine cycle. The temperature distribution in the initial condition can be seen in Figure 7.19.

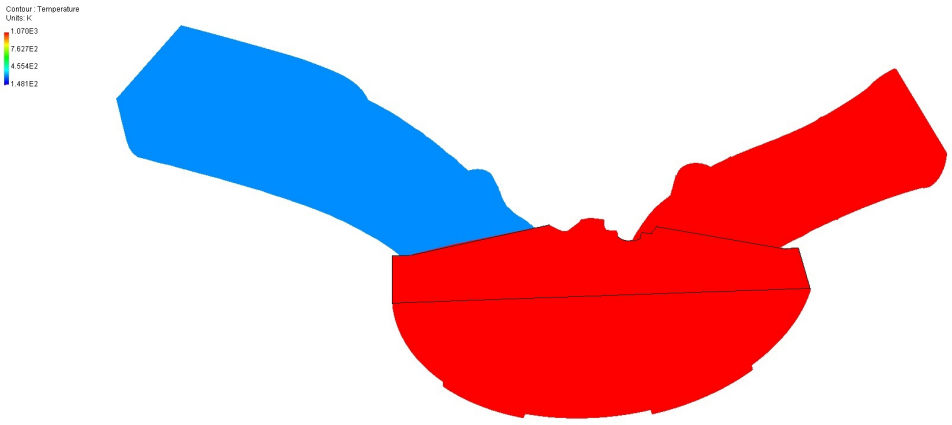

Figure 7.19: Temperature distribution at a crank angle of 328 degrees. The general shape of the cylinder has been drawn in for clarity.

It is immediately very clear what is going on in this picture, and this was also what was to be expected. The initial conditions are set for each of the three volumes; the inlet, the combustion chamber and the exhaust. For each of these three volumes, a temperature is specified, which results in a condition in which the temperature throughout each of the individual volumes is constant. Logic tells us that this is most likely not something that will happen in real life, so it is expected that the temperature distribution at the same crank angle in the fourth engine cycle will look quite different. This distribution can be seen in Figure 7.20.

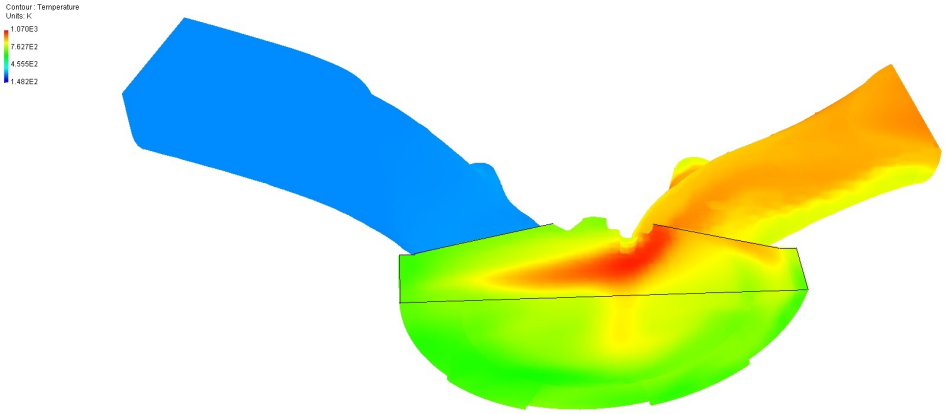

Figure 7.20: Temperature distribution at a crank angle of 2488 degrees (328 degrees in the fourth engine cycle). The general shape of the cylinder has been drawn in for clarity.

And indeed, the temperature distribution in the combustion chamber and the exhaust differ greatly from the initial condition. In general, the flow in these two volumes is much cooler than in the initial condition. Interestingly, the temperature in the inlet is the same as in the initial condition. But this makes sense of course, as this is the temperature of the air that is drawn into the engine, which has a constant temperature. From these two figures, it could be concluded that the initial conditions that were selected do not match the flow that they are trying to approximate, and are therefore wrong. However, that would be jumping to conclusions, for even though the chosen initial conditions might not exactly match real life conditions, they might still suffice. Because, to be able to say whether the initial conditions are wrong, or do not suffice, we need to think about what they are meant to do. The initial conditions in this case are trying to recreate the conditions near the end of the exhaust stroke post-combustion, when the piston is almost at top dead centre again. This means that between the initial condition and the moment of combustion, there are the intake stroke and the compression stroke. That is actually the reason that 328 degrees was chosen as the initial condition. Because after the initial condition, the combustion chamber will be 'flushed' with the intake air, which means that the conditions before the intake stroke virtually do not matter. At least, that is the idea. To find out if this is actually the case, we look at Figure 7.21 and Figure 7.22.

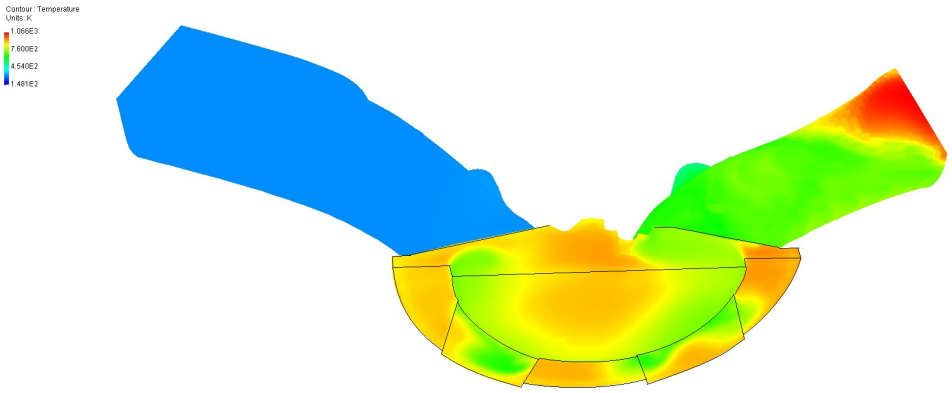

Figure 7.21: Temperature distribution at a crank angle of 715 degrees. The general shape of the cylinder has been drawn in for clarity.

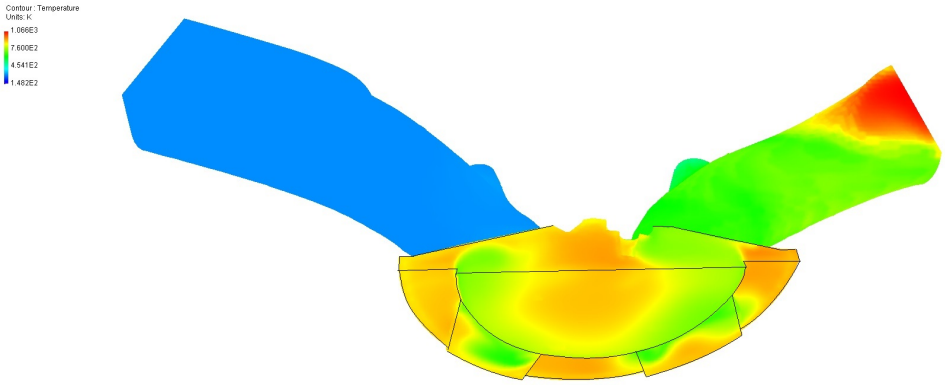

Figure 7.22: Temperature distribution at a crank angle of 2875 degrees (715 degrees in the fourth engine cycle). The general shape of the cylinder has been drawn in for clarity.

These two images are taken at the same moment in the engine cycle, but the first one is from the first engine cycle and the second one is from the fourth engine cycle. It is very hard to see any differences, but to prove that these are not just the same figure, please look at the exhaust, where the shape of the hot spot is slightly different.

So it can be seen that the temperature distributions just before TDC are virtually the same, but what about the hydrogen distribution? For this, please have a look at Figure 7.23 and Figure 7.24.

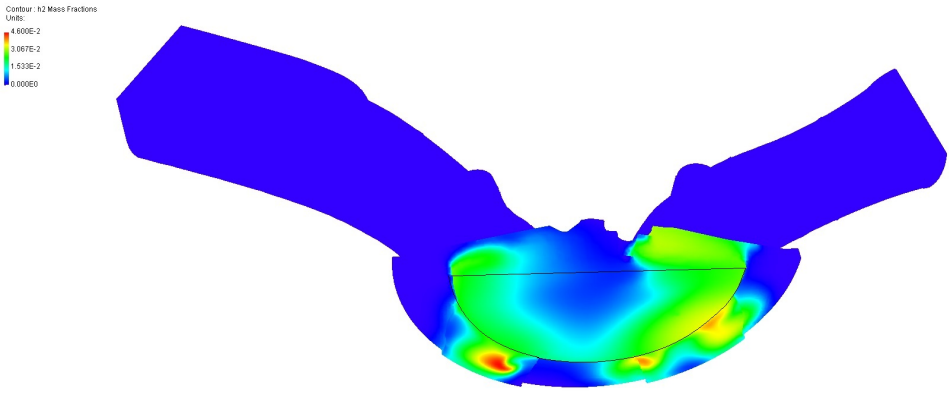

Figure 7.23: Hydrogen distribution at a crank angle of 720 degrees. The general shape of the cylinder has been drawn in for clarity.

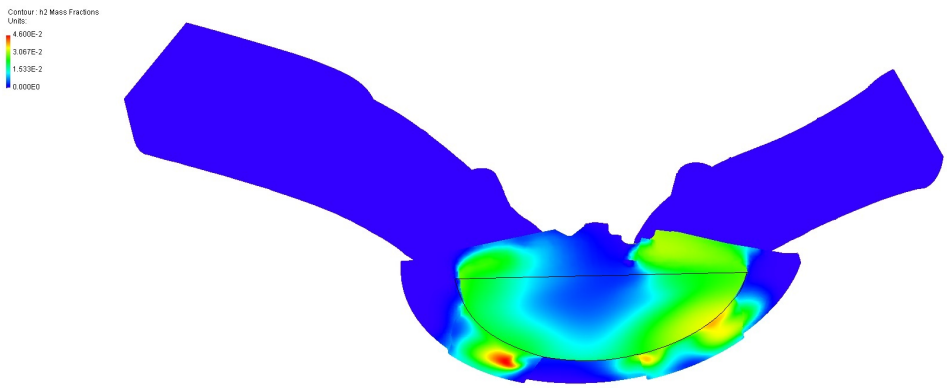

Figure 7.24: Temperature distribution at a crank angle of 2880 degrees (720 degrees in the fourth engine cycle). The general shape of the cylinder has been drawn in for clarity.

Again, the figures look almost identical, but small differences can be seen. These differences are deemed too small to have any significant influence on the combustion process and thus on the result of the simulation. This is once again confirmed by looking back at Figure 7.18. The first pressure peak is slightly lower than the other three peaks, but the difference is quite small, less than 3%. This difference would be an issue if the simulations in this research were used to make quantitative predictions about a hydrogen internal combustion engine. However, no such predictions will be made. Instead, the simulations will be used to make qualitative recommendations about hydrogen internal combustion engines. These recommendations are mainly based on the hydrogen flow and temperature distribution in the combustion chamber at the time of combustion and as can be seen from the figures in this section, those are hardly affected by the difference between the initial conditions and the actual post-combustion situation.

7.2. Validation

An integral part of any conducted research is validation of the model that is used. This is especially true for complex models such as CFD simulations. One can make predictions or draw conclusions based on CFD simulations, but without providing any validation for the model, those predictions and conclusions are worthless. The best way of validating the CFD model, would be to perform actual engine tests on an engine with the same geometry and under the same conditions, and then compare the results of those two. Unfortunately, at the time of writing, the engine test set-up that will be part of this project is not yet ready and will not be available before the end of this thesis work. Therefore, the results of the CFD simulations could not be validated directly in the optimal fashion. However, there is of course another option, which is to validate the CFD model using the work of others. Several pieces of work have been published that discuss tests with a hydrogen internal combustion engine, of which three were found suitable to use as validation material. Firstly, a study by Scarcelli et al. [27] looked at hydrogen injection, both on a physical engine and using their own CFD simulation. The second and third study, by Eichlseder et al. [52] and Dhyani and Subramanian [25] respectively, present results from two different engine tests on hydrogen internal combustion engines. Based on the comparison between these three sources and the results obtained from the ANSYS Forte simulations, the validity of those simulations will be discussed.

7.2.1. Hydrogen injection

In their work, Scarcelli et al. [27] performed experiments on a visual internal combustion engine, which let them examine the hydrogen flow inside the cylinder, using both the Schlieren and the PLIF techniques. A more extensive explanation on the work by Scarcelli et al. is given in subsection 4.2.1. In this section, the results from their work are compared to a ANSYS Forte simulation that tries to replicate the hydrogen flow in the Schlieren/PLIF images. The hydrogen injection in the reference paper starts at 137 degrees BTDC and lasts for 17 degrees, until 120 degrees BTDC and hydrogen is injected with a pressure of 100 bar. This is the full extend of the information provided in the reference work and it leaves one important gap, which

is that it is not specified how much hydrogen is injected. The injection mass flux is given in kg/ms^2, but since the injection duration was only given in degrees and not in seconds, the amount of hydrogen injected could not be calculated exactly. Therefore, the amount of hydrogen that is injected does not match the amount injected in the reference work. Another difference is the geometry of the engine. As can be seen in Figure 7.25, the engine used in this work is slightly longer than the one used in the reference work. The second difference is the location of the injection point. In the reference paper, the injector is located in the center of the cylinder, while in the Forte engine, the injector is located slightly to the left. It is difficult to see in these images, but looking at Figure 5.1, it can clearly be seen that there is a spark plug of quite a significant size located to the right of the injector. This will prove important when the results of the simulation will be analysed. The last difference between the Forte engine and the reference engine is the shape of the piston bowl. As can be seen in Figure 7.25, the bowl in the reference paper is completely flat, whereas the one in the Forte engine is not.

All these differences will impact the flow of the hydrogen in the cylinder. With that being said, let's look at the results of the comparison. Figure 7.25 shows four sets of images, each set consisting of three images. The column on the left shows the hydrogen injection according a CFD simulation by Scarcelli et al. The middle column first shows two Schlieren images of the early stages of combustion, which are replaced by PLIF images as the injection continues. On the right are the images from the CFD simulations performed for this work.

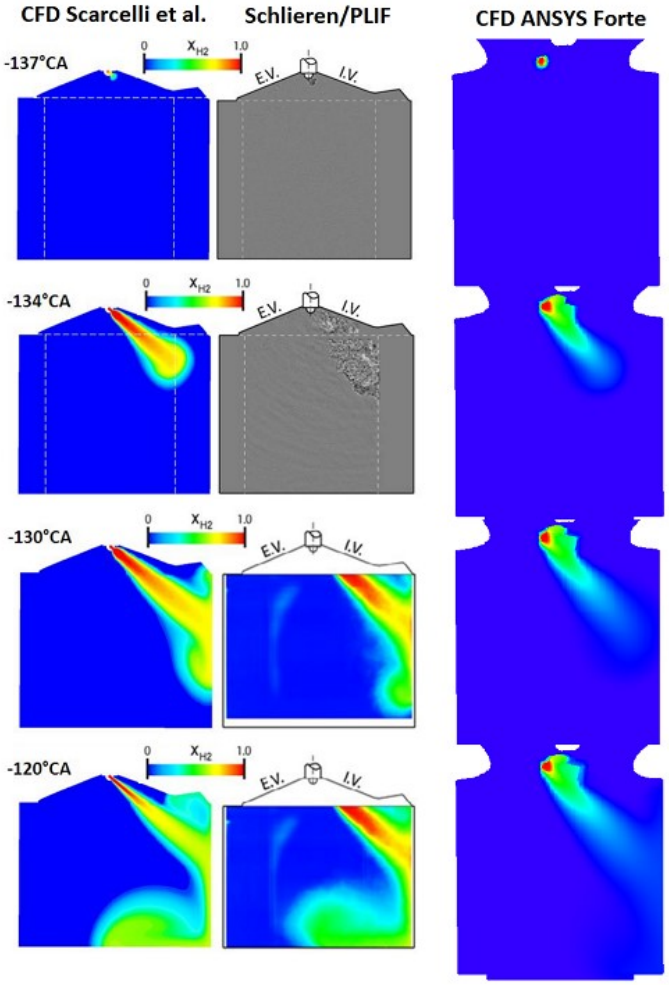

Figure 7.25: Comparison of hydrogen injection in Forte model with work by Scarcelli et al. [27]

At 134 degrees BTDC, a clear difference can be seen in the angle of injection between the reference CFD and the Forte CFD. This is because, as is stated in their work, the injection angle of the CFD injection and the real injection do not match. In this work, the injection angle is equal to that of the real injection, which is why it differs from the Scarcelli CFD angle. The second thing that can be noticed from the CFD ANSYS Forte

images, is that the hydrogen is hitting the spark plug and because of that, the hydrogen accumulates somewhat behind the spark plug. But maybe the most obvious difference between the images from this work and that from the reference paper is that while in the reference paper, the hydrogen jet seems to steadily grow, in this work's images, the jet seems to hardly increase in size. This, however, only appears to be the case at first glance, because when examining the hydrogen distribution more closely, it can be seen that the front of the hydrogen jet is moving at about the same pace as the one in the reference work, but the density of the hydrogen in the most forward part of the hydrogen jet is much lower and is therefore harder to see. The reason for this difference is the different methods of hydrogen injection in the two models. In the reference paper, a nozzle is used that guides the hydrogen in the desired jet direction. In the Forte model, an inlet boundary condition is created, which is given an inlet direction that corresponds to the desired jet direction. The result is that in the reference paper, a nice clean jet can be seen, whereas the jet in the Forte simulation is wider, less focused and seems to leak hydrogen towards the head of the cylinder. It is clear from this that the hydrogen jet in the Forte simulation does not resemble an actual hydrogen jet at this pressure. However, before discarding the hydrogen injection system used in this work, let's first look at how the hydrogen propagates throughout the combustion chamber and compare that to the experiments done by Scarcelli et al.

After 120 degrees BTDC, no more additional hydrogen is injected into the combustion chamber, but the hydrogen that has been injected up to that point still propagates through the combustion chamber. This can be seen in Figure 7.26, where six sets of images are shown, from 100 degrees BTDC to 30 degrees BTDC. Like in the previous image, the left most column consists of CFD images from Scarcelli et al., the middle column consists of PLIF images from Scarcelli et al. and the right most column consists of images taken from CFD ANSYS Forte analysis.

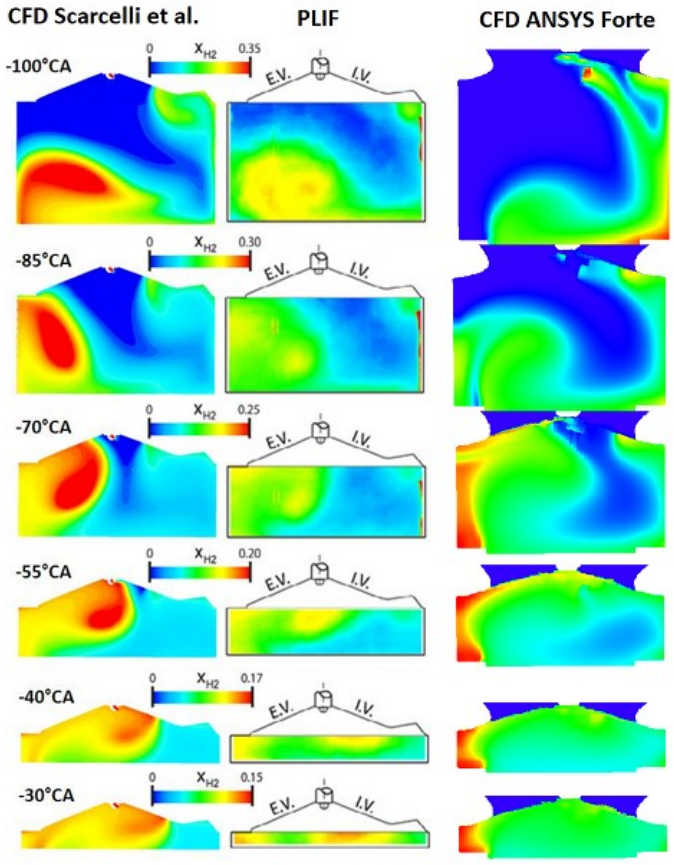

Figure 7.26: Comparison of hydrogen injection in Forte model with work by Scarcelli et al. [27], continued

Looking at the first row of images, it can be seen that the hydrogen in the right most picture seems to 'lag' behind the hydrogen in the other two images. In those two pictures, the hydrogen has 'bounced' off the right cylinder wall, hit the piston, is now travelling upwards again and has made it halfway up the cylinder. In the

right most image, the hydrogen has at this crank angle not reached the left cylinder wall. One of the reasons for this, is that in the engine on the right, the hydrogen has to travel further because the cylinder is simply longer. It takes longer for the hydrogen to reach the piston and therefore it takes longer for the hydrogen to move upwards again. One additional explanation for this lagging behind, could be that the hydrogen is moving slower in the engine on the right. However, as the hydrogen seems to be lagging behind by the same amount in all the images in Figure 7.26, it is believed that this is mainly due to the difference in cylinder length and that the velocity difference is negligible. Additionally, when the hydrogen is first injected into the combustion chamber in the Forte analysis, it is injected to the left of the centre of the cylinder, whereas the hydrogen in the reference work is injected in the centre. This means that since the hydrogen jet is aimed at the right wall, it will take longer for the hydrogen in the Forte simulation to reach that wall than for the hydrogen in the reference work, as the distance is simply longer. This again increases the 'lag' that the hydrogen in the Forte analysis seems to have.

When we look at the differences between the way the hydrogen moves through the combustion chamber in the images from Scarcelli et al., we can spot one big difference between the CFD and the PLIF images. The general direction and location of the hydrogen matches quite well, but the way in which the hydrogen mixes with the air in the combustion chamber seems to differ. In the CFD imagery, the majority of the hydrogen seems to be located in one bubble, which moves through the combustion chamber and becomes smaller as it 'sheds' hydrogen along the way. In the PLIF images however, there is less off a bubble of hydrogen and the hydrogen and air seem to mix a lot more as the hydrogen moves through the combustion chamber. As a result, the hydrogen in the last PLIF image is mixed with the air much better than in the last reference CFD image. If we now compare that to the Forte images, we can see that Forte seems to do a better job of capturing the hydrogen distribution over the combustion chamber. There is still a pocket of hydrogen on the left side of the cylinder, but that is due to the different shape of the piston bowl, which traps some of the hydrogen in that corner.

There is of course one glaring difference between both CFD images and the images from the test. Especially in the Schlieren images, it can be seen that, where the CFD images predict a smooth flow of hydrogen, no such thing is present in the real combustion chamber. The real hydrogen flow is not so smooth and this of course makes complete sense. Both CFD simulations use a RANS model to simulate turbulence, which means that the resulting flow is averaged and smoothed over. An example of this can be seen in the work of Som et al. [64], from which Figure 7.27 is taken.

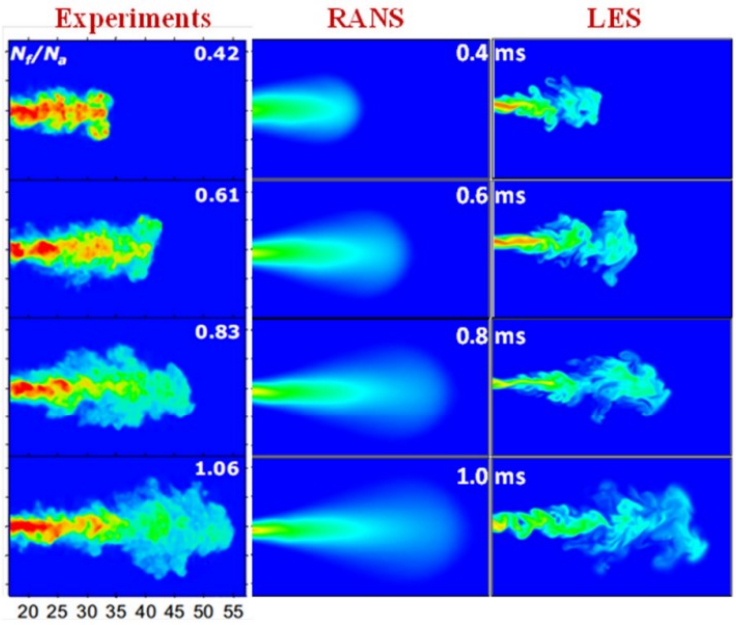

Figure 7.27: Images comparing the calculated equivalence ratio contours using RANS and LES models, against experimental data [64]

In this figure, it can clearly be seen that the shape and structure of the injected fuel differs completely between the experiments and the RANS simulations. However, the average distribution of the injected fuel matches the experiment quite well and the penetration distance of the fuel matches as well. It can also be seen from this image that LES is able to capture the structure of the flow much better, but it still differs quite a lot from the actual flow.

From this validation effort, it can be concluded that the hydrogen jet that results from the inlet boundary condition in the Forte simulation does not resemble the hydrogen jet in the experimental work by Scarcelli et al. However, looking at how the hydrogen further propagates through the combustion chamber, it can be said that the RANS model that is used in the Forte simulation does a good job at simulating the average movement and mixing of the hydrogen in the combustion chamber. It is therefore concluded that the injection method used is an adequate model of hydrogen injection, although it is recommended that further investigations be performed into the improvement of this method and potentially the development of a method that more accurately captures the hydrogen jet.

7.2.2. Eichlseder et al.

The first reference paper of the set of two papers with experimental data that will be used to validate the CFD model, was written by Eichlseder et al. [52]. In their experiment, the researchers run engine cycles of both direct and indirect injection on a single cylinder test engine. The lay-out of this engine can be seen in Figure 7.28.

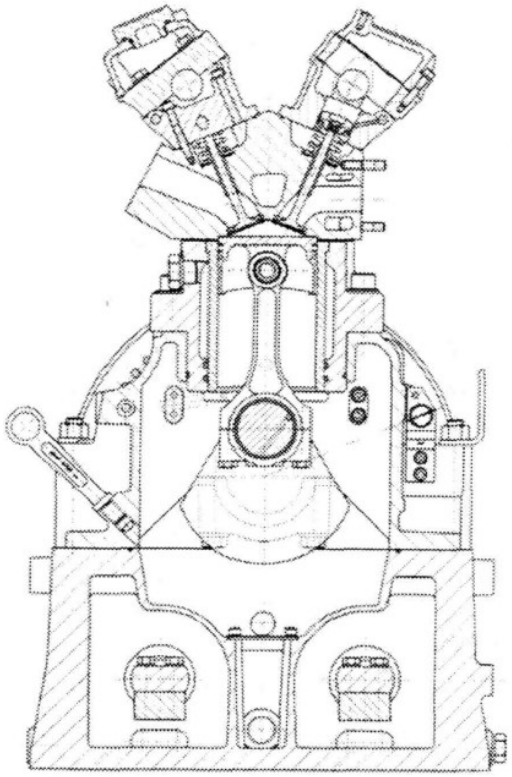

Figure 7.28: Technical drawing the single cylinder engine used in the reference paper by Eichlseder et al. [52]

This engine is very similar to the engine used in the Forte CFD simulations in this report. It also employs four valves, two for the inlet and two for the outlet. Furthermore, the dimensions of the two engines are very similar, as can be seen in Table 7.2.

Table 7.2: Geometrical properties of both engines

Engine	Eichlseder et al. [52]	ANSYS Forte
Stroke [mm]	86	90
Bore [mm]	86	84
Volume [cm^3]	499.6	498.8
Compression ratio [-]	10.5:1	10.3:1

Even though the engines are very similar, and the experiments conducted in the reference paper include both direct and indirect injection engine cycles, the value of the paper as a validation source is quite underwhelming. About half of the graphs in the paper do not include any numbers on the y-axis, and most of the graphs that do, plot variables that are either not very interesting for this research, or are not variables that are provided as an output in ANSYS Forte. However, the work by Eichlseder et al. is not mentioned in this validation effort for nothing, as there is one figure in the paper that provides valuable validation material. This graph is a pressure vs. volume diagram, and can be seen in Figure 7.29. For more information on pV-diagrams, please refer to Figure 6.27.

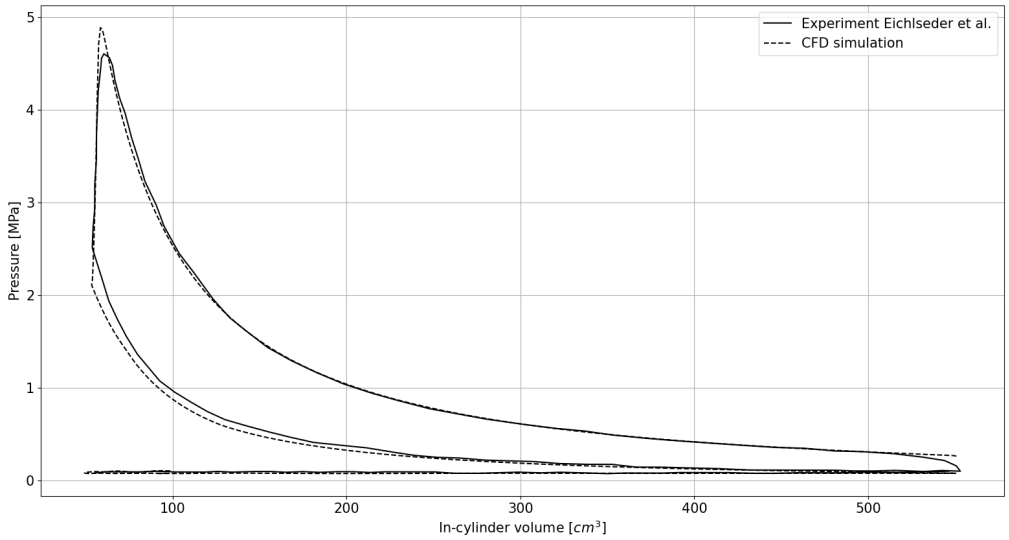

Figure 7.29: In-cylinder pressure vs. volume graph comparing the experimental results of Eichlseder et al. [52] with CFD Forte results

The graph also includes the pV-diagram of the corresponding CFD simulation in Forte. Unfortunately, not a lot of information is given about the engine cycle parameters that resulted in the pV-diagram from the reference paper. It was therefore difficult to reproduce the engine conditions exactly, as they were not known exactly. The resulting pV-diagrams are quite similar, but some differences can definitely be noticed. First of all, the pressure due to compression is clearly higher in the experimental results, which peaks at about 2.5 MPa, whereas the CFD pressure peaks at just over 2 MPa. Reasons for this could be the different geometries of the engines, different injection timings, different amounts of hydrogen injected, different temperatures of the injected hydrogen, different initial conditions, etc. Once combustion happens, it can be seen that the two lines overlap, indicating that combustion happens at roughly the same speed and pressure rise. However, the pressure peak in the CFD simulation is slightly higher than the peak in the experimental results. This is most likely due to a mismatch in equivalence ratios between the two engine cycles. The equivalence ratio in the CFD simulation is most likely slightly higher than the equivalence ratio in the experiment, which results in the higher pressure peak. But once the piston is travelling down again, the lines almost overlap again.

All in all, despite some differences that can be explained by differences in operating conditions of the engines, the pV-diagrams match quite well.

7.2.3. Dhyani and Subramanian

The second and final reference paper with experimental data that will be used in this validation effort was written by Dhyani and Subramanian [25] and looks at the characterisation of backfire in a hydrogen internal combustion engine, both using experiments and CFD simulations. The experiments that were performed in this research, were most likely performed on the same type of research engine that was used in the experiments by Eichlseder et al. Again, the operating conditions of the engine are not exactly known, so it was difficult to fully recreate the engine cycle of the reference paper. Nevertheless, the resulting pressure curves of the experiment and both CFD simulations (the one performed by Dhyani and Subramanian and the one performed in this work) are quite similar, as can be seen in Figure 7.30.

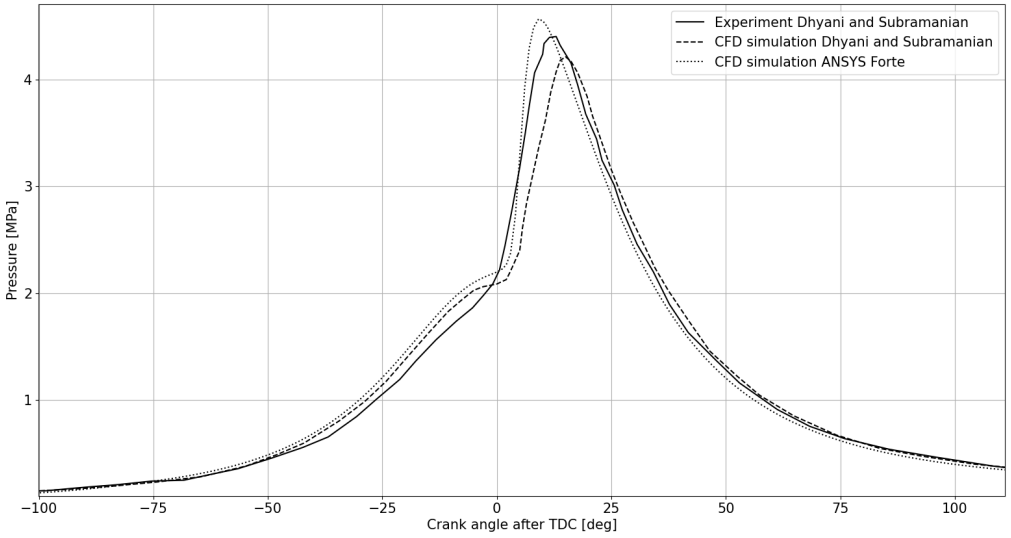

Figure 7.30: The pressure curves from the experimental and CFD results by Dhyani and Subramanian [25] and the CFD Forte results

It is quite interesting to see that both of the CFD simulations do not exactly match the experimental data, but both are not far off. Both simulations have higher pressures during the compression phase of the engine cycle and in both, combustion seems to occur later than during the experiment. But where the pressure peak in the reference paper simulation is lower and later than the experiment, the pressure peak in the Forte simulation is higher and comes earlier in the cycle. Once again the differences here can be explained by a myriad of reasons, such as different engine geometry and different operating conditions. Despite these differences, the overall trend and resulting pressure curve match that of the experiment quite well, meaning that the ANSYS Forte model accurately represents the combustion processes in a hydrogen internal combustion engine.

8
Lycoming IO-360-1AB6

As has been discussed before, this work is part of a larger project that aims to convert one of the engines of a Cessna 337 Skymaster to run on hydrogen, to see if such a conversion would be a viable solution to make this type of aircraft more environmentally sustainable. The research performed in this work is meant as preparation for the conversion of a Lycoming IO-360-1AB6 engine to run on hydrogen inside a testcell that is currently under construction. However, the insights that have been gained from this work have either been specific for the ANSYS Forte engine used in the simulation, or have been for a general hydrogen internal combustion engine. This chapter therefore attempts to translate those insights to be used on the Lycoming engine.

8.1. Lycoming vs. ANSYS Forte engine

In this first section, the differences and similarities between the Forte engine model and the Lycoming engine will be discussed, as well as what those differences and similarities mean for the insights that have been gained from the CFD simulations.

Figure 8.1 and Figure 8.2 show two different viewing angles of a Lycoming IO-360 engine. The IO-360 engine is a four-cylinder, port fuel injection, flat engine. In Figure 8.1, the crankshaft is located in the centre and there are two cylinders on either side. In the figure, two spark plugs are indicated, but it can be seen that each individual cylinder is equipped with two spark plugs. This is a feature that is very common in aircraft engines, as it adds a layer of redundancy. If one of the spark plugs fails, there is still a second spark plug there and full engine operation can continue.

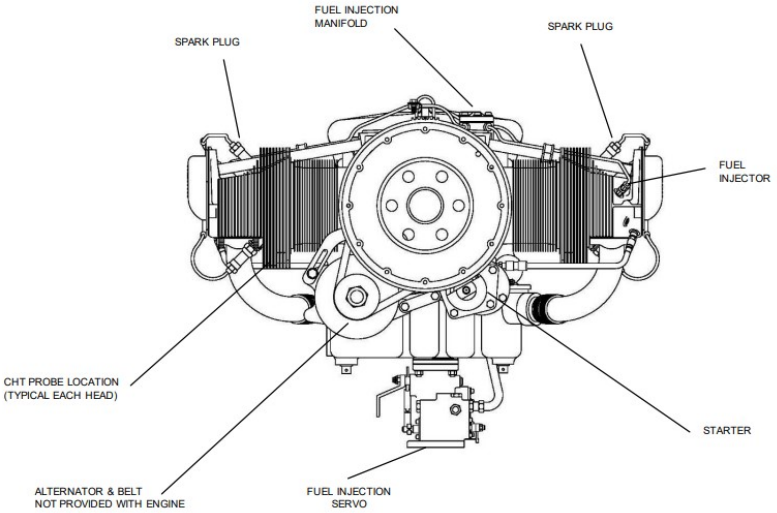

Figure 8.1: Front view of a IO-360 Lycoming engine [65]

The I in IO-360 stands for injection, and indeed a fuel injector can be seen, which injects aviation gasoline into the combustion chamber inlet. Figure 8.2 shows a side view of the same engine, where two out of the four cylinders can be seen.

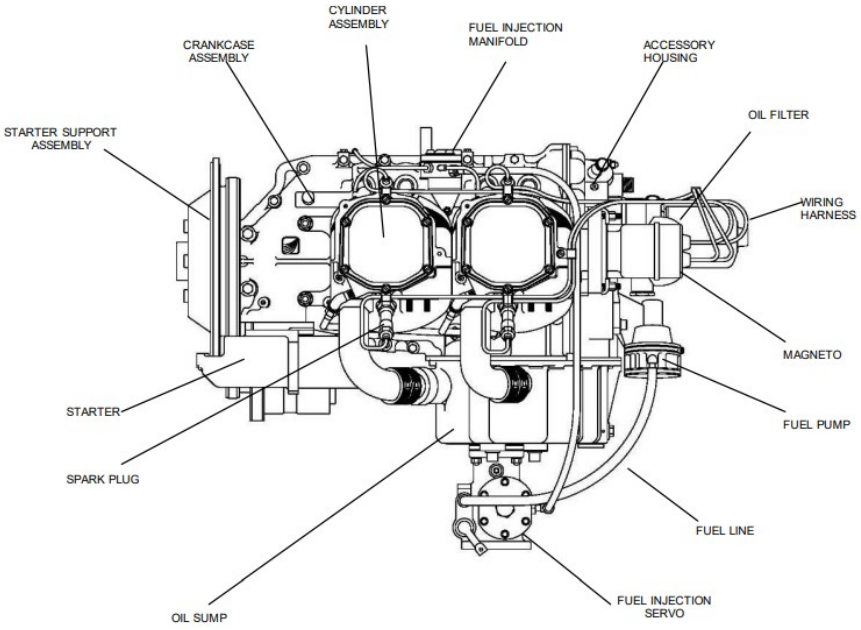

Figure 8.2: Left side view of a IO-360 Lycoming engine [65]

What can't be seen in these figures is the shape of the combustion chamber, so of the cylinder head and of the piston. However, it is known that the piston has a flat bowl and can be seen in Figure 8.4, unlike the Forte engine, which can be seen in Figure 8.3. Here, the piston has a more complex shape, which also influences the flow inside the combustion chamber. It was already shown in subsection 7.2.1 that a different piston bowl leads to different hydrogen flows within the engine. It should therefore be noted that the hydrogen flows that were shown in this work are not indicative of the hydrogen flows in the Lycoming engine.

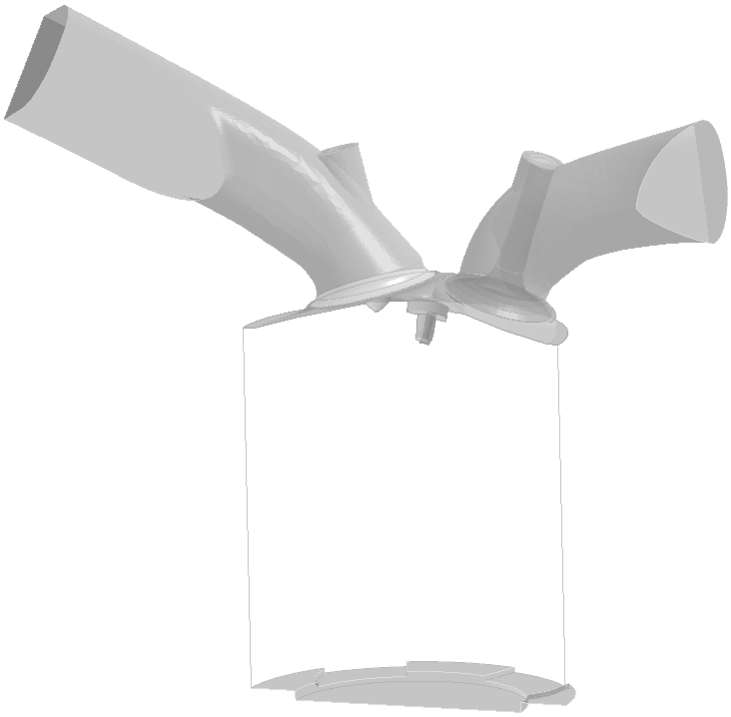

Figure 8.3: View of the Ansys Forte engine

Although the exact shape of the Lycoming engine head is not known, it can be derived from the images provided above, that the general shape differs quite a bit from the Forte engine. The major difference, is

that where on the Forte engine, all of the components are located on the top of the cylinder head, most of the components on the Lycoming cylinder head seem to be located on either side. Another difference is of course the different number of spark plugs. However, one of the spark plugs in the Lycoming engine will most likely be replaced by an injector, in order to make direct injection possible. This will be discussed later on in this chapter, but what it means is that the injector will be located on the side of the combustion chamber, whereas it is located in the centre of the Forte engine. For early injection, where the hydrogen has time to mix with the air, this should not pose a problem, but for later injection, the hydrogen flows in the two engines will differ. This is especially important if the implementation of optimised hydrogen injection is going to be attempted, as the hydrogen flow is the most important factor there.

One difference that is not apparent from the images shown above, is the size difference. Table 8.1 shows the geometrical properties of both engines.

Table 8.1: Geometrical properties of both engines, both for 1 cylinder

Engine	Lycoming IO-360-1AB6	ANSYS Forte
Volume [cm^3]	1478.9	498.8
Stroke [mm]	111	90
Bore [mm]	130	84
Compression ratio [-]	8.7:1	10.3:1

It is very clear that the Lycoming engine is much larger than the Forte engine. Furthermore, the ratio between the bore and the stroke is very different. In the Lycoming engine, the bore is wider than the stroke, while the stroke is longer than the bore in the Forte engine. This will again influence the hydrogen flow in the engine. The last difference that can be noted from the table is the difference in compression ratio. The Lycoming engine has a lower compression ratio, resulting in a lower pressure at the moment of combustion and therefore most likely also a lower peak pressure.

Finally, it is clear that there are large differences between the Lycoming engine and the engine used in the CFD simulations. Therefore, it is wise to repeat the conditions under which the CFD results, as reported in this work, should be used. The general trends for power and NO_x emissions as functions of spark timing and equivalence ratio hold for hydrogen internal combustion engines in general and can be applied to the Lycoming engine as well. Values and results of hydrogen flow-based combustion processes are specific to the engine used in the simulations and to the conditions of the CFD simulations and can therefore not be used to make any predictions for the Lycoming or any other engine. The insights that were gained from these hydrogen flows however, can be used to potentially optimise the injection in other hydrogen internal combustion engines, but this must be done on an engine per engine basis.

8.2. Conversion of the Lycoming

From the contents of this work, it is clear that converting an internal combustion engine to run on hydrogen is not as simple as just replacing the fuel. Changes have to be made to the engine in order to ensure safe and efficient operation. In this section, some of the changes that will have to be made to the Lycoming IO-360-1AB6 engine are discussed.

8.2.1. Direct injection

During the literature study part of this thesis work, a great amount of attention was given to figuring out what changes would have to be made to the injection part of the engine cycle. From the CFD results, it can be concluded that, in order to meet the power requirements for an aircraft engine, direct injection is necessary. However, the Lycoming engine that will be used during testing, does not have direct injection. A necessary change to the Lycoming engine will therefore have to be to replace one of the spark plugs in each cylinder with an injector. Of course, it will have to be seen if the selected injector will fit inside the hole that is left by the spark plug, or if some further modifications will have to be made.

Using direct injection means that the injector will need to inject hydrogen at high pressures and, as hydrogen has a low density, a high volume has to be injected. This report has discussed some of the injectors that could be used, but modifying a different injector or developing one from the ground up are also possibilities. If one of these options is chosen, it should be noted that the non-lubricity of hydrogen poses a real problem that has to be addressed.

8.2.2. Fuel system

Of course, the injector is not the only part of the fuel system that has to be modified. As hydrogen will be stored and injected at pressures that are much higher than that of aviation gasoline, the fuel system that is currently used on the Lycoming engine and that can partly be seen in Figure 8.1 and Figure 8.2 can not be used. Depending on the storage and injection pressures, components should be selected that can safely handle those pressures and from which the hydrogen will not leak.

8.2.3. Sealing rings

Upon hearing about the conversion of one of their engines to run on hydrogen, Lycoming expressed their concerns regarding the piston rings, and whether they would provide enough of a seal to keep the hydrogen from leaking into the crank case. These piston rings can be seen in Figure 8.4, marked by numbers 9 and 10.

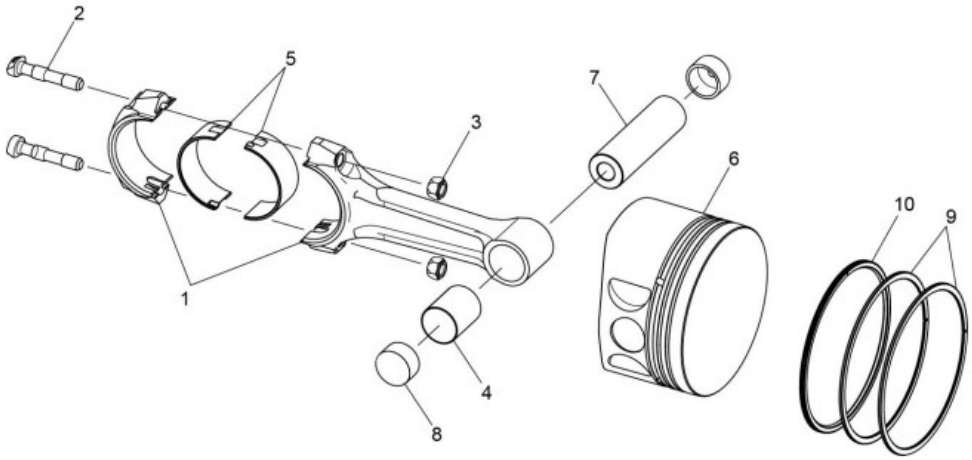

Figure 8.4: View of the piston assembly of a IO-360 engine [66]

Leakage of hydrogen must of course be avoided, so there are two courses of action here. The first option is to leave the rings as they are, but closely monitor the hydrogen density inside the crank case, to make sure that no hydrogen leaks past the rings. The second option is to preemptively replace the current piston rings for ones that provide more of a seal. In the second case, the hydrogen density inside the crank case should still be monitored, but probably less heavily.

8.2.4. Spark Plugs

The final modification that should be applied to the Lycoming engine, is the installation of a cold rated spark plug. Hydrogen has the potential to pre-ignite on a hot surface, which the spark plug could potentially be. A cold rated spark plug dissipates more of its heat to the rest of the cylinder, which means it stays cooler. More explanation on this topic was given in subsection 4.2.2. No pre-ignition was observed during the CFD simulations, but that is because during the simulations, all boundaries of the engine, including the spark plugs, were kept at the same temperature, so no hot spots ever developed. In order to see if cold rated spark plugs are necessary, further research could be performed, where hot spots would be created artificially in the CFD simulations, to observe if any pre-ignition would occur.

8.3. Recommendations for Engine Testing

The maximum pressure that would be reached inside the combustion chamber at the moment of peak pressure was a very important concern before this research began. Previous work had shown that hydrogen's high flame speed could produce a very fast and violent combustion, that would result in high and steep pressure peaks. Such pressure peaks could potentially damage the engine and therefore this potential problem had to be assessed.

In section 6.6, it has already been discussed how the pressure peak due to combustion could be lowered, such that safe operation could be guaranteed. However, these measures come at a cost to the performance of the engine, so the pressure peak should not be reduced to a level lower than is strictly necessary.

By contacting Lycoming directly, it was found that the maximum pressures that occurs in a Lycoming IO-360-1AB6 engine during normal operation on 100LL aviation gasoline is 6.4 MPa. This is not the maximum pressure that the engine can handle before being damaged, as Lycoming does not provide maximum burst pressures for their engine heads. However, they have warned that a 1.5 safety factor is not always used on all of the engine components, so 6.4 MPa should be considered the maximum pressure at which the engine should operate.

Going through the results presented in this work, it can be seen that for early injection, high equivalence ratio engine cycles, the peak pressures are well beyond this maximum of 6.4 MPa. The concerns that were raised in previous work about the dangers of hydrogen combustion inside an internal combustion engine were therefore not unwarranted. However, if the recommendations that were given in section 6.6 and in chapter 10 are followed, safe operation of the Lycoming engine using hydrogen should be attainable. Starting off with low equivalence ratios and retarded spark timings, the pressure peaks should be relatively low. Once this has been established, the equivalence ratio can be increased and the spark timing advanced. During such operation, a close watch should be kept on the maximum pressures that occur inside the combustion chamber, as they should always be kept below the maximum of 6.4 MPa.

But how should the pressure inside the combustion chamber be monitored? Like most internal combustion engines, the Lycoming does not have a pressure transducer built into the combustion chamber. Therefore, in order to monitor the pressure inside the combustion chamber, modifications need to be made. Basically, there are two options here. The first one is to drill a hole in the combustion chamber and insert a pressure transducer at this location. For that to work, there needs to be a location in the combustion chamber where there is enough space and material to support the transducer. Additionally, this location needs to be a suitable location to place a pressure transducer. The second option is one that can be seen in Figure 8.5.

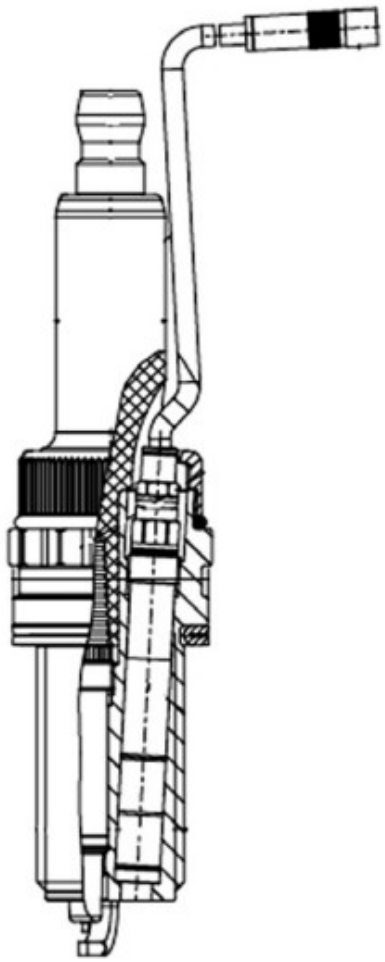

Figure 8.5: Part section through a typical combined spark plug and cylinder pressure transducer[67]

In this figure, a combined spark plug and cylinder pressure transducer is shown. On the left side, the spark plug can be seen, while on the right side, a pressure transducer is visible. By combining these two, no extra holes need to be drilled and the structural integrity of the combustion chamber stays intact. Of course, a combined spark plug and cylinder pressure transducer needs to be selected that fits into the existing spark plug hole. Also, it should be checked whether such a configuration does not create extra hot spots, where preignition could occur.

9
Conclusions

In this thesis work, a CFD model of a hydrogen internal combustion engine was used to evaluate the performance of such an engine, to find the challenges and opportunities of the conversion of an aviation gasoline internal combustion engine to a hydrogen internal combustion engine. Prior to this work, a literature study was performed, from which it was concluded that the following modifications should be made to an aviation internal combustion engine to convert it into a competitive hydrogen internal combustion engine. One of the spark plugs should be replaced by a hydrogen injector. This is because direct injection of hydrogen is the only way to match the power output of a gasoline internal combustion engine. The remaining spark plug should be replaced by a cold-rated spark plug, to reduce the likelihood of preignition occurring inside the combustion chamber.

From the verification and validation efforts in this work, it was concluded that the results from the CFD simulations match with the results from engine tests of a hydrogen internal combustion engine. As such, the results of the simulations are indicative for the performance of a real engine. However, it was also found that the flow inside the combustion chamber is highly dependent on the mesh geometry. It was therefore concluded that, although the results can be used as a first assessment of the performance of a hydrogen internal combustion engine, the model can not be used to make exact predictions.

Using the CFD simulations, it was found that early injection results in a fairly homogeneous mixture inside the combustion chamber. This results in fast and hot combustion, resulting in high NO_x emissions. Through trial and error, it was found that the hydrogen injection can be optimised such that the combustion process is slowed down. This results in lower pressure peaks, higher output powers and lower NO_x emissions. It was also concluded that any hydrogen internal combustion engine with a high-power use case requires direct injection, as indirect injection results in too high volumetric losses. Using direct injection, a hydrogen internal combustion engine is able to come close to or even match the performance of a gasoline internal combustion engine. Using optimised hydrogen injection, the performance of hydrogen might even exceed that of gasoline.

By reviewing pressure peak reduction measures, it was concluded that safe operation can be achieved by starting off with lower equivalence ratio engine cycles and later spark timings. The maximum allowable pressure inside the combustion chamber is 6.4 MPa and this pressure should not be exceeded. To ensure this, a pressure transducer should be installed in the combustion chamber. By starting off with lower equivalence ratios and later spark timings, the maximum pressure inside the combustion chamber stays relatively low. Once it is ensured that safe operation is possible, the performance of the engine can be optimised by optimising the spark timing and the equivalence ratio. The optimum spark timing will most likely be later than the spark timing for a gasoline engine. This later spark timing will result in higher power output, but lower NO_x emissions. Higher equivalence ratios result in higher power outputs, but due to a lower thermal efficiency at higher equivalence ratios, the rate of return on additional hydrogen diminishes at these higher equivalence ratios. Furthermore, higher equivalence ratios may result in preignition, something that should be investigated in future CFD studies.

In conclusion, hydrogen internal combustion engines promise to be a viable alternative to traditional internal combustion engines. They can provide similar, or with optimised hydrogen injection even better, performance figures, while emitting no carbon oxides. During future engine testing, the results from this report will have to be validated further, and the feasibility of converting aircraft engines to run on hydrogen on a larger scale will have to be assessed.

10
Recommendations

The recommendations of this thesis work can be split into two parts, the recommendations for future CFD studies and the recommendations for the continuation of the project, in which the next step is going to be engine testing.

10.1. Future CFD Studies

Although the CFD study performed in this work has resulted in many insights into the workings of a hydrogen internal combustion engine, there are still areas that have not been covered or require further investigation. Therefore, the following recommendations are made:

- Further investigate the behaviour of hydrogen inside the combustion chamber, mapping the conditions under which optimised injection is possible.
- Investigate the effects of different engine speeds on the performance of a hydrogen internal combustion engine, focusing on optimised hydrogen injection.
- Model the Lycoming IO-360-1AB6 engine in ANSYS Forte to further study its particular behaviour under hydrogen operation.
- Model the engine of the Cessna 337 Skymaster in ANSYS Forte to further study its particular behaviour under hydrogen operation.
- Look at different hydrogen injection models to more accurately mimic the behaviour of a real hydrogen injector.
- Investigate the possibility of multiple injection moments to prevent misfire. Some preliminary investigation into this topic has been performed, but many more scenarios can be considered, such as different number of injections and different timings.
- Investigate the possibility of multiple spark firings, to ensure combustion. Some preliminary investigation into this topic has been performed, but many more scenarios can be considered, such as different spark timings and different engine conditions.
- During the literature study that was performed prior to this thesis, it was found that engine knock can become a problem for hydrogen internal combustion engines at higher equivalence ratios. Since higher equivalence ratios are most likely necessary to attain the required power outputs, the knocking behaviour of hydrogen internal combustion engines should be investigated further. This could be done by artificially by creating a hotspot at, for example, the spark plug in the CFD model and observe if any pre-ignition occurs.

For any future CFD study, it should also be contemplated whether ANSYS Forte or a different solver should be used. In this work, Forte was chosen because it was designed specifically for internal combustion engines and because it was available to the student. There are however three major points that might make a future student want to reconsider the choice for Forte, based on the experience and knowledge gained from this work. Firstly, there is the fact that ANSYS does not seem to put a lot of their resources towards Forte. The program itself looks very dated, the integration with other programs, whether from ANSYS or third-party developers, is very bad and the support from ANSYS does not go beyond anything that a first time user can deduce by themselves in no-time. Secondly, there is the geometry import issue. The engine geometry that was used in this work stems from an ANSYS Forte tutorial. Fortunately, this model fits the requirements for this research very well, but any attempt to import a different geometry seemed fruitless. Again, the ANSYS support was no help at all on this issue and looking through online fora, it seems that many people are

suffering from the same issue. This once again shows that ANSYS does not seem to pay much attention to Forte. Lastly, there is the injector model in ANSYS Forte. The injector model does everything that anyone could expect it to do, apart from injecting non-liquid fuels. This means it can not be used for hydrogen and an inlet boundary condition had to be used instead. Not only was it quite a challenge to control the amount of hydrogen that was injected this way, but the shape of the injection cone could not be altered much and no additional cones could be added.

These factors should be taken into account by anyone who wants to model a hydrogen internal combustion engine using CFD. As was shown in this report, the solver in ANSYS Forte works well and the results are very usable, but if a solver could be found that would address these issues, that solver might be a better choice for this specific application.

10.2. Engine Testing

Because this thesis work is in preparation for the engine testing of the Lycoming IO-360-1AB6 engine, this sections makes some recommendations on the modifications that should be made to the Lycoming engine and some practices that should be applied in order to ensure safe engine testing. These are the recommendations:

- A hydrogen injector should be selected or manufactured that can inject hydrogen at high pressure into the combustion chamber. It should be able to operate under higher temperatures and should not wear due to the non-lubricity of hydrogen.
- On each individual cylinder, one of the spark plugs should be replaced by an injector.
- The existing fuel system should be replaced by a system that can handle high-pressure hydrogen.
- The spark plugs should be replaced by cold-rated spark plugs.
- The piston rings should be monitored closely for hydrogen leaks or should be replaced altogether to prevent hydrogen leakage into the crank case.
- A pressure transducer should be placed inside the combustion chamber.
- If not present, an NO_x sensor should be placed inside the exhaust of the engine.
- A hydrogen sensor should be placed inside the exhaust of the engine. This sensor is used to evaluate the efficiency of the combustion, to see if all hydrogen is burned.
- The performance of the Lycoming engine on aviation gasoline should be mapped before any modifications are made, to later compare to the performance on hydrogen.
- The pressure inside the combustion chamber should be kept below 6.4 MPa.
- When first running the Lycoming engine on hydrogen, the equivalence ratio should be kept low and the spark timing should be retarded to decrease the pressure peak.
- If misfires occur, the injection timing should be advanced or the equivalence ratio should be increased.

Furthermore, the research into optimised hydrogen injection would benefit greatly from developing a visual hydrogen internal combustion engine, where instruments could follow the flow of hydrogen inside the engine. Similar experiments have been performed before, but those just looked at the injection stage of the engine cycle. A visual engine where actual combustion occurs will be hard to accomplish, as the modifications will weaken the integrity of the engine. However, if two identical engines were acquired, where one was modified so a visual of the combustion chamber could be captured, the flow of the hydrogen in that engine could be matched to the combustion performance of the second engine. In doing so, the findings of this report about optimised hydrogen injection could be validated and the engine performance could be optimised further.

Bibliography

[1] B. Khandelwal, A. Karakurt, P. R. Sekaran, V. Sethi, and R. Singh, "Hydrogen powered aircraft : The future of air transport," *Progress in Aerospace Sciences*, vol. 60, pp. 45–59, 2013.

[2] S. Verhelst and T. Wallner, "Hydrogen-fueled internal combustion engines," *Progress in Energy and Combustion Science*, vol. 35, no. 6, pp. 490–527, 2009.

[3] A. Delorme, A. Rousseau, P. Sharer, S. Pagerit, and T. Wallner, "Evolution of hydrogen fueled vehicles compared to conventional vehicles from 2010 to 2045," 2009.

[4] E. Peeters, "Literature Study: The Challenges of a Hydrogen Internal Combustion Engine ," Master's thesis, Delft University of Technology, 2021.

[5] W. Pulkrabek, *Engineering fundamentals of the internal combustion engine*. New Jersey: Prentice Hall, 1997.

[6] L. Das, "Fuel induction techniques for a hydrogen operated engine," *International Journal of Hydrogen Energy*, vol. 15, pp. 833–842, 1990.

[7] A. Welch, D. Mumford, S. Munshi, J. Holbery, B. Boyer, M. Younkins, and H. Jung, *Challenges in Developing Hydrogen Direct Injection Technology for Internal Combustion Engines*. 2008.

[8] R. H. Stanglmaier and C. E. Roberts, "Homogeneous charge compression ignition (hcci): Benefits, compromises, and future engine applications," *SAE Transactions*, vol. 108, pp. 2138–2145, 1999.

[9] F. Zhao, T. N. Asmus, D. N. Assanis, J. E. Dec, J. A. Eng, and P. M. Najt, "Homogeneous charge compression ignition (hcci) engines," 2003.

[10] D. K. Srivastava, A. K. Agarwal, A. Datta, and R. K. Maurya, *Advances in internal combustion engine research*. Singapore: Springer, 2017.

[11] M. Christensen and B. Johansson, "Influence of mixture quality on homogeneous charge compression ignition," *SAE transactions*, pp. 951–963, 1998.

[12] P. M. Najt and D. E. Foster, "Compression-ignited homogeneous charge combustion," *SAE Transactions*, pp. 964–979, 1983.

[13] M. Christensen, B. Johansson, and P. Einewall, "Homogeneous charge compression ignition (hcci) using isooctane, ethanol and natural gas-a comparison with spark ignition operation," *SAE transactions*, pp. 1104–1114, 1997.

[14] T. Ullman, "Investigation of the effects of fuel composition on heavy-duty diesel engine emissions," *SAE International*, 1989.

[15] P. Talebizadeh Sardari, M. Babaie, R. Brown, H. Rahimzadeh, Z. Ristovski, and M. Arai, "The role of non-thermal plasma technique in nox treatment: A review," *Renewable and Sustainable Energy Reviews*, vol. 40, pp. 886–901, 2014.

[16] L. Hosking, "Literature Study: A Flying Test Bed for Sustainable Aviation: Alternative Fuel-powered Aircraft ," Master's thesis, Delft University of Technology, 2020.

[17] W. Frijters, "A Flying Test Bed for Sustainable Aviation - Hydrogen Propulsion ," Master's thesis, Delft University of Technology, 2020.

[18] M. A. R. Sadiq Al-Baghdadi, "Effect of compression ratio, equivalence ratio and engine speed on the performance and emission characteristics of a spark ignition engine using hydrogen as a fuel," *Renewable Energy*, vol. 29, no. 15, pp. 2245–2260, 2004.

[19] X. Tang, D. M. Kabat, R. J. Natkin, W. F. Stockhausen, and J. Heffel, "Ford p2000 hydrogen engine dynamometer development," *SAE Technical Papers*, 2002.

[20] H. L. Yip, A. Srna, A. C. Y. Yuen, S. Kook, R. A. Taylor, G. H. Yeoh, P. R. Medwell, and Q. N. Chan, "A review of hydrogen direct injection for internal combustion engines: Towards carbon-free combustion," *Applied Sciences*, vol. 9, no. 22, p. 4842, 2019.

[21] H. Li and G. A. Karim, "Knock in spark ignition hydrogen engines," *International Journal of Hydrogen Energy*, vol. 29, no. 8, pp. 859–865, 2004.

[22] C. M. White, R. R. Steeper, and A. E. Lutz, "The hydrogen-fueled internal combustion engine: a technical review," *International Journal of Hydrogen Energy*, vol. 31, no. 10, pp. 1292–1305, 2006.

[23] B. Lewis and G. Von Elbe, *Combustion, flames, and explosions of gases*. New York: Academic Press, 2d ed. ed., 1961.

[24] W. Stockhausen, R. Natkin, D. Kabat, L. Reams, X. Tang, S. Hashemi, S. Szwabowski, and V. Zanardelli, "Ford p2000 hydrogen engine design and vehicle development program," *SAE Technical Papers*, 2002.

[25] V. Dhyani and K. A. Subramanian, "Fundamental characterization of backfire in a hydrogen fuelled spark ignition engine using cfd and experiments," *International Journal of Hydrogen Energy*, vol. 44, no. 60, pp. 32254–32270, 2019.

[26] R. Hari Ganesh, V. Subramanian, V. Balasubramanian, J. M. Mallikarjuna, A. Ramesh, and R. P. Sharma, "Hydrogen fueled spark ignition engine with electronically controlled manifold injection: An experimental study," *Renewable Energy*, vol. 33, no. 6, pp. 1324–1333, 2008.

[27] R. Scarcelli, T. Wallner, N. Matthias, V. Salazar, and S. Kaiser, "Mixture formation in direct injection hydrogen engines: Cfd and optical analysis of single- and multi-hole nozzles," *SAE International Journal of Engines*, vol. 4, pp. 2361–2375, 2011.

[28] G. Settles, *Schlieren and Shadowgraph Techniques*. Springer, 2001.

[29] J. Norbeck, M. Barth, J. Farrell, and J. Heffel, "Development and evaluation of a hydrogen fuel power plant for a hybrid electric vehicle — phase ii," 1997.

[30] A. Mohammadi, M. Shioji, Y. Nakai, W. Ishikura, and E. Tabo, "Performance and combustion characteristics of a direct injection si hydrogen engine," *International Journal of Hydrogen Energy*, vol. 32, no. 2, pp. 296–304, 2007.

[31] T. Wallner, N. Matthias, R. Scarcelli, and J. Kwon, "Evaluation of the efficiency and the drive cycle emissions for a hydrogen direct-injection engine," *Proceedings of the Institution of Mechanical Engineers, Part D: Journal of Automobile Engineering*, vol. 227, pp. 99–109, 2013.

[32] P. G. Aleiferis and M. F. Rosati, "Controlled autoignition of hydrogen in a direct-injection optical engine," *Combustion and Flame*, vol. 159, no. 7, pp. 2500–2515, 2012.

[33] Z. Huang, J. Wang, B. Liu, K. Zeng, J. Yu, and D. Jiang, "Combustion characteristics of a direct-injection engine fueled with natural gas–hydrogen blends under different ignition timings," *Fuel*, vol. 86, no. 3, pp. 381–387, 2007.

[34] J. Wang, Z. Huang, Y. Fang, B. Liu, K. Zeng, H. Miao, and D. Jiang, "Combustion behaviors of a direct-injection engine operating on various fractions of natural gas–hydrogen blends," *International Journal of Hydrogen Energy*, vol. 32, no. 15, pp. 3555–3564, 2007.

[35] D. Kabat and J. Heffel, "Durability implications of neat hydrogen under sonic flow conditions on pulse-width modulated injectors," *International Journal of Hydrogen Energy - INT J HYDROGEN ENERG*, vol. 27, pp. 1093–1102, 2002.

[36] K. Yamane, M. Nogami, Y. Umemura, M. Oikawa, Y. Sato, and Y. Goto, "Development of high pressure h2 gas injectors, capable of injection at large injection rate and high response using a common-rail type actuating system for a 4-cylinder, 4.7-liter total displacement, spark ignition hydrogen engine," *SAE Technical Papers*, 2011.

[37] D. R. Pearl, "O-ring seals in the design of hydraulic mechanisms," *SAE Technical Paper*, vol. 470247, p. 10, 1947.

[38] K. Alvine, V. Shutthanandan, W. Bennett, C. Bonham, D. Skorski, S. Pitman, M. Dahl, and C. Henager, "High-pressure hydrogen materials compatibility of piezoelectric films," *Applied Physics Letters*, vol. 97, pp. 221911–221911, 2010.

[39] J. Topinka, M. D. Gerty, J. Heywood, and J. Keck, "Knock behavior of a lean-burn, h2 and co enhanced, si gasoline engine concept," *SAE Technical Papers*, 2004.

[40] S. Verhelst, Sierens, and S. Verstraeten, "A critical review of experimental research on hydrogen fueled si engines," *SAE Technical Papers*, 2006.

[41] R. J. Natkin, A. R. Denlinger, M. Younkins, A. Z. Weimer, S. Hashemi, and A. T. Vaught, "Ford 6.8l hydrogen ic engine for the e-450 shuttle van," *SAE Technical Papers*, 2007.

[42] P. Huyskens, S. Oost, P. J. Goemaere, K. Bertels, and M. Pecqueur, "The technical implementation of a retrofit hydrogen pfi system on a passenger car," *SAE Technical Papers*, 2011.

[43] H. Osamura and N. Abe, *Development of New Iridium Alloy for Spark Plug Electrodes*, vol. 108. 1999.

[44] L. M. Das, "Near-term introduction of hydrogen engines for automotive and agricultural application," *International Journal of Hydrogen Energy*, vol. 27, no. 5, pp. 479–487, 2002.

[45] B. L. Salvi and K. A. Subramanian, "Experimental investigation on effects of compression ratio and exhaust gas recirculation on backfire, performance and emission characteristics in a hydrogen fuelled spark ignition engine," *International Journal of Hydrogen Energy*, vol. 41, no. 13, pp. 5842–5855, 2016.

[46] J. W. Heffel, "Nox emission reduction in a hydrogen fueled internal combustion engine at 3000 rpm using exhaust gas recirculation," *International Journal of Hydrogen Energy*, vol. 28, no. 11, pp. 1285–1292, 2003.

[47] J. W. Heffel, "Nox emission and performance data for a hydrogen fueled internal combustion engine at 1500rpm using exhaust gas recirculation," *International Journal of Hydrogen Energy*, vol. 28, no. 8, pp. 901–908, 2003.

[48] M. Berckmuller and H. Rottengruber, "Potentials of a charged si-hydrogen engine," *Proceedings of the International Hydrogen Energy Forum; 2004 May 25-28; Beijing, China*, pp. 59–67, 2004.

[49] B. Nagalingam, M. Dubel, and K. Schmillen, *Performance of the Supercharged Spark Ignition Hydrogen Engine*. 1983.

[50] S. Furuhama, M. Hiruma, and Y. Enomoto, "Development of a liquid hydrogen car," *International Journal of Hydrogen Energy*, vol. 3, pp. 61–81, 1978.

[51] L. Hosking, "Safety Considerations for Developing an H2ICE for Aviation Applications ," Master's thesis, Delft University of Technology, 2021.

[52] H. Eichlseder, T. Wallner, R. Freymann, and J. Ringler, "The potential of hydrogen internal combustion engines in a future mobility scenario," *SAE Technical Papers*, 2003.

[53] S. Furuhama, K. Yamane, and I. Yamaguchi, "Combustion improvement in a hydrogen fueled engine," *International Journal of Hydrogen Energy*, vol. 2, pp. 329–340, 1975.

[54] "Ansys forte theory manual," *ANSYS Inc.*, 2019. Manual as included with the 2019 R3 edition of Ansys Forte.

[55] A. A. Amsden, "Kiva-3v: A block-structured kiva program for engines with vertical or canted valves," 1997.

[56] V. Yakhot and S. Orszag, "Renormalization group analysis of turbulence. i. basic theory.," *J Sci Comput*, vol. 1, pp. 3–51, 1986.

[57] Z. Han and R. Reitz, "Turbulence modeling of internal combustion engines using rng k-ϵ models," *Combustion Science and Technology*, vol. 106, pp. 267–295, 1995.

[58] L. Fan and R. Reitz, "Development of an ignition and combustion model for spark-ignition engines," *SAE Technical Paper 2000-01-2809*, 2000.

[59] R. Tan, Z.; Reitz, "An ignition and combustion model for spark ignition engine multidimensional modeling," *Combustion and Flame, 145*, pp. 1–15, 2006.

[60] N. Peters, *Turbulent combustion*. Cambridge University Press, 2000.

[61] R. Liang, L.; Reitz, "Spark ignition engine combustion modeling using a level set method with detailed chemistry," *SAE TEchnical Paper 2006-01-0243*, 2006.

[62] L. Liang, R. Reitz, C. Iyer, and J. Yi, "Modeling knock in spark-ignition engines using a g-equation combustion model incorporating detailed chemical kinetics," *SAE Technical Paper 2007-01-0165*, 2007.

[63] K. M. Rahman, *Experimental Investigation and CFD Simulation of Mixture Formation and Combustion in Hydrogen Direct Injection Spark-Ignition Engine*. Thesis, 2018.

[64] S. Som, P. K. Senecal, and E. Pomraning, "Comparison of rans and les turbulence models against constant volume diesel experiments," 2012.

[65] "Installation & operation manual - o-360 and io-360 series engines," *Superior Air Parts*, 2014.

[66] "Io-360-p1a engine - illustrated parts catalog," *Lycoming*, 2017.

[67] A. Martyr and M. Plint, *Engine Testing*. Oxford: Butterworth-Heinemann, fourth ed., 2012.